WASHINGTON UNIVERSITY

SEVER INSTITUTE OF TECHNOLOGY

DEPARTMENT OF CIVIL ENGINEERING

TORSIONALLY COUPLED RESPONSE CONTROL OF EARTHQUAKE EXCITED ASYMMETRIC BUILDINGS: DEVELOPMENT AND APPLICATION OF EFFECTIVE CONTROL SYSTEMS USING SMART DAMPERS

by

Osamu Yoshida

Prepared under the direction of Professor Shirley J. Dyke

A dissertation presented to the Sever Institute of
Washington University in partial fulfillment
of the requirements of the degree of

DOCTOR OF SCIENCE

May, 2003

Saint Louis, Missouri

WASHINGTON UNIVERSITY
SEVER INSTITUTE OF TECHNOLOGY
DEPARTMENT OF CIVIL ENGINEERING

ABSTRACT

TORSIONALLY COUPLED RESPONSE CONTROL OF EARTHQUAKE EXCITED ASYMMETRIC BUILDINGS: DEVELOPMENT AND APPLICATION OF EFFECTIVE CONTROL SYSTEMS USING SMART DAMPERS

by Osamu Yoshida

ADVISOR: Professor Shirley J. Dyke

May 2003
St. Louis, Missouri

This dissertation focuses on the development and validation of control systems that can effectively reduce seismic responses due to torsional coupling in asymmetric building structures. Due to their attractive characteristics for seismic response control, semiactive control systems using magnetorheological (MR) dampers are specifically examined in the numerical and experimental studies.

To experimentally verify the applicability of the proposed semiactive control system to torsionally coupled responses of an asymmetric building, laboratory studies are conducted using a 2-story experimental building model with asymmetric column distribution, and the performance is evaluated through shaking table testing.

The efficacy of the proposed control system when applied to numerical models of full scale irregular buildings is also discussed. Two full scale buildings, a 9-story building with

an asymmetric structural plan, and an L-shaped, 8-story building with additional vertical irregularity due to setbacks, are considered in these studies.

Through the research presented herein, it is verified that the controlled performance of the proposed semiactive control system using MR dampers is significantly better than that of passive control systems and as good as an ideal active control system.

To whom always give me joy in life:

my wife Koaru, my daughter Mayu, and my son Yusei

Contents

Tables

Figures

Acknowledgments

First of all, I would like to address my gratitude to Dr. Shirley J. Dyke for accepting me as a graduate student under her supervision and for keeping giving me valuable advice and suggestions. I have learned a lot from her, not only on research itself but also on how to think as a researcher and how to get through difficult situations. I have always been encouraged by her to complete my degree. Without her direction, this dissertation would not have been completed.

Also, I would like to express my gratitude to my doctoral committee members, Dr. Kevin Z. Truman, Dr. Phillip L. Gould, Dr. Thomas G. Harmon, and Dr. Philip V. Bayly for providing me valuable advice and comments. This dissertation has been improved by their advice and comments.

I would also like to thank Dr. Satish Nagarajaiah and Mr. Sriram Narasimhan of Rice University for helping me with the analytical model of the full scale 8-story, L-shaped building studied in the chapter 6.

I would like to thank Mr. Luca M. Giacosa, a former visiting researcher, for helping me with the experiment described in the chapter 5

I would like to thank Mr. Carlos Monroy, a former visiting researcher, for helping me with the genetic algorithm code described in the chapter 6.

I would like to thank graduate students of Structural Control and Earthquake Engineering Laboratory, Mr. Juan M. Caicedo, Mr. Diego F. Giraldo, Mr. Steven R. Williams, and a postdoctoral researcher, Dr. Ping Tan for sharing wonderful time in the lab with me. They have always been good friends and helped me in my work.

I would also like to thank graduate students of civil engineering department, Ms. Dongmei Chu, Ms. Lizzy Li, Mr. Yoo Jae Kim, and Mr. Wei Huang for their friendship. I had really good times with them.

Next, I would like to express my acknowledgement to my employer, Obayashi Corporation for giving me the opportunity to study at Washington University. Their generous support is gratefully acknowledged.

I would like to address my gratitude to my bosses, Dr. Yutaro Omote, the director of Obayashi Corporation Technical Research Institute, and Dr. Matsutaro Seki, the manager of Building Vibration Control Department of Obayashi Corporation Technical Research Institute. Their generous support and encouragement is gratefully acknowledged.

I would also like to address my gratitude to my former bosses of Obayashi Corporation Technical Research Institute, Dr. Toshikazu Takeda, Dr. Tetsuo Suzuki, and Dr. Yuzuru Yasui for having encouraged me to study in the United States.

I would like to thank Mr. Akira Teramura, a former manager of Obayashi Corporation Technical Research Institute, for taking care of the jobs I have left behind while I have been studying at Washington University.

I would also like to thank Dr. Mitsuru Nakamura, a senior research engineer of Obayashi Corporation Technical Research Institute, for giving me valuable advice as a pioneer who have experienced studying in the United States. I have always been encouraged and motivated by him.

I would also like to thank Mr. Kazutaka Shirai, a research engineer of Obayashi Corporation Technical Research Institute, for helping me with the analytical model of the full scale 9-story building studied in the chapter 6.

Finally, I would like to say thank you to my family, my wife Kaoru, my daughter Mayu, and my son Yusei for sharing wonderful days in St. Louis with me.

Chapter 1

Introduction

Recently, several sizeable earthquakes have caused severe damage in civil structures all over the world, including Northridge, California (1994), Kobe, Japan (1995), Kocaeli, Turkey (1999), Chi-Chi, Taiwan (1999), and Bhuj, India (2001). To protect civil structures from significant damage, the response reduction of civil structures under such severe earthquakes has become an important topic in structural engineering.

During the last three decades, significant efforts have been made to apply modern control technology to civil structures for enhancing structural safety against natural hazards. Various types of passive and active control systems have been developed and experimentally verified. A number of them have been implemented in full scale civil structures [48]. Passive systems are well understood and widely accepted, but they are limited in their ability to adapt to changes in the structure or environmental loading. Active systems can adapt their performance to different loading conditions and can be implemented in different structures, but their ability to input mechanical energy into the structural system raises concerns about stability. Semiactive systems have a promising future for control technology applied to civil structures, because they combine the adaptability of active system and reliability of passive systems.

One semiactive device that appears to be particularly promising is the magnetorheological (MR) damper. Recently developed MR fluids appear to be attractive for use in controllable fluid dampers [5,7]. When magnetic field is applied to the fluid, MR fluid

becomes a semi-solid and exhibits visco-plastic behavior. MR fluid can operate at temperatures from -40 to 150°C with only slight variations in the yield stress. Moreover, MR fluids are not sensitive to impurities and can be readily controlled with a low voltage (*e.g.*, ~12-24V), current-driven power supply outputting only ~1-2 Amps. MR fluid technology appears to be scalable to the size required for seismic control applications. In fact, 200kN MR dampers have been constructed and tested [6,22,44,45,50]. Since semiactive devices are intrinsically nonlinear, nonlinear control algorithms which explicitly incorporate the model of MR damper have been developed to effectively use the unique characteristics of this device, and their performance has been verified both numerically and experimentally.

One important issue in seismic response control which has not been studied to a large extent, is torsionally coupled response control in asymmetric structures. If a structure has an asymmetric distribution of either mass or stiffness, a lateral seismic load can cause a response in which the torsional and lateral motions of the structure are coupled. This may cause larger responses than in a symmetric structure, resulting in severe structural damage. As a practical example, a building which had been moderately damaged during the Kocaeli Earthquake (Turkey, August 17, 1999) and had been repaired only at one corner of the structure, was subjected to the Duzce Earthquake (Turkey, November 12, 1999). As a result, the structure was severely damaged due to the torsional irregularity created by the partial strengthening of the structure [54]. One promising approach for retrofit or new construction such cases is the implementation of control systems designed to be effective for such systems.

This dissertation focuses on the development and validation of control systems that can effectively reduce the seismic responses due to such torsional coupling in asymmetric building structures. Due to their attractive characteristics for seismic response control, semiactive control systems are specifically examined in the numerical and experimental studies.

In the remainder of this chapter previous research including torsional response and control of asymmetric structures, various semiactive control systems, and semiactive control using MR dampers, is summarized. An overview of the dissertation follows.

1.1 Literature Review

1.1.1 Torsional Responses of Asymmetric Structures

Although torsional responses are an important consideration in the design of an irregular building, little research is available to examine issues regarding the response of such structures. Kan and Chopra [28] have studied the elastic earthquake responses of a torsionally-coupled single story building using response spectrum analysis. It was concluded that the maximum base shear in a torsionally-coupled system is smaller than in the corresponding uncoupled (symmetric) system, while the torque generally increases with the eccentricity between the center of resistance and the center of mass. It is also concluded that this effect depends strongly on the ratio of the natural frequencies of the torsional and lateral motions of the corresponding uncoupled system.

Ferhi and Truman [19,20] studied inelastic behavior of an asymmetric single story building under monotonic loads. In these studies, asymmetric building systems were classified into three groups according to the ratio between the stiffness eccentricity and strength eccentricity, and the behavior of each group was summarized. They concluded that the elastic deformations are dependent primarily on the stiffness eccentricity (not strength eccentricity), while the inelastic deformations are strongly dependent on both stiffness and strength eccentricities.

1.1.2 Torsional Response Control of Asymmetric Buildings

Torsional responses in buildings may be induced by wind loads even if the structure is symmetric. This effect becomes more critical when the building is taller, and initial work

FIGURE 1-1. Kyobashi Seiwa Building.

FIGURE 1-2. Riverside Sumida Building.

in torsional response control focused on this issue. The Kyobashi Seiwa building (Figure 1-1), the first full-scale application of active control to a building in the world, employs an Active Mass Damper (AMD) system to reduce torsional motions [41]. Also, the Riverside Sumida building (Figure 1-2) is equipped with a set of AMDs to reduce the first three translational modes of the building as well as the first torsional mode [53]. Another example in the United States is the John Hancock Tower in Boston, where tunes mass dampers have been installed to reduce the torsional responses caused by wind loads as well as translational responses (Engineering News Record, Oct. 1975).

Fewer researchers have examined seismic response control for such irregular structures. Singh et al. [42] examined the use of tuned mass dampers (TMD) to control torsional responses due to seismic excitations. In this study, four TMDs are applied to control the torsional responses of a multi-story building. Optimal controller designs were obtained using genetic algorithms. Chi et al. [8] studied the performance of passive, active and semiactive control of a base isolated, four story building with a setback on the third floor. The focus of this study was to develop a smart isolation system to reduce the

motion of the structure. Gavin et al. [23] have also examined a base-isolated, L-shaped, eight story building, considering the effects of yield force, yield displacement, natural period and damping of the isolation devices. This building is also the subject of a benchmark control problem for smart base isolation systems [34].

1.1.3 Semiactive Control Systems

Semiactive devices have been shown to possess the advantages of active control devices without requiring the associated large power sources, and are inherently stable [21,47]. For these reasons, they have a promising future in structural control. If the power fails, a semi-active device behaves like a passive device. The inherently stable nature of these devices makes it possible to implement high authority control strategies, which can result in better performance than comparable active systems. Preliminary analytical and experimental studies indicate that appropriately implemented semiactive systems perform significantly better than passive devices [10,11,39,40] and have the potential to achieve or even surpass the performance of fully active systems [12].

Various types of semiactive devices have been proposed for structural control applications. One type of such devices utilizes forces generated by surface friction to dissipate vibratory energy in a structural system. Akbay and Aktan [2] examined the effect of an energy dissipation device which consists of a friction shaft which is rigidly connected to the structural bracing of a structure. Another means of achieving a variable-damping device is to use a controllable, electromechanical, variable-orifice valve to alter the resistance to flow of a conventional hydraulic fluid damper. The concept of applying this type of semiactive device to control the motion of bridges experiencing seismic motion was discussed by Feng and Shinozuka [18] and Kawashima et al. [29]. Sack and Patten [39] conducted experiments in which a hydraulic actuator with a controllable orifice was implemented in a single-lane model bridge to dissipate the energy induced by vehicle traffic. They also conducted a full-scale experiment on a bridge on interstate highway I-

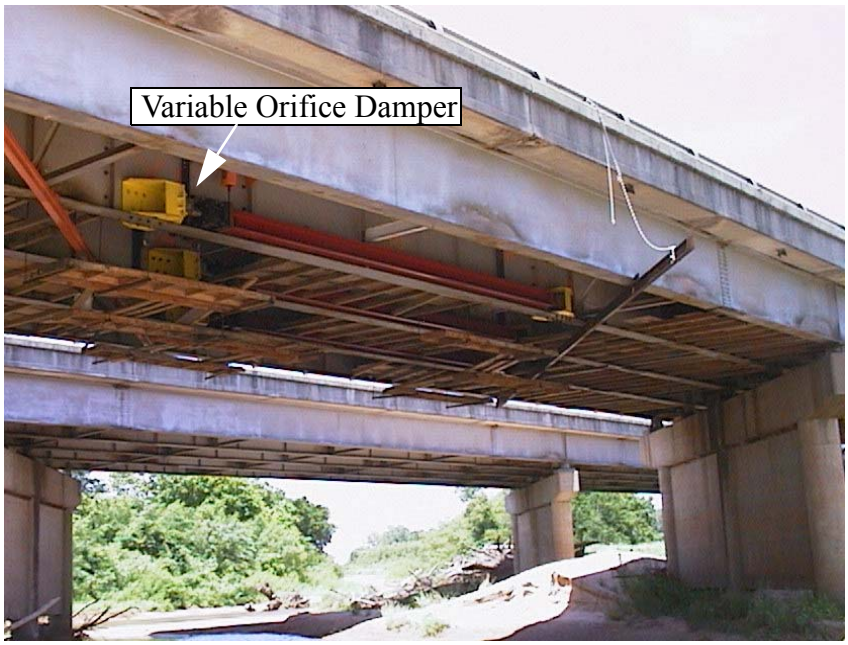

FIGURE 1-3. Bridge on Interstate Highway I-35 in Oklahoma.

35 in Oklahoma (Figure 1-3) to demonstrate this technology. This experiment constitutes the first full-scale implementation of structural control in the United-States. A similar device has also been studied by Constantinou and Symans [9].

Another very promising class of semiactive devices uses controllable fluids, including electrorheological (ER) fluid and magnetorheological (MR) fluids. These devices contain no moving parts except the piston, which makes them very reliable. Initial research on ER fluid was performed by Klass and Martinek [30,31]. The application of ER devices in civil structures has been considered by Ehrgott and Masri [16], by Burton et al. [4] and Makris et al. [33], and by Gavin et al. [24]. Control systems based on MR fluids and devices have attracted a great deal of attention from the civil engineering community. Prior research on MR fluid devices will be discussed in the following section.

1.1.4 Semiactive Control Using Magnetorheological (MR) Dampers

MR dampers have demonstrated a great deal of promise for civil engineering applications in both analytical and experimental studies. Spencer et al. [49] developed a phenomenological model for an MR damper based on the Bouc-Wen hysteresis model [55]. This model was subsequently used to demonstrate the capabilities of MR dampers [12,13]. Further, Dyke, et al. [14] and Yi et al. [61] performed experimental verification of the use of MR dampers for the control of civil engineering structures. Jansen and Dyke conducted studies to consider a variety of nonlinear control algorithms to examine their efficacy with MR devices [26]. Various phenomenological models have been developed for MR dampers of different designs [56,57,60,61]. In the last few years, 200kN MR dampers have been constructed and tested [6,22,44,45,50]. In addition to demonstrating the scalability of MR devices to full scale, these devices are now commercially available for implementation in civil engineering structures.

Various semiactive control algorithms have been evaluated for use with MR dampers in numerical studies [11,26]. The results of these studies demonstrated that the performance of the controlled system is highly dependent on the choice of algorithm. So, one challenge in the use of semiactive technology is in developing nonlinear control algorithms that are appropriate for implementation in full-scale structures. In previous studies, the clipped-optimal control algorithm has been effective for use with the MR damper [26,60,61].

1.2 Overview of the Dissertation

This dissertation focuses on the development and validation of control systems that can effectively reduce the seismic responses due to torsional coupling in asymmetric buildings. Both numerical and experimental studies are performed to verify the application of semiactive control systems, specifically those using MR devices, to this problem.

Chapter 2 provides the background information for this research, describing modeling and control using MR dampers. Adequate modeling of the control devices is essential for predicting the behavior of the controlled system, and the MR damper is modeled using a Bouc-Wen hysteresis model in this research. Additionally, in controlling MR dampers, the desired control force cannot be commanded directly because the control forces generated by MR dampers are dependent on the structure's local responses where the devices are installed, and the Bouc-Wen model used for the device is not invertible. Only the voltage applied to the MR dampers can be controlled to induce the MR device to apply the desired force. Thus, a clipped-optimal control and a modified version of this algorithm are proposed in this chapter for use with the MR damper. The H_2/LQG (Linear Quadratic Gaussian) strategy is advocated as a nominal linear controller for clipped-optimal control.

In chapter 3, the proposed semiactive control systems using MR dampers are applied to a full scale building model to verify the effectiveness of the control systems. The full scale building used in this study is the 20-story building model developed for the benchmark control problem for seismically-excited, nonlinear buildings [36,37]. The responses of the building examined include the maximum and normed interstory drift ratio, maximum and normed acceleration, and required control forces. These are evaluated for ten earthquake excitations. The results of the proposed control systems using MR dampers are compared to active and ideal semiactive system.

Chapter 4 discusses the basic dynamics of torsional responses in an asymmetric building. Parametric studies are conducted to examine important responses including base shear and torque. The eccentricity ratio and the uncoupled natural frequency ratio between the translational and torsional modes are used as the parameters. Further, practical cases are studied to examine deformation and acceleration responses for a simple structural model similar to the experimental model used in laboratory tests. As a preliminary control study, a passive control system using viscous dampers and active control

systems based on an LQG algorithm are applied to this simple asymmetric building. Ideal devices are used in both cases. Studies are also conducted for the multiple story asymmetric building.

In Chapter 5, the performance of the proposed method is studied experimentally using a 2-story building model with an asymmetric stiffness distribution. An automated system identification methodology is developed and implemented to obtain a control-oriented model of the experimental system. The parameters of the MR damper model are identified using experimental data to develop an integrated model of the structure and MR dampers. To demonstrate the performance of this control system on the experimental structure, a shake table is used to reproduce an El Centro 1940 N-S earthquake as well as a broadband random excitation. The responses for the proposed control system are compared to those of passive control cases in which a constant voltage is applied to the MR damper.

Chapter 6 addresses the performance of the proposed control system when applied to numerical models of full scale asymmetric buildings. Two cases are studied. One of them is a 9-story building with an asymmetric structural plan due to the distribution of shear walls. The other is an L-shaped, 8-story building with additional vertical irregularity due to setbacks. A device placement scheme using genetic algorithms (GA) is used to place them effectively. The responses due to the El Centro 1940 and the Kobe 1995 earthquake excitations are evaluated for the proposed semiactive control system using MR dampers. These results are compared to those of ideal active control systems and to passive control systems in which constant voltages are applied to MR dampers. A two dimensional earthquake input is considered in the second case.

Chapter 7 summarizes the conclusions of this dissertation and discusses some topics for future work.

Chapter 2

Background

This chapter provides background material for the dissertation, including models and algorithms used in semiactive control systems with MR dampers. Adequate modeling of the control devices is essential for predicting the behavior of the controlled system. Here, the MR damper is modeled using a Bouc-Wen hysteresis model. In controlling an MR damper, the desired control force cannot be directly commanded because the control force generated by the device is dependent on the local responses of the structure where it is installed. Only the voltage applied to the MR damper can be controlled. In this chapter the model of the device, and the semiactive control algorithm used with the device, the clipped-optimal control algorithm, are discussed. A modified version of this algorithm is also proposed in this chapter.

2.1 Mechanical Model of MR damper

The semiactive control device used in this study is the MR damper. The MR dampers have demonstrated a great deal of promise for civil engineering applications in both analytical and experimental studies. Adequate modeling of the control devices is essential for predicting the behavior of the controlled system. The simple mechanical model shown in Figure 2-1 was developed and shown to accurately predict the behavior of a prototype shear-mode MR damper over a wide range of inputs in a set of experiments [15,26,60,61]. This model has also been successfully used to model the behavior of a scaled-up version of the MR damper [56,57].

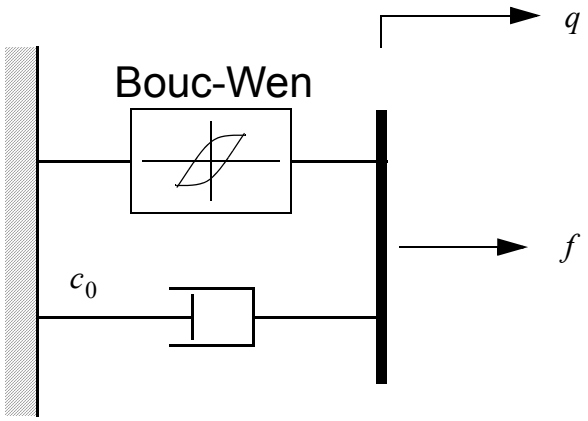

FIGURE 2-1. Mechanical Model of the MR Damper.

The equations governing the force f produced by this device model are

$$f = c_0\dot{q} + \alpha z \qquad \dot{z} = -\gamma|\dot{q}|z|z|^{n-1} - \beta\dot{q}|z|^n + A\dot{q} \tag{2-1}$$

where q is the displacement of the device, and z is the evolutionary variable that accounts for the history dependence of the response. By adjusting the parameters of the model γ, β, n, and A, one can control the linearity in the unloading and the smoothness of the transition from the preyield to the postyield region. The functional dependence of the device parameters on the command input u is modeled as

$$\alpha = \alpha(u) = \alpha_a + \alpha_b u \qquad c_0 = c_0(u) = c_{0a} + c_{0b}u \quad . \tag{2-2}$$

In addition, the current driver circuit of the MR damper introduces dynamics into the system. These dynamics are typically considered to be a first order time lag in the response of the device to changes in the command input. These dynamics are accounted for with the first order filter on the control input given by

$$\dot{u} = -\eta(u - v) \tag{2-3}$$

where v is the command voltage applied to the control circuit.

2.2 Semiactive Control Algorithm

Consider a seismically excited structure controlled with n MR dampers. Thus, the equations of motion can be written as

$$\mathbf{M}_s\ddot{\mathbf{x}} + \mathbf{C}_s\dot{\mathbf{x}} + \mathbf{K}_s\mathbf{x} = \Lambda\mathbf{f} - \mathbf{M}_s\Gamma\ddot{x}_g \tag{2-4}$$

where $\mathbf{M}_s$, $\mathbf{C}_s$, and $\mathbf{K}_s$ are the mass, damping and stiffness matrices of the building, $\mathbf{x}$ is a vector of the relative displacements of the floors of the structure, $\ddot{x}_g$ is a one-dimensional ground acceleration, $\mathbf{f} = \left[f_1\, f_2\, \ldots f_n\right]^T$ is the vector of control forces, defined by Eqs. (2-1) through (2-3), generated by the n MR dampers, Γ is a column vector of ones, and Λ is a vector determined by the placement of the MR dampers in the structure. This equation can be written in state-space form as

$$\dot{\mathbf{z}} = \mathbf{A}\mathbf{z} + \mathbf{B}\mathbf{f} + \mathbf{E}\ddot{x}_g \tag{2-5}$$

$$\mathbf{y}_r = \mathbf{C}_r\mathbf{z} + \mathbf{D}_r\mathbf{f} + \mathbf{F}_r\ddot{x}_g \tag{2-6}$$

$$\mathbf{y}_m = \mathbf{C}_m\mathbf{z} + \mathbf{D}_m\mathbf{f} + \mathbf{F}_m\ddot{x}_g + \mathbf{v}_m \tag{2-7}$$

where $\mathbf{A}$, $\mathbf{B}$, $\mathbf{E}$, $\mathbf{C}_r$, $\mathbf{D}_r$, $\mathbf{F}_r$, $\mathbf{C}_m$, $\mathbf{D}_m$, and $\mathbf{F}_m$ are the state-space matrices, $\mathbf{z}$ is the state vector, and $\mathbf{y}_r$ is the vector of regulated responses, $\mathbf{y}_m$ is the vector of measured outputs, and $\mathbf{v}_m$ is the measurement noise vector. For these applications, the

measurements typically available for control force determination include the absolute acceleration of selected points on the structure, the displacement of each control device, and a measurement of each control force.

2.2.1 Clipped-Optimal Control

Dyke et al. [12,13] proposed a clipped-optimal control strategy based on acceleration feedback for controlling a single MR damper. Dyke and Spencer [10] extended the control algorithm to control multiple MR devices, and Yi et al. [60,61] experimentally verified the performance of this algorithm. This control algorithm is selected as one candidate semiactive control algorithm for this research, and is summarized herein.

In the clipped-optimal control algorithm, the approach is to append *n* force feedback loops to induce each MR damper to produce approximately a desired control force. The desired control force of the *i*th MR damper is denoted f_{ci} . A linear optimal controller $\mathbf{K}_c(s)$ is designed that calculates a vector containing the desired control forces, $\mathbf{f}_c = \left[f_{c1}\, f_{c2}\, \ldots\, f_{cn}\right]^T$, based on the measured structural response vector $\mathbf{y}_m$ and the measured control force vector $\mathbf{f}_m$, *i.e.*,

$$\mathbf{f}_c = L^{-1}\left\{-\mathbf{K}_c(s)L\left\{\begin{matrix}\mathbf{y}_m\\ \mathbf{f}_m\end{matrix}\right\}\right\} \tag{2-8}$$

where $L\{\cdot\}$ is the Laplace transform. Although the controller $\mathbf{K}_c(s)$ can be obtained from a variety of synthesis methods, H_2/LQG (Linear Quadratic Gaussian) strategies are advocated herein because of the stochastic nature of earthquake ground motions and because of their successful application in other civil engineering structural control applications [12,13,14,60,61].

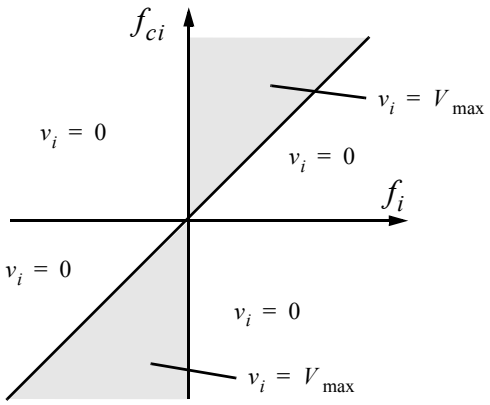

FIGURE 2-2. Graphical Representation of Clipped-Optimal Control Algorithm.

Because the force generated in the MR damper is dependent on the local responses of the structural system, the desired optimal control force f_{ci} cannot always be produced by the MR damper. Only the control voltage v_i can be directly controlled to increase or decrease the force produced by the device. Thus, a force feedback loop is incorporated to induce the MR damper to generate approximately the desired optimal control force f_{ci} .

To induce the MR damper to generate approximately the desired optimal control force, the command signal is selected as follows. When the *i*th MR damper is providing the desired optimal force (*i.e.*, $f_i = f_{ci}$), the voltage applied to the damper should remain at the present level. If the magnitude of the force produced by the damper is smaller than the magnitude of the desired optimal force and the two forces have the same sign, the voltage applied to the current driver is increased to the maximum level so as to increase the force produced by the damper to track the desired control force. Otherwise, the commanded voltage is set to zero. The algorithm for selecting the command signal for the *i*th MR damper is graphically represented in Figure 2-2 and can be stated as

$$v_i = V_{\max} H(\{f_{ci} - f_i\} f_i) \tag{2-9}$$

where $V_{\max}$ is the maximum voltage to the current driver, and $H(\cdot)$ is the Heaviside step function.

2.2.2 Modified Clipped-Optimal Control

In the original clipped-optimal control algorithm, the command voltage takes on values of either zero or the maximum value. In some situations when the dominant frequencies of the system under control are low, large changes in the forces applied to the structure may result in high local acceleration values. This behavior is dependent on the time lag in the generation of the control voltage modeled by Eq. (2-3). Here a modification to the original clipped-optimal control algorithm is proposed to reduce this effect, resulting in another candidate control design.

In the modified version of the control algorithm, the control voltage can be any value between 0 and $V_{\max}$. The control voltage, denoted V_{ci}, is determined using a linear relationship between the applied voltage and the maximum force of MR damper. When

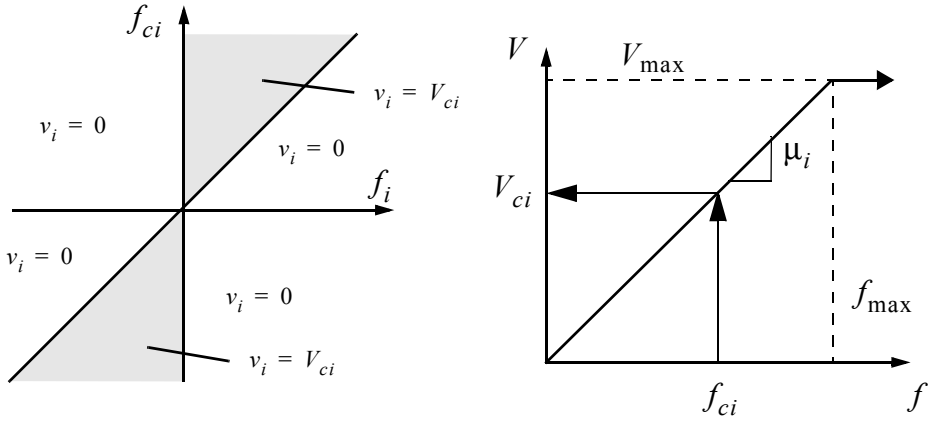

FIGURE 2-3. Graphical Representation of the Modified Clipped-Optimal Control Algorithm.

the desired force is larger than the maximum force that the device can produce, the maximum voltage $V_{\max}$ is applied. This modified clipped-optimal control algorithm is graphically represented in Figure 2-3 and can be given as

$$v_i = V_{ci} H(\{f_{ci} - f_i\} f_i) \tag{2-10}$$

where

$$V_{ci} = \begin{cases} \mu_i f_{ci} & \text{for } f_{ci} \le f_{\max} \\ V_{\max} & \text{for } f_{ci} > f_{\max} \end{cases} \tag{2-11}$$

and where $f_{\max}$ is the maximum force produced by the control device and μ_i is the coefficient relating the voltage to the force.

2.3 Nominal Controller

Both of the clipped-optimal control algorithms presented above are based on a nominal controller design. An effective nominal control design is important for obtaining good controlled performance in the semiactive system. Here an H_2/LQG control algorithm is employed for the nominal controller.

In the design of the H_2/LQG controller, the ground acceleration input, $\ddot{x}_g$, is taken to be a stationary white noise, and an infinite horizon performance index is chosen as

$$J = \lim_{\tau \to \infty} \frac{1}{\tau} E\left[\int_0^{\tau} \{(\mathbf{C}_r \mathbf{z} + \mathbf{D}_r \mathbf{f})^T \mathbf{Q} (\mathbf{C}_r \mathbf{z} + \mathbf{D}_r \mathbf{f}) + \mathbf{f}^T \mathbf{R} \mathbf{f}\} dt \right] \tag{2-12}$$

where $\mathbf{Q}$ and $\mathbf{R}$ are weighting matrices for the vectors of regulated responses and of control forces, respectively. For design purposes, the measurement noise vector, $\mathbf{v}_m$, is assumed to contain identically-distributed, statistically-independent Gaussian white noise processes, with $S_{\ddot{x}_g\ddot{x}_g} / S_{v_{mi}v_{mi}} = \gamma_g = 25$.

The nominal controller is represented as

$$\dot{\hat{\mathbf{z}}} = (\mathbf{A}_r - \mathbf{L}\mathbf{C}_r)\hat{\mathbf{z}} + \mathbf{L}\mathbf{y}_m + (\mathbf{B}_r - \mathbf{L}\mathbf{D}_r)\mathbf{f}_m \tag{2-13}$$

$$\mathbf{f}_c = -\mathbf{K}\hat{\mathbf{z}} \tag{2-14}$$

where $\mathbf{L}$ is the gain matrix for state estimator and $\mathbf{K}$ is the gain matrix for Linear Quadratic Regulator, and $\mathbf{f}_m$ is the vector of measured control forces. For more information on the determination of these gain matrices, see [14] or [61]. As described in the previous section, the control force determined using this algorithm is compared to the measured control force, and, using either Eq. (2-9) or (2-10), the appropriate control voltage is applied to the control devices.

Note that in the case of ideal active control, the applied (measured) control force $\mathbf{f}_m$ is equal to the desired control force $\mathbf{f}_c$. Thus Eq. (2-13) can be rewritten as

$$\dot{\hat{\mathbf{z}}} = (\mathbf{A}_r - \mathbf{B}_r\mathbf{K} - \mathbf{L}\mathbf{C}_r + \mathbf{L}\mathbf{D}_r\mathbf{K})\hat{\mathbf{z}} + \mathbf{L}\mathbf{y}_m, \tag{2-15}$$

and force feedback is not required to implement this algorithm. However, in the case of semiactive control, Eq. (2-13) is needed as the measured force $\mathbf{f}_m$ is not always equal to the desired control force $\mathbf{f}_c$, and feedback of measured force is needed.

2.4 Summary

In this chapter the model of MR device and two candidate control algorithms were presented for the semiactive control system. The linear control design used as the nominal controller for the clipped optimal designs has been presented. These will be used in subsequent chapters to design and validate the performance of the semiactive controllers.

Chapter 3

Full Scale Verification of Semiactive Control

In this chapter, the proposed semiactive control system using MR dampers is applied to a model of a full scale building to verify its effectiveness. The model used in this study is the full scale 20-story building model developed for the benchmark control problem for seismically-excited nonlinear buildings [36,37]. The responses of the building, including the maximum and normed interstory drift ratio, maximum and normed acceleration, required control forces, are evaluated due to various earthquake excitations. The results of the proposed control system are compared to active and ideal semiactive systems [62].

3.1 Benchmark Problems

Benchmark problems provide a means of directly comparing various control strategies on a representative problem. The first benchmark problem in seismic response control dealt with two laboratory scale structures equipped with an active control devices [51]. Two second generation benchmark problems were developed to study a wider variety of issues in structural control of buildings. One of them was developed to address issues related to the control of a building excited by wind loads [58], and the second problem was developed to further examine the seismic control problem [52]. Subsequently these problems evolved into third generation benchmark problems [36,37,59]. The wind control problem was enhanced with more realistic models of the wind loading, and the

seismic benchmark was modified to consider nonlinear behavior of structures. This third generation (nonlinear) seismic benchmark problem is the subject of this study.

3.2 Nonlinear Benchmark Building

The benchmark building considered herein is the 20-story benchmark building specified in the benchmark problem statement [36,37]. The structure used for this benchmark study was designed by Brandow & Johnston Associates for the SAC Phase II Steel Project to represent a typical high-rise building designed for the Los Angeles, California region. SAC is a joint venture of three non-profit organizations: The Structural Engineers Association of California (SEAOC), the Applied Technology Council (ATC) and Consortium of Universities for Research in Earthquake Engineering (CUREE). Although not actually constructed, this structure was designed to meet seismic code. The structure is 30.48 m (100 ft) by 36.58 m (120 ft) in plan, and 80.77 m (265 ft) in elevation. The bays are 6.10 m (20 ft) on center, in both directions, with five bays in the north-south (N-S) direction and six bays in the east-west (E-W) direction.

The building's lateral load resisting system is comprised of steel perimeter moment-resisting frames (MRFs). This benchmark study focuses on an in-plane (2-D) analysis of the benchmark structures. The frames considered in the development of the evaluation models are the N-S MRFs (the short, or weak, direction of the buildings) and control devices can be implemented throughout these N-S frames of the structure. The damping matrix is determined based on an assumption of Rayleigh damping. The first ten natural frequencies of the 20-story benchmark building model are: 0.261, 0.753, 1.30, 1.83, 2.40, 2.44, 2.92, 3.01, 3.63 and 3.68 Hz.

Structural member nonlinearities are included to capture the inelastic behavior of the building during strong earthquakes. The beams and columns of the structure are modeled as plane-frame elements, and mass and stiffness matrices for the structure are

determined. A bilinear hysteresis model is used to characterize the nonlinear bending stiffness of the structural members [36,37].

3.3 Control System Design

Four control systems have been designed and applied to the numerical model of the benchmark structure, and the approach adopted to design these controllers is described in this section. The control action is based primarily on acceleration feedback, but also uses measurements of the control forces applied to the structure in determining the control action. MR dampers are applied as the control devices. Each control device is oriented horizontally, and is rigidly attached between the two adjacent floors of the building. The phenomenological model of the MR damper discussed in chapter 2 is employed in the numerical simulations. The control input is determined by application of two types of clipped-optimal controllers. The various components of the control systems (*i.e.*, sensors, control devices) and design of nominal controller are described in this section.

3.3.1 Sensors

Because accelerometers can readily provide reliable and inexpensive measurements of the absolute accelerations of arbitrary points on a structure, the control system used in this study is based primarily on acceleration feedback. Additionally, the clipped-optimal control algorithm, described subsequently, requires measurement of each of the control forces applied to the structure. Thus, one force transducer is used to measure each unique force.

Because accelerometers and force transducers are readily available with a natural frequency that is at least an order of magnitude above the dominant dynamics of this benchmark structure, each sensor is modeled as having a constant magnitude and phase.

The sensitivity of each accelerometer is s_a = 10 V/g = 10 V/9.81 m/sec^2. The sensitivity of each force transducer is s_f = 10 V/1000 kN. Thus, in state space form, the sensor model can be written as

$$\dot{\mathbf{x}}^{\mathrm{s}} = \mathbf{0}, \qquad \mathbf{y}^{\mathrm{s}} = \mathbf{D}_{\mathrm{s}} \begin{bmatrix} \mathbf{y}_m \\ \mathbf{f}_m \end{bmatrix} \tag{3-1}$$

where $\mathbf{x}^{\mathrm{s}}$ is the state vector of the sensor model, $\mathbf{y}^{\mathrm{s}}$ is the output of the sensor model, and $\mathbf{D}_{\mathrm{s}} = \begin{bmatrix} s_a\mathbf{I} & \mathbf{0} \\ \mathbf{0} & s_f\mathbf{I} \end{bmatrix}$.

Five absolute acceleration measurements were identified as measured outputs: on levels 4, 8, 12, 16, and 20. The vector of measured responses is $\mathbf{y}_m = \begin{bmatrix} \ddot{x}_{a4} & \ddot{x}_{a8} & \ddot{x}_{a12} & \ddot{x}_{a16} & \ddot{x}_{a20} \end{bmatrix}^T$. The vector of measurements for each of the control forces applied to the structure is $\mathbf{f}_m = \begin{bmatrix} f_{m1} & f_{m2} & \cdots & f_{mn} \end{bmatrix}^T$. As specified in the benchmark problem statement [36,37], each of these measured responses are assumed to contains an RMS noise of 0.03 Volts, which are modeled as Gaussian rectangular pulse processes with a pulse width of 0.01 sec.

3.3.2 Control Devices

The mechanical modeling of the MR damper is described in the previous chapter. The parameters of the MR damper were selected so that the device has a capacity of 1000 kN, as follows: α_a = 1.0872e5 N/cm, α_b = 4.9616e5 N/(cm·V), c_{0a} = 4.40 N·sec/cm, c_{0b} = 44.0 N sec/(cm·V),n = 1, A = 1.2, γ = 3 cm^{-1}, β = 3 cm^{-1},

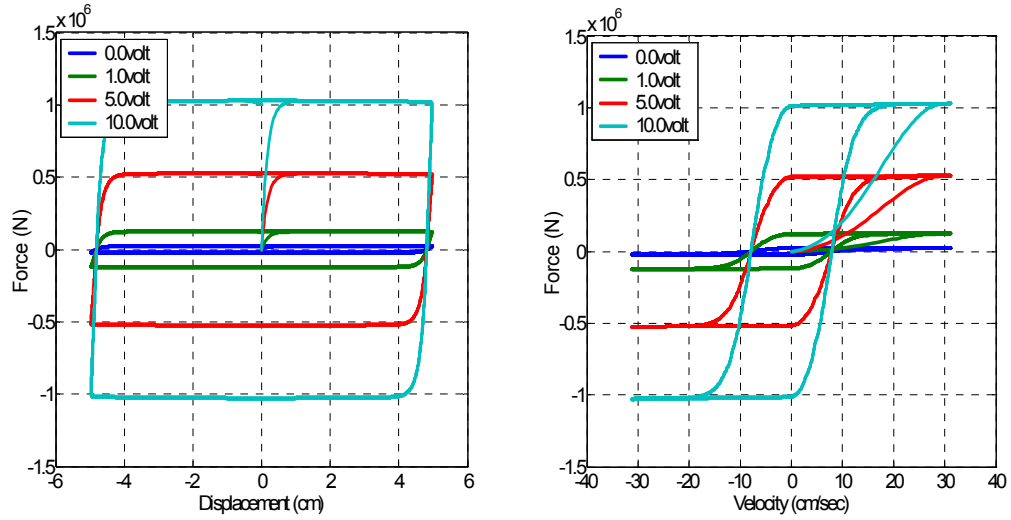

(a) Force-Displacement Hysteresis Loop **(b) Force-Velocity Hysteresis Loop**

FIGURE 3-1. Typical Responses of Employed MR Damper.

and η = 50 sec^{-1}. These parameters are based on the identified model of a shear-mode prototype MR damper tested at Washington University [60,61] and scaled up to have maximum capacity of 1000 kN with maximum command voltage V_{max} = 10 V. According to the device manufacturer's expectations, the device described here is assumed to require a maximum power of 50 Watts.

Typical force-displacement and force-velocity hysteresis loops for this device model are shown in Figure 3-1. Here the device response is shown for various constant voltages applied to the control input to the MR damper, and a 1.0 Hz sinusoidal displacement with an amplitude of 5 cm. Note that this device has a dynamic range of 50.

3.3.3 Design of the Nominal Controller

In this benchmark study, two types of semiactive control algorithms, original and modified clipped-optimal control, are used for controlling MR dampers where an H_2/LQG

control algorithm is employed for the nominal controller. The controller is designed using the linear, reduced-order building model, which is provided with the benchmark files. This reduced order model has twenty states.

Parametric studies were performed with various weighting matrices $\mathbf{Q}$ corresponding to various regulated output vectors $\mathbf{y}_r$. During these parameter studies $\mathbf{R}$ remained as $\mathbf{R} = diag\left(\left[n_1{}^2 \; n_2{}^2 \; \ldots \; n_{20}{}^2\right]\right)$, where n_i is number of devices employed on *i*th floor, so as to have equal weighting on the forces of each floor. The parameter studies were performed using the linear, reduced-order building model provided with the benchmark problem statement. The model was subjected to the four earthquakes specified in the benchmark paper. Evaluation of the controllers focused on minimizing the interstory drifts and absolute accelerations.

The results of these parameter studies indicated that an effective controller could be designed by selecting a vector of regulated responses, $\mathbf{y}_r$, to include the velocities of each floor relative to the ground, *i.e.*, $\mathbf{y}_r = \left[\dot{\mathbf{x}}\right]^T$. These studies indicates that the weighting matrix for the regulated response should be selected as $\mathbf{Q} = q \cdot diag([\mathbf{1}_{1\times 20}])$, and $q = 10^{13}$.

The Northridge earthquake was used to determine the number of 1000 kN devices on each floor because it requires the largest control forces in the structure. In the proposed designs, four devices are located on the first eight stories, three devices are located on the next nine stories, and two devices are located on the top three stories. The total number of devices is 65.

As required in the benchmark statement paper [36,37], the digitally implemented controller has a sampling time of 0.01 seconds. The continuous-time controller described in Eqs. (2-13) and (2-14) is approximated as a discrete-time controller using the bilinear transformation [3]. The AD and DA converters on this digital control implementation have 16-bit precision and a span of ± 10 Volts.

3.4 Benchmark Control Design Evaluation

To evaluate this control system, the seventeen evaluation criteria defined in the benchmark problem statement [36,37] are evaluated for each control design. Two additional criteria are proposed for this nonlinear benchmark design. All of the evaluation criteria are summarized in Table 3-1.

TABLE 3-1. Summary of Evaluation Criteria for the Nonlinear Benchmark Problem.

Building Responses

Interstory Drift Ratio

$$J_1 = \max_{\substack{\text{El Centro}\\\text{Hachinohe}\\\text{Northridge}\\\text{Kobe}}} \left\{ \frac{\max_{t,i} \dfrac{|d_i(t)|}{h_i}}{\delta^{\max}} \right\}$$

Floor Acceleration

$$J_2 = \max_{\substack{\text{El Centro}\\\text{Hachinohe}\\\text{Northridge}\\\text{Kobe}}} \left\{ \frac{\max_{t,i} |\ddot{x}_{a_i}(t)|}{\ddot{x}_a^{\max}} \right\}$$

Base Shear

$$J_3 = \max_{\substack{\text{El Centro}\\\text{Hachinohe}\\\text{Northridge}\\\text{Kobe}}} \left\{ \frac{\max_{t} \left| \sum_i m_i \ddot{x}_{a_i}(t) \right|}{F_b^{\max}} \right\}$$

Normed Interstory Drift Ratio

$$J_4 = \max_{\substack{\text{El Centro}\\\text{Hachinohe}\\\text{Northridge}\\\text{Kobe}}} \left\{ \frac{\max_{i} \dfrac{\|d_i(t)\|}{h_i}}{\|\delta^{\max}\|} \right\}$$

Normed Floor Acceleration

$$J_5 = \max_{\substack{\text{El Centro}\\\text{Hachinohe}\\\text{Northridge}\\\text{Kobe}}} \left\{ \frac{\max_{i} \|\ddot{x}_{a_i}(t)\|}{\|\ddot{x}_a^{\max}\|} \right\}$$

Normed Base Shear

$$J_6 = \max_{\substack{\text{El Centro}\\\text{Hachinohe}\\\text{Northridge}\\\text{Kobe}}} \left\{ \frac{\left\| \sum_i m_i \ddot{x}_{a_i}(t) \right\|}{\|F_b^{\max}\|} \right\}$$

Building Damage

Ductility

$$J_7 = \max_{\substack{\text{El Centro}\\\text{Hachinohe}\\\text{Northridge}\\\text{Kobe}}} \left\{ \frac{\max_{t,j} \dfrac{|\phi_j(t)|}{\phi_{yj}}}{\phi^{\max}} \right\}$$

Dissipated Energy

$$J_8 = \max_{\substack{\text{El Centro}\\\text{Hachinohe}\\\text{Northridge}\\\text{Kobe}}} \left\{ \frac{\max_{t,j} \dfrac{\int dE_j}{F_{yj} \cdot \phi_{yj}}}{E^{\max}} \right\}$$

Plastic Connections

$$J_9 = \max_{\substack{\text{El Centro}\\\text{Hachinohe}\\\text{Northridge}\\\text{Kobe}}} \left\{ \frac{N_d^C}{N_d} \right\}$$

Normed Ductility

$$J_{10} = \max_{\substack{\text{El Centro}\\\text{Hachinohe}\\\text{Northridge}\\\text{Kobe}}} \left\{ \frac{\max_{j} \dfrac{\|\phi_j(t)\|}{\phi_{yj}}}{\|\phi^{\max}\|} \right\}$$

Control Devices

Control Force

$$J_{11} = \max_{\substack{\text{El Centro}\\\text{Hachinohe}\\\text{Northridge}\\\text{Kobe}}} \left\{ \frac{\max_{t,l} |f_l(t)|}{W} \right\}$$

Control Device Stroke

$$J_{12} = \max_{\substack{\text{El Centro}\\\text{Hachinohe}\\\text{Northridge}\\\text{Kobe}}} \left\{ \frac{\max_{t,i} |y_i^a(t)|}{x^{\max}} \right\}$$

Control Power

$$J_{13} = \max_{\substack{\text{El Centro}\\\text{Hachinohe}\\\text{Northridge}\\\text{Kobe}}} \left\{ \frac{\max_{t} \left[\sum_l P_l(t) \right]}{\dot{x}^{\max} W} \right\}$$

Normed Control Power

$$J_{14} = \max_{\substack{\text{El Centro}\\\text{Hachinohe}\\\text{Northridge}\\\text{Kobe}}} \left\{ \frac{\sum_l \int_0^{t_f} P_l(t)}{\dot{x}^{\max} W} \right\}$$

Control Strategy

Control Devices

J_{15} = Number of control devices

Sensors

J_{16} = Number of required sensors

Computational Resources

$$J_{17} = dim(x_k^c)$$

Permanent Interstory Drift

Maximum Permanent Interstory Drift Ratio

$$P_1 = \max_{\substack{\text{El Centro}\\\text{Hachinohe}\\\text{Northridge}\\\text{Kobe}}} \left\{ \frac{\max_{i} \dfrac{|d_{pi}|}{h_i}}{\delta_p^{max}} \right\}$$

Total Permanent Interstory Drift Ratio

$$P_2 = \max_{\substack{\text{El Centro}\\\text{Hachinohe}\\\text{Northridge}\\\text{Kobe}}} \left\{ \frac{\sum_i \dfrac{|d_{pi}|}{h_i}}{\delta_p^{sum}} \right\}$$

3.4.1 Evaluation Criteria

The seventeen criteria are defined in detail in the benchmark problem statement paper and summarized here in Table 3-1. For the semi-active systems, the evaluation criteria describing the required maximum control power and normed control power, J_{13} and J_{14}, are calculated based on the actual power required by the devices. Here the instantaneous power required is determined by assuming that the maximum power required by each MR damper at the maximum voltage is 50 Watts, based on the expectation provided by the device manufacturer, and for lower instantaneous voltages, the power required is approximated by linearly relating it to the applied control voltage. For the ideal semiactive system, no specific type of device has been selected (*e.g.*, variable friction, variable orifice, etc.) and thus associating this device with a set power requirement is not possible. Thus, for purposes of this analysis, each ideal semiactive device in the control system is assumed to require 50 Watts at every time instant.

In addition to the seventeen evaluation criteria specified in the benchmark statement paper, two other criteria are considered to describe the performance of the controlled system. The two newly proposed criteria correspond to nondimensionalized values of the permanent interstory drift, which results from the formation of a plastic connection after severe earthquake. All nineteen criteria are to be evaluated for the four earthquakes at various magnitudes, for a total of ten cases.

The first newly proposed evaluation criterion, designated P_1, is a nondimensionalized measure of the maximum permanent interstory drift ratio, and is given by

$$P_1 = \max_{\substack{\text{El Centro}\\ \text{Hachinohe}\\ \text{Northridge}\\ \text{Kobe}}} \left\{ \frac{\max_i \dfrac{|d_{pi}|}{h_i}}{\delta_p^{max}} \right\} \tag{3-2}$$

where d_{pi} is the permanent interstory drift of the *i*th floor, h_i is the height of the *i*th floor, and δ_p^{max} is the maximum permanent interstory drift ratio of the uncontrolled structure calculated by $\max_i (|d_{pi}|/h_i)$. Note that the value of d_{pi} is determined as an average of the last t_p seconds of the response because there is a small fluctuation in the response over this time period. This value is calculated using

$$d_{pi} = \frac{1}{t_p}\int_{(t_f - t_p)}^{t_f} d_i dt \tag{3-3}$$

where t_f is final time of response time history data. Here, t_p is selected to be 10 seconds.

The second newly proposed evaluation criterion, designated P_2, is a nondimensionalized measure of the total permanent interstory drift ratio, and is given by

$$P_2 = \max_{\substack{\text{El Centro}\\ \text{Hachinohe}\\ \text{Northridge}\\ \text{Kobe}}} \left\{ \frac{\sum_i \frac{|d_{pi}|}{h_i}}{\delta_p^{sum}} \right\} \tag{3-4}$$

where δ_p^{sum} is the total permanent interstory drift ratio of the uncontrolled structure calculated by $\sum_i (|d_{pi}|/h_i)$. These evaluation criteria are also summarized in Table 3-1.

3.4.2 Active and Semiactive Control Systems

For purposes of comparison, an active control system and an ideal semiactive control system are also designed. For both cases, sensor location and device distribution are identical to those considered with the MR damper system.

In the active control system, ideal force actuators which have maximum capacity of 1000 kN are used. Ideal actuators are assumed to have ability to instantaneously and precisely supply the force commanded by the nominal control algorithm. Thus, the force provided by the *i*th active control devices is given by

$$f_i = f_{ci} \tag{3-5}$$

where *i*th command force f_{ci} are determined by Eqs. (2-14–2-15).

In the ideal semiactive control system, ideal semiactive devices having a maximum capacity of 1000 kN are used. Ideal semiactive devices are assumed to be purely dissipative devices. That is, these devices are capable of generating any control forces that are in the second and fourth quadrants of the force velocity plane. Thus the force provided by the *i*th semiactive devices is given by

$$f_i = \begin{cases} f_{ci} & \text{for } \dot{x}_{di} f_{ci} \le 0 \\ 0 & \text{Otherwise} \end{cases} \tag{3-6}$$

where *i*th command force f_{ci} are determined by Eqs. (2-13–2-14) and $\dot{x}_{di}$ is the relative velocity across the *i*th device. Note that in order to reduce the potential for high accelerations caused by switching on and off the actuators, lowpass filters, which are first order

filters with same characteristics as the MR damper dynamics, are applied to the ideal semiactive control force.

Note that when the ideal semiactive controller is used, the controller described in Eqs. (2-13 through 2-14) are applicable. These equations were developed based on an estimator that employs acceleration feedback as well as control force measurements.

The flow chart in Figure 3-2 provides a summary of the steps taken and equations used for each of the control designs considered.

3.5 Numerical Results

The proposed controllers are evaluated by considering the time histories of the controlled structure using the simulation code provided in the benchmark problem. This simulation employs the full model of the structural system, and includes member nonlinearities [36,37].

Two control designs are considered for the MR damper. The first controller, denoted OCO, is designed using the original clipped-optimal algorithm with $V_{\max}$ = 10 Volts [12–14,60,61]. The second controller, denoted MCO, is designed using the modified clipped-optimal control design algorithm with $V_{\max}$ = 10 Volts. To assess the controlled performance, the responses obtained with MR-based control systems are also compared to an active control system and an ideal semiactive control system. Ideally, it would be appropriate to compare active, ideal semi-active, and MR control systems with the same force requirements. Because multiple earthquake records are used for evaluation of the designs, this approach is not possible. Additionally, the time required to run the benchmark problem restricts the number of designs to be considered. Thus, active, ideal semiactive, and MR-based control systems that are based on the same nominal controller (the same control gains **K**) are compared. The ideal active and ideal

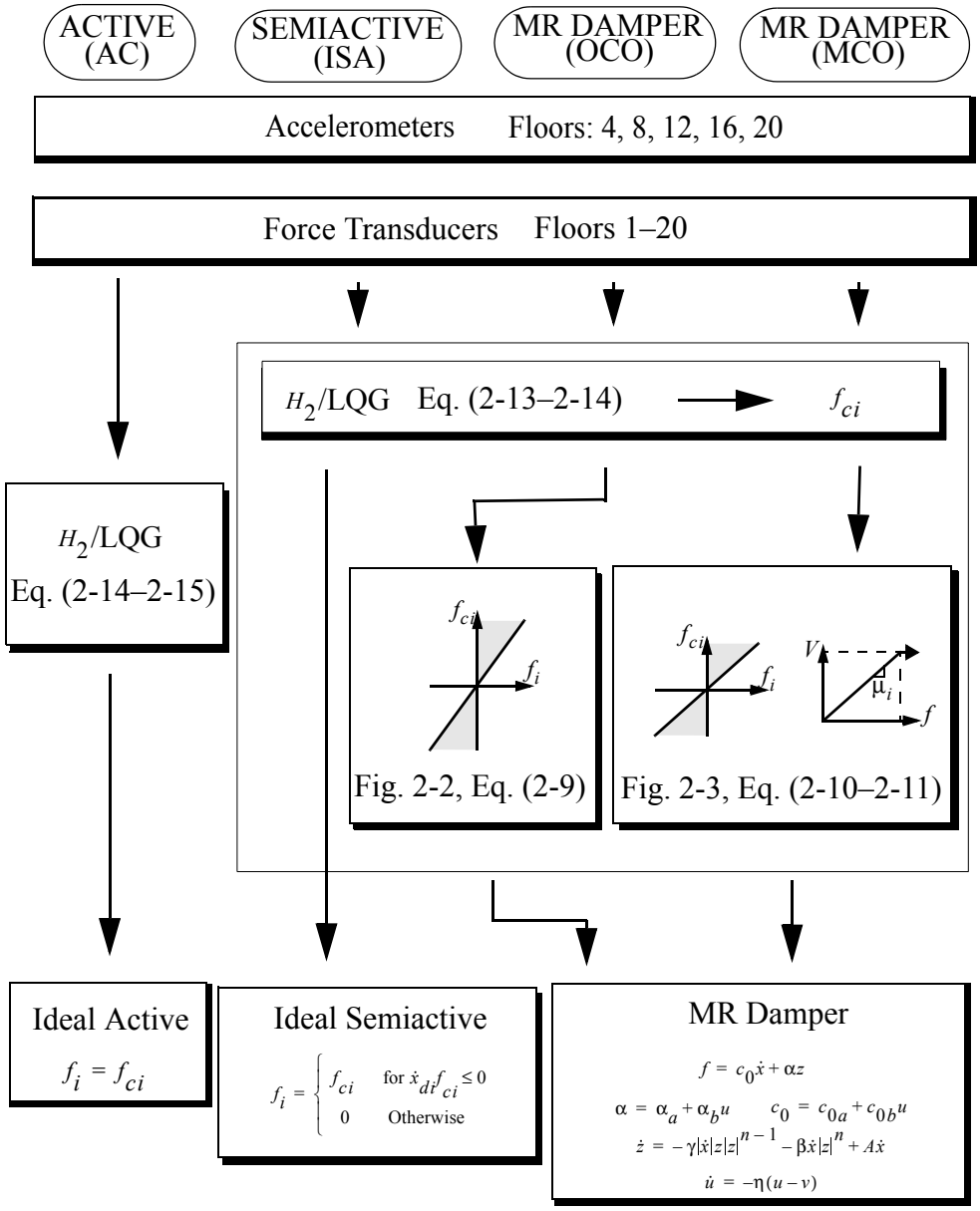

FIGURE 3-2. Description of the Various Controllers.

semiactive control system are denoted AC and ISA, respectively. Results are obtained using an integration step of 0.001 sec for the semiactive systems, and 0.01 sec for the active system. The smaller integration time step is required for the semiactive systems because of their nonlinear control algorithms and device models. However, the responses for the semiactive systems are decimated by 10 for determining the evaluation criteria so as to have the same time step as in the active system.

3.5.1 Time History Responses

Representative responses of the controlled systems (controller MCO) to the full-scale earthquakes (100% magnitude of the original earthquakes) are shown in Figure 3-3. Time histories are provided for the absolute acceleration of the 20th floor of the building and the interstory drift between the 19th and 20th floors. This response is selected because the maximum drift often occurs at the 20th floor. Maximum acceleration and maximum interstory drift ratio response profiles are provided for all floors of the building.

According to these time history results, the both peak acceleration and peak interstory drift are significantly reduced when an MR damper is used to control the structure. The response profiles show that peak story drifts are reduced at all floors. The maximum floor acceleration (among all floors) is always reduced in Figure 3-3, although in some cases the peak acceleration on a specific floor may increase.

In addition, it is obvious that in the case of severe earthquake such as full scale Northridge and Kobe, significant permanent drifts remain for uncontrolled building due to the development of plastic connections, which are suppressed with control using the MR damper.

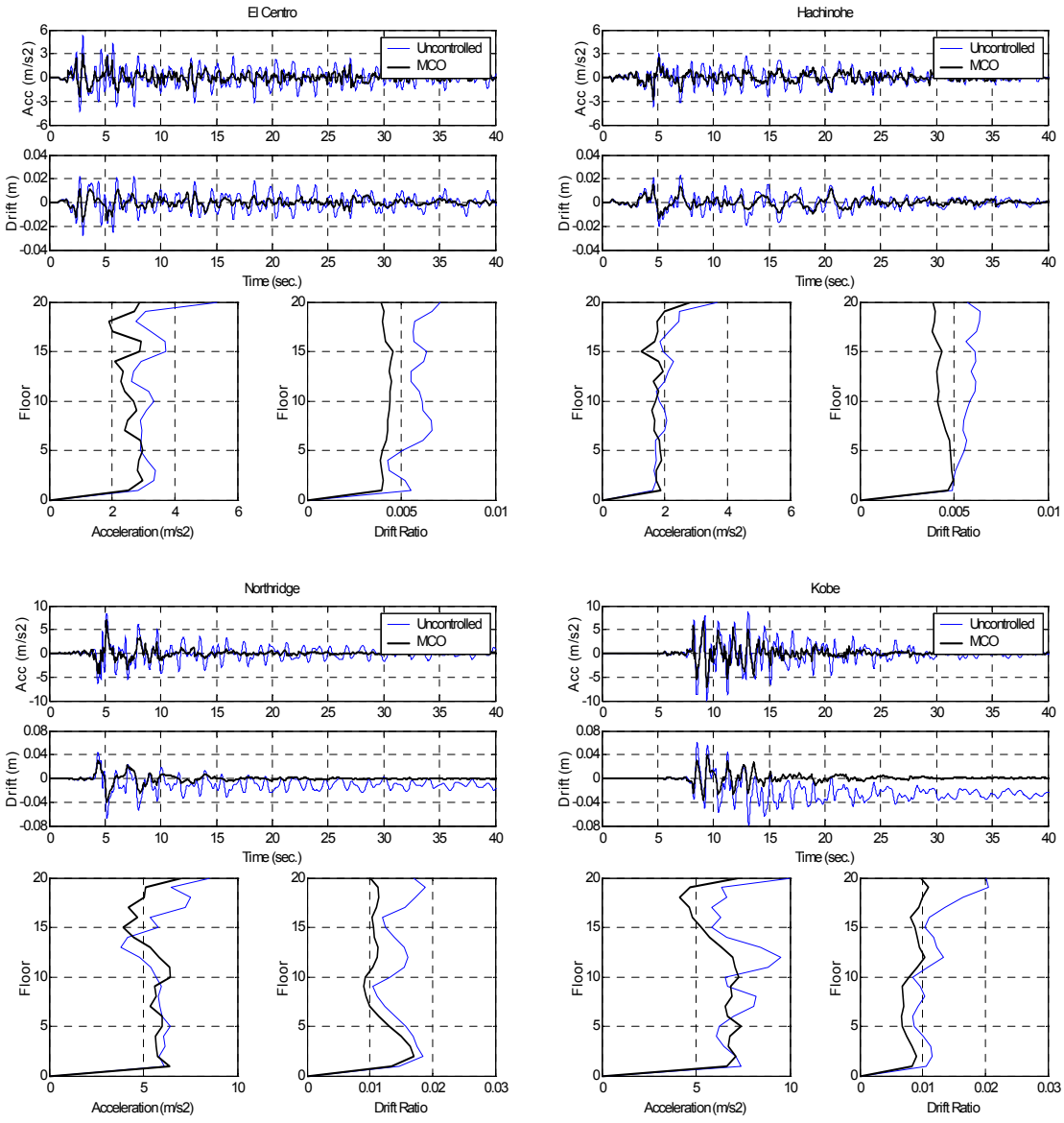

FIGURE 3-3. Comparison of Controlled and Uncontrolled Responses for Full-Scale Earthquakes.

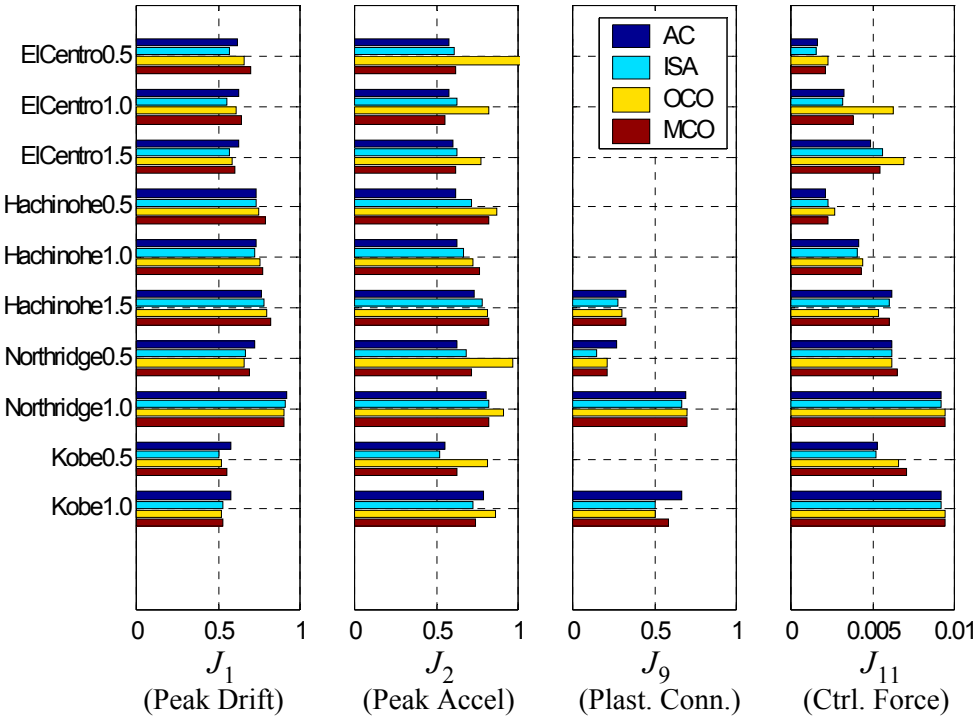

FIGURE 3-4. Bar Chart Comparing the Evaluation Criteria for Various Controllers.

3.5.2 Evaluation Criteria

The values of the evaluation criteria for the four control systems are provided in Tables 3-2 through 3-5. To compare the performance of the controlled systems, the bar chart in Figure 3-4 provides a graphical comparison of the various control systems for earthquakes at each magnitude specified in the benchmark problem definition [36,37]. Figure 3-4 shows the values for the maximum interstory drift ratio (J_1), maximum absolute acceleration (J_2), number of plastic connections (J_9), and maximum control force (J_{11}).

First note that the force requirements of each of the control systems are approximately the same for a given earthquake and magnitude. An exception to this case is for the OCO algorithm (using the MR damper) for the full-scale and 1.5 scale El Centro cases because the OCO (original clipped-optimal) algorithm only applies the maximum voltage or zero. Thus, larger forces may be required when this algorithm is used to control the MR damper. Note that, although approximately the same forces are required, all semiactive control systems require significantly less power than the active controller. Additionally, because the semiactive systems cannot insert energy into the structural system, they are considered to be inherently stable. Thus, in terms of stability, the semiactive systems are significantly more robust than the active system.

Examining the first graph in this figure, it is found that all controllers have the ability to reduce the peak drift ratio to nearly 50% of the uncontrolled value for all magnitudes of El Centro and Kobe earthquakes. Note that in several of these cases the semiactive results are smaller than the active results. For the half-scale Northridge and the Hachinohe earthquake at all levels, all controllers reduce the responses to 60–70% of the uncontrolled responses. Modest reduction is achieved for the full-scale Northridge earthquake.

The second graph in Figure 3-4 compares the evaluation criteria corresponding to the peak acceleration of the structure. Note that the acceleration reduction achieved is often similar for the active, ISA, and MCO controllers. No general trends are observed in comparing the performance of these algorithms (*i.e.*, neither of the approaches is always more effective). In certain cases the MCO and ISA results are better than the active results (*e.g.*, full-scale Kobe earthquake), and in some cases the active results are somewhat better than the MCO results (*e.g.* Hachinohe earthquake at all levels).

In comparing the two MR designs, the OCO and MCO control systems, the resulting peak drift ratios are slightly smaller with the OCO algorithm in general. However, the

MCO (modified algorithm) is typically able to achieve a significant reduction in the peak accelerations over that of the OCO algorithm. Therefore, if the control objective is to reduce accelerations, this controller would offer significant advantages over the OCO algorithm.

It is particularly interesting that the application of a controller results in reducing the number of plastic connections significantly. For instance, the uncontrolled structure developed plastic connections when subjected to the half-scale Kobe earthquake. However, when control is applied, the formation of plastic connections is completely prevented. This is also observed in the results for the 1.5 scale El Centro earthquake. Further, in all of the cases in which plastic connections form in the uncontrolled structure, the number of plastic connections that are formed is significantly reduced when control is applied. Thus, damage in the structure is significantly minimized.

As is evident in the time history response of the drifts in Figure 3-3, when the structure develops plastic connections, a residual permanent deformation may be present in the structure. The degree of permanent deformation can only be indirectly controlled by minimizing the drifts of the structure throughout the earthquake. Because information about the earthquake input at future times is not available, this response cannot be directly controlled. The newly proposed evaluation criteria, P_1 and P_2 take this into account.

Tables 3-2 through 3-5 also provide values for the additional evaluation criteria. In most cases the permanent deformations present in the controlled structure are smaller than in the uncontrolled structure. Note that in every case the value of P_2 is less than 1.0, indicating that the overall permanent drifts in the structure are smaller than the uncontrolled responses. Additionally, in all but one case, the value of P_1 is less than 1. In one case, that of the full-scale Northridge earthquake, the value of P_1 is above 1.0. Thus, for this

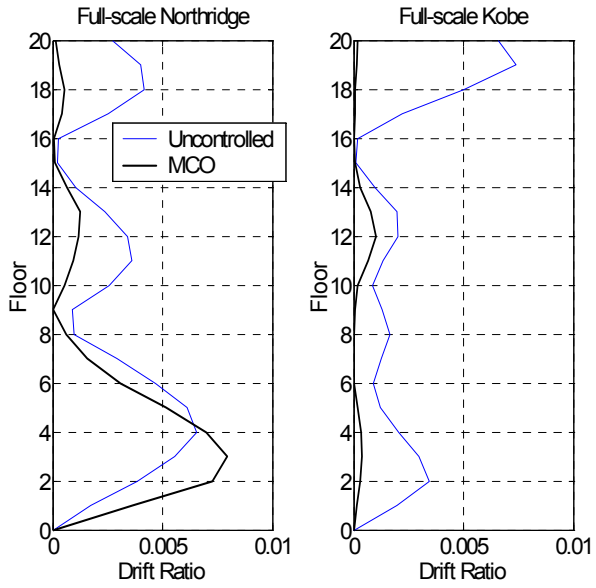

FIGURE 3-5. Distribution of Permanent Interstory Drift Ratio.

large earthquake, there is a tradeoff between allowing a larger permanent deformation on one floor, and minimizing the total permanent deformation (given by P_2).

To examine this issue further, the permanent drift ratio response for the full-scale Northridge and Kobe earthquakes are shown in Figure 3-5. Although the maximum permanent drift ratio over the structure is larger for the controlled case in the Northridge earthquake, the permanent offset at each floor in the controlled structure is generally a fraction that of the uncontrolled structure. In the full-scale Kobe earthquake, the controlled permanent offset is generally significantly smaller than the uncontrolled offset. Additionally, note that the existence of the permanent offset results in evaluation criteria J_4 for normed drift ratio being larger than 1.0 in Tables 3-2 through 3-5 for the full-scale Northridge earthquake.

TABLE 3-2. Evaluation Criteria for Active Control.

Earthquake intensity	*El Centro 0.5/1.0/1.5*	*Hachinohe 0.5/1.0/1.5*	*Northridge 0.5/1.0*	*Kobe 0.5/1.0*	*Max Value*
J_1 Peak Drift Ratio	0.6193 0.6227 0.6230	0.7307 0.7341 0.7648	0.7197 0.9222	0.5796 0.5748	0.9222
J_2 Peak Acceleration	0.5752 0.5808 0.5994	0.6164 0.6260 0.7278	0.6294 0.8089	0.5521 0.7895	0.8089
J_3 Peak Base Shear	0.8623 0.8597 0.9973	1.0307 1.0243 1.0672	1.0211 1.0960	0.8475 1.1029	1.1029
J_4 Normed Drift Ratio	0.5091 0.5039 0.5075	0.7309 0.7331 0.7510	0.4528 1.2592	0.3734 0.1478	1.2592
J_5 Normed Acceleration	0.4308 0.4266 0.4397	0.5317 0.5269 0.5399	0.4025 0.5059	0.4112 0.5693	0.5693
J_6 Normed Base Shear	0.6242 0.6162 0.6195	0.7676 0.7645 0.7767	0.5083 0.7434	0.4712 0.6699	0.7767
J_7 Ductility	0.6947 0.6983 0.6509	0.8806 0.8841 0.8332	0.6814 0.9609	0.4888 0.5968	0.9609
J_8 Dissipated Energy	–[a] – 0	– – 0.1420	0.0340 0.3312	0 0.0936	0.3312
J_9 Plastic Connections	– – 0	– – 0.3256	0.2708 0.6875	0 0.6667	0.6875
J_{10} Norm Ductility	0.5566 0.5509 0.4912	0.6981 0.7000 0.7109	0.3554 1.2624	0.3480 0.1898	1.2624
J_{11} Control Force	0.001659 0.003268 0.004892	0.002095 0.004169 0.006175	0.006160 0.009166	0.005295 0.009203	0.009203
J_{12} Device Stroke	0.06921 0.06955 0.07013	0.07047 0.07077 0.07519	0.07425 0.09801	0.09618 0.09854	0.09854
J_{13} Control Power	0.003055 0.005914 0.009265	0.003379 0.006485 0.010151	0.010342 0.019434	0.009030 0.023773	0.023773
J_{14} Normed Control Power	0.000131 0.000256 0.000404	0.000148 0.000287 0.000455	0.000174 0.000402	0.000130 0.000312	0.000455
J_{15} Control Devices	65				65
J_{16} Sensors	5				5
J_{17} Computational Resources	20				20
P_1 Max Permanent Drift Ratio	– – 0	– – 0.4028	0.0676 1.2912	0 0.0821	1.2912
P_2 Total Permanent Drift Ratio	– – 0	– – 0.2496	0.0497 0.8113	0 0.1146	0.8113

a.Note that uncontrolled structure does not yield in some cases.

TABLE 3-3. Evaluation Criteria for Ideal Semiactive Control.

Earthquake intensity	*El Centro 0.5/1.0/1.5*	*Hachinohe 0.5/1.0/1.5*	*Northridge 0.5/1.0*	*Kobe 0.5/1.0*	*Max Value*
J_1 Peak Drift Ratio	0.5729 0.5558 0.5714	0.7316 0.7266 0.7817	0.6643 0.9091	0.5077 0.5286	0.9091
J_2 Peak Acceleration	0.6105 0.6286 0.6270	0.7184 0.6687 0.7787	0.6841 0.8171	0.5222 0.7233	0.8171
J_3 Peak Base Shear	0.7993 0.8002 0.9661	1.0336 1.0281 1.0570	0.9811 1.0764	0.7941 1.0938	1.0938
J_4 Normed Drift Ratio	0.4984 0.4996 0.5111	0.7292 0.7336 0.7535	0.4462 1.2412	0.3435 0.1310	1.2412
J_5 Normed Acceleration	0.3738 0.3754 0.3898	0.4830 0.4848 0.4956	0.3767 0.4749	0.3619 0.5164	0.5164
J_6 Normed Base Shear	0.5809 0.5819 0.5986	0.7486 0.7542 0.7719	0.4990 0.7409	0.4374 0.6356	0.7719
J_7 Ductility	0.6760 0.6683 0.6492	0.9039 0.8976 0.8770	0.6910 0.9406	0.4418 0.5207	0.9406
J_8 Dissipated Energy	–[a] – 0	– – 0.2177	0.0397 0.2653	0 0.0778	0.2653
J_9 Plastic Connections	– – 0	– – 0.2791	0.1458 0.6667	0 0.5000	0.6667
J_{10} Norm Ductility	0.5527 0.5547 0.5032	0.7063 0.7095 0.7825	0.3848 1.2506	0.3535 0.1331	1.2506
J_{11} Control Force	0.001549 0.003195 0.005648	0.002253 0.004048 0.006041	0.006172 0.009202	0.005239 0.009198	0.009202
J_{12} Device Stroke	0.06689 0.06591 0.06954	0.07229 0.07178 0.07747	0.07431 0.09897	0.08816 0.09074	0.09897
J_{13} Control Power	0.000065 0.000033 0.000023	0.000066 0.000033 0.000024	0.000018 0.000015	0.000023 0.000016	0.000066
J_{14} Normed Control Power	0.000065 0.000033 0.000023	0.000066 0.000033 0.000024	0.000018 0.000015	0.000023 0.000016	0.000066
J_{15} Control Devices	65				65
J_{16} Sensors	25				25
J_{17} Computational Resources	20				20
P_1 Max Permanent Drift Ratio	– – 0	– – 0.8358	0.1604 1.2717	0 0.0713	1.2717
P_2 Total Permanent Drift Ratio	– – 0	– – 0.3508	0.0659 0.7288	0 0.0567	0.7288

a.Note that uncontrolled structure does not yield in some cases.

TABLE 3-4. Evaluation Criteria for Original Clipped-Optimal Control.

Earthquake intensity	*El Centro 0.5/1.0/1.5*	*Hachinohe 0.5/1.0/1.5*	*Northridge 0.5/1.0*	*Kobe 0.5/1.0*	*Max Value*
J_1 Peak Drift Ratio	0.6564 0.6098 0.5826	0.7500 0.7587 0.7954	0.6585 0.9040	0.5242 0.5216	0.9040
J_2 Peak Acceleration	1.0472 0.8221 0.7699	0.8675 0.7227 0.8096	0.9653 0.9082	0.8112 0.8606	1.0472
J_3 Peak Base Shear	0.8121 0.8937 1.0156	1.0972 1.0754 1.1027	1.0229 1.0947	0.8097 1.1713	1.1713
J_4 Normed Drift Ratio	0.4943 0.4922 0.5049	0.7402 0.7323 0.7464	0.4355 1.2067	0.3214 0.1393	1.2067
J_5 Normed Acceleration	0.5346 0.4466 0.4318	0.6415 0.5593 0.5435	0.3908 0.5069	0.4107 0.5264	0.6415
J_6 Normed Base Shear	0.6327 0.6092 0.6098	0.8147 0.7692 0.7734	0.4920 0.7267	0.4204 0.6248	0.8147
J_7 Ductility	0.6608 0.7096 0.6525	0.9249 0.9270 0.8806	0.6824 0.9289	0.3996 0.4941	0.9289
J_8 Dissipated Energy	–[a] – 0	– – 0.2236	0.0344 0.2401	0 0.0693	0.2401
J_9 Plastic Connections	– – 0	– – 0.3023	0.2083 0.6979	0 0.5000	0.6979
J_{10} Norm Ductility	0.5414 0.5466 0.4936	0.7184 0.7051 0.7832	0.3660 1.2303	0.3131 0.1540	1.2303
J_{11} Control Force	0.002240 0.006280 0.006913	0.002719 0.004371 0.005344	0.006180 0.009427	0.006619 0.009391	0.009427
J_{12} Device Stroke	0.06599 0.07254 0.07064	0.07379 0.07336 0.07722	0.07337 0.09757	0.07821 0.08732	0.09757
J_{13} Control Power	0.000060 0.000031 0.000023	0.000064 0.000032 0.000024	0.000017 0.000014	0.000022 0.000016	0.000064
J_{14} Normed Control Power	0.000017 0.000009 0.000006	0.000018 0.000009 0.000007	0.000005 0.000004	0.000006 0.000004	0.000018
J_{15} Control Devices	65				65
J_{16} Sensors	25				25
J_{17} Computational Resources	20				20
P_1 Max Permanent Drift Ratio	– – 0	– – 1.0161	0.1435 1.2367	0 0.0988	1.2367
P_2 Total Permanent Drift Ratio	– – 0	– – 0.5142	0.0681 0.7505	0 0.0677	0.7505

a.Note that uncontrolled structure does not yield in some cases.

TABLE 3-5. Evaluation Criteria for Modified Clipped-Optimal Control.

Earthquake intensity	*El Centro 0.5/1.0/1.5*	*Hachinohe 0.5/1.0/1.5*	*Northridge 0.5/1.0*	*Kobe 0.5/1.0*	*Max Value*
J_1 Peak Drift Ratio	0.6957 0.6450 0.6007	0.7867 0.7707 0.8180	0.6910 0.9060	0.5495 0.5324	0.9060
J_2 Peak Acceleration	0.6149 0.5568 0.6156	0.8171 0.7673 0.8175	0.7167 0.8195	0.6228 0.7410	0.8195
J_3 Peak Base Shear	0.8145 0.8283 0.9612	1.0519 1.0507 1.0623	1.0019 1.0777	0.7660 1.0793	1.0793
J_4 Normed Drift Ratio	0.5568 0.5261 0.5206	0.7761 0.7553 0.7649	0.4557 1.1881	0.3563 0.1716	1.1881
J_5 Normed Acceleration	0.5656 0.4833 0.4620	0.6647 0.5900 0.5699	0.4043 0.4909	0.4237 0.5480	0.6647
J_6 Normed Base Shear	0.6733 0.6303 0.6179	0.8230 0.7840 0.7831	0.5091 0.7429	0.4395 0.6352	0.8230
J_7 Ductility	0.6992 0.7098 0.6533	0.9569 0.9367 0.8999	0.6837 0.9276	0.4292 0.4985	0.9569
J_8 Dissipated Energy	–[a] – 0	– – 0.2567	0.0351 0.2546	0 0.0719	0.2567
J_9 Plastic Connections	– – 0	– – 0.3256	0.2083 0.6979	0 0.5833	0.6979
J_{10} Norm Ductility	0.6136 0.5875 0.5137	0.7519 0.7288 0.8343	0.3858 1.2044	0.3394 0.2070	1.2044
J_{11} Control Force	0.002092 0.003820 0.005435	0.002315 0.004334 0.006041	0.006470 0.009429	0.007067 0.009408	0.009429
J_{12} Device Stroke	0.07083 0.07125 0.07095	0.07562 0.07395 0.07793	0.07372 0.09833	0.08558 0.08767	0.09833
J_{13} Control Power	0.000009 0.000009 0.000010	0.000011 0.000011 0.000012	0.000009 0.000010	0.000011 0.000013	0.000013
J_{14} Normed Control Power	0.000001 0.000001 0.000001	0.000001 0.000001 0.000001	0.000000 0.000000	0.000000 0.000000	0.000001
J_{15} Control Devices	65				65
J_{16} Sensors	25				25
J_{17} Computational Resources	20				20
P_1 Max Permanent Drift Ratio	– – 0	– – 1.3284	0.1438 1.2149	0 0.1398	1.3284
P_2 Total Permanent Drift Ratio	– – 0	– – 0.7127	0.0598 0.7214	0 0.1057	0.7214

a.Note that uncontrolled structure does not yield in some cases.

3.6 Summary

This chapter focuses on the application of the proposed semiactive control system using MR dampers to a model of a full scale building to verify the effectiveness of the control system. The full scale building used in this chapter is the 20-story building used for the nonlinear benchmark study. To investigate the achievable capabilities of the control system, four control systems were designed and evaluated, including: an active control system, an ideal semiactive control system, and two semiactive systems using 1000 kN MR dampers. Acceleration feedback was employed in the control designs. In addition, the semiactive systems also employed measurements of the forces produced by each device for control force determination. The MR damper was controlled using a clipped-optimal control algorithm which falls into the class of bang-bang controllers, as well as a newly proposed modified clipped-optimal control algorithm that supplies continuously-varying command voltages.

In comparing the active, ideal semi-active and MR control systems, it was observed that similar performance could typically be achieved by all of these systems, reinforcing the result obtained by previous studies that semiactive systems can achieve similar performance levels to that of active systems. In several cases the semiactive systems performed better than the active, while requiring significantly less power than the active system.

In comparing the two control algorithms used with the MR damper, the modified clipped-optimal control algorithm was found to be significantly more effective at reducing the accelerations of this structure while achieving nearly the same reduction in interstory drifts. Furthermore, for low-level excitations, the clipped-optimal control algorithm required significantly more force to control this structure than the modified algorithm. Of particular interest was the result that the permanent offset in the interstory

drifts was generally reduced by a significant margin in the controlled results. The number of plastic connections formed was also reduced significantly by the controllers.

Chapter 4

Basic Behavior of Asymmetric Buildings

This chapter demonstrates the basic behavior of an asymmetric building. Parametric studies are performed using a single story asymmetric structure to examine the responses, including base shear and torque, under ground excitation. The eccentricity ratio and the uncoupled natural frequency ratio between the translational and torsional modes are taken as the parameters. Further, practical cases are studied to examine deformation and acceleration responses for a simple structural model similar to the experimental model available in the laboratory. As a preliminary control study, a passive control system using viscous dampers and an active control system based on H_2/LQG methods using ideal actuators are implemented on this simple asymmetric building. Studies are also conducted for multistory asymmetric buildings.

4.1 Basic Behavior of Torsional Responses of Asymmetric Buildings

To examine the effect of asymmetry on the dynamic behavior of a typical structure, a parametric study is performed using a mathematical model of a one-story building with an asymmetric stiffness distribution along one axis. (See Figure 4-1). The model is subjected to a uniaxial lateral disturbance, exciting both lateral and torsional motions. The equation of motion of this structure can be written as follows [28]

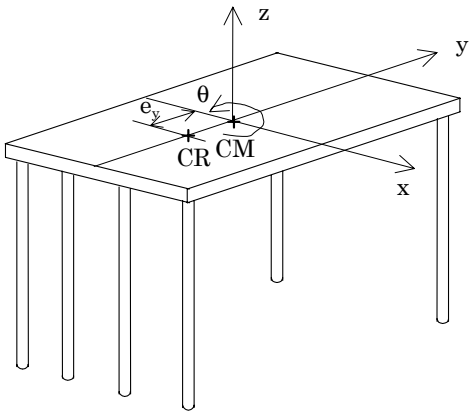

FIGURE 4-1. Single-story Asymmetric Building.

$$\begin{Bmatrix} \ddot{x} \\ r\ddot{\theta} \end{Bmatrix} + \begin{bmatrix} \omega_x^2 & -\frac{e_y}{r}\omega_x^2 \\ -\frac{e_y}{r}\omega_x^2 & \omega_\theta^2 \end{bmatrix} \begin{Bmatrix} x \\ r\theta \end{Bmatrix} = -\begin{Bmatrix} 1 \\ 0 \end{Bmatrix} \ddot{x}_g \tag{4-1}$$

where x is the relative displacement of mass center to ground, θ is the rotation about the vertical axis, $\ddot{x}_g$ is the ground acceleration along x-direction, e_y is the static eccentricity (distance from center of mass along y-axis to center of resistance), r is the radius of gyration of the deck about a vertical axis through the center of mass. The frequency parameters, ω_x, and ω_θ, may be interpreted as the natural frequencies of the system if it were not coupled (*i.e.*, $e_y = 0$).

The variation of the responses for various eccentricity ratios and frequency ratios is examined herein. The structural responses considered in this study include normalized measures of the base shear and base torque (previously considered in [28]), as well as the maximum acceleration and column drift. The *rms* response values for a stationary,

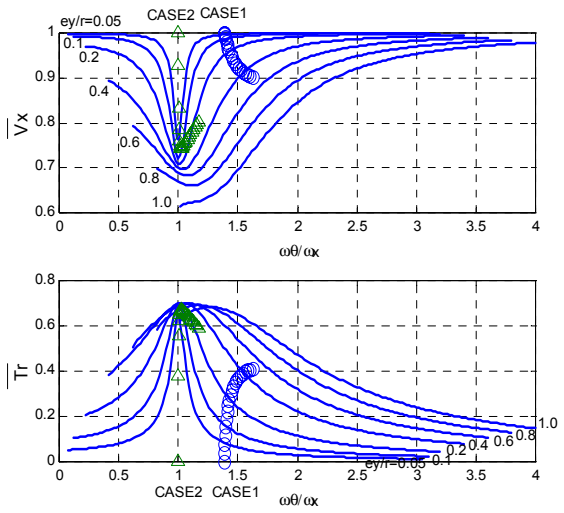

FIGURE 4-2. Normalized Base Shear and Torque.

white noise excitation are determined for comparison, and results are obtained by solving the associated Lyapunov equation [46].

The maximum responses for various eccentricity values, e_y/r, are shown in Figure 4-2 as a function of the uncoupled frequency ratio, ω_θ/ω_x. The base shear and the base torque are normalized using the base shear of the uncoupled system, V_{xo}, given by

$$\overline{V_x} = \frac{V_x}{V_{x0}} \qquad \overline{T_r} = \frac{T_r}{rV_{x0}} \tag{4-2}$$

From these results, it is clear that base torque increases and base shear decreases with an increasing eccentricity, and this effect is most pronounced when the translational and torsional natural frequencies of the uncoupled system are equal. These results agree with the results provided by Kan and Chopra [28]. Note that the results in [28] are determined

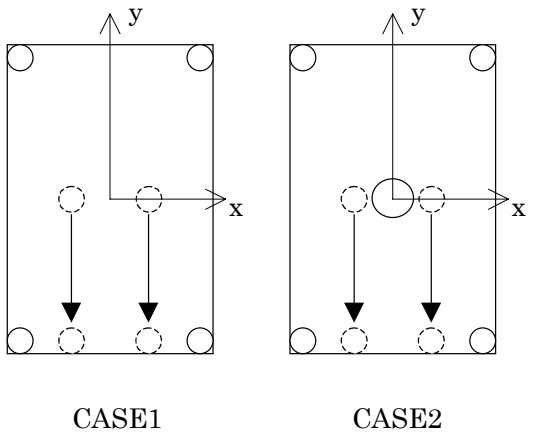

FIGURE 4-3. Schematic of Cases Studied.

based on response spectrum analysis, whereas the results obtained in this study are determined as *rms* responses due to a stationary, white noise excitation.

To examine the acceleration and column drift responses, the parameters of the one story building model are selected to be similar to those of an experimental structure available in the lab. The mass of the floor is 23.3 kg (51.12 lb.). The stiffness is supplied by a permanent column at each corner, plus additional columns that are employed to vary the eccentricity of the system. Every column, permanent and variable column, in this numerical study has the stiffness of a circular steel rod with a 0.64cm (1/4in) outer diameter. The following two practical cases are considered (see Figure 4-3 for schematic).

- *Case1:* The floor mass is supported by four identical columns (one per corner), and two extra columns whose locations move from the center to one edge of the mass along the *y*-axis.

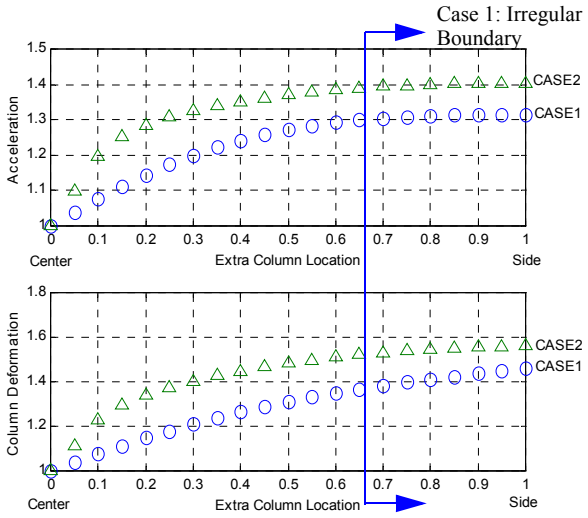

FIGURE 4-4. Normalized Responses for an Asymmetric Building.

- *Case2:* The floor mass is supported by four identical columns (one per corner), plus one column at the center to have the same uncoupled torsional and translational frequencies, and two extra columns whose locations move from the center to one edge of the mass along the *y*-axis.

The base shear and torque responses for these two cases are shown in Figure 4-2. The maximum acceleration and maximum column deformation responses, which are normalized by the acceleration and column deformation of the corresponding uncoupled system, are shown in Figure 4-4 as a function of the location of the extra columns. From these figures, it is clear that asymmetry of the building results in an increase in torsional response and a decrease in translational response, which concentrates the deformation at some columns and amplifies the maximum acceleration of the floors. In the example, the maximum column deformation and maximum floor acceleration are 40–60% and 30–40% larger than those of uncoupled building, respectively.

According to FEMA recommendations [17], an irregular structure is defined as one in which the ratio e_y/d is greater than 0.1, where d is a building dimension perpendicular to the direction of the seismic excitation. The set of parameters that defines the boundary for an irregular structure is identified in Figure 4-4 for Case 1. For Case 2, when the extra columns are located at the edge of the structure, the ratio e_y/d is only 0.078, well within the range of a regular structure, although the responses are significantly larger than those of the irregular building of Case 1. This is the reason that a core-type building does not perform well in strong earthquakes, although it is not classified as an irregular building.

The same series of studied have been performed for a 2-story building with an asymmetric stiffness distribution. The parameters of each story were identical to the structural system in the first example. The results show almost the same behavior of base shear, base torque, maximum floor acceleration and maximum column deformation, and are not included here.

4.2 Preliminary Control Study

As a preliminary control study, a passive control system using viscous dampers and active control systems based on H_2/LQG (Linear Quadratic Gaussian) control using ideal actuators are implemented on this system. These control systems are applied to the single-, 2-, 3-, and 4-story buildings with an asymmetric stiffness distribution. The parameters of each story in the multistory buildings are identical to the structural system in the single-story building. In each control system, two devices are installed between the ground and the first floor and equally spaced from the center of mass.

Figure 4-5 shows the results for the passive control system applied to the 2-story building as a function of the passive system's damping coefficient. These results are the *rms* responses due to stationary white noise input (Lyapunov solution [46]). Base shear, base

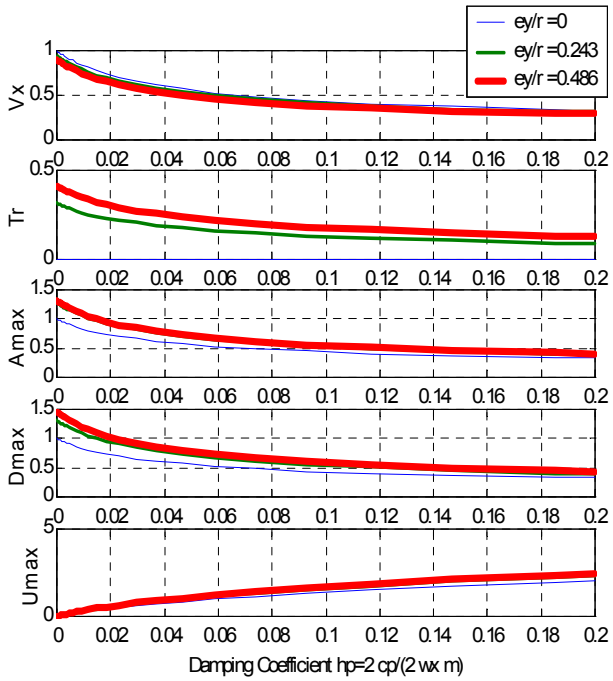

FIGURE 4-5. Passive Control for 2-story Asymmetric Building.

torque, maximum floor acceleration, maximum column deformation, and maximum control force are shown for three different eccentricities. As discussed in the previous study, the base shear and base torque are normalized using the base shear of the corresponding uncoupled system, the maximum floor acceleration and column deformation are normalized by those of the uncoupled system, and the maximum control force is normalized by the input force. As shown in these figures, the passive control system can typically reduce the responses significantly. However, when the eccentricity becomes large, smaller performance gains can be achieved with the addition of the passive devices.

Figure 4-6 shows the controlled performance using the active control system as compared to the results using the passive control system as a function of the maximum *rms* control force (of the 2 devices). Two controllers based on H_2/LQG methods are designed for the active system. One, denoted LQG-a, is designed by placing equal

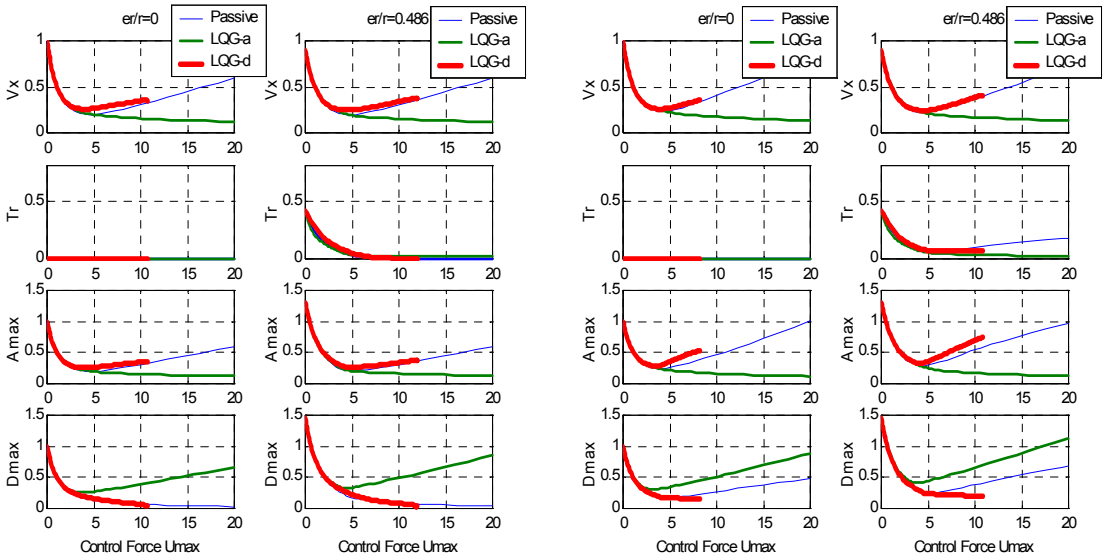

a) Single-story Building

b) 2-story Building

c) 3-story Building

d) 4-story Building

FIGURE 4-6. Comparison between Active and Passive Control for Asymmetric Building.

weighting on all acceleration outputs, and the second, denoted LQG-d, is designed by placing equal weighting on all deformation outputs. Base shear, base torque, maximum floor acceleration and maximum column deformation are compared for the single-, 2-, 3-, and 4-story buildings. The results are the normalized *rms* responses due to a stationary white noise input.

In the case of the single-story building, when the passive control system is applied, the base torque and the maximum column deformation decrease with increasing control force, while the base shear and the maximum acceleration increase after reaching their minimum values. This behavior is also observed when the LQG-d controller is applied. When the LQG-a controller is applied, the base shear, the base torque, and the maximum floor acceleration decrease with increasing control force, while the maximum column deformation increases after reaching its minimum value.

In the case of multistory buildings, when the passive control system is applied, all responses increases with increasing control force after reaching their minimum values. The LQG-a controller can reduce the base shear, the base torque, and the maximum floor acceleration more than the passive control system can achieve, and the LQG-d controller can reduce the maximum column deformation more than the passive control system can achieve. Note that the maximum performance achieved by the passive control system is getting worse with increasing number of stories in the building and with larger eccentricity. The application of active control has advantages.

4.3 Summary

In this chapter the basic behavior of torsional responses of asymmetric building has been examined, and as a preliminary numerical control study, a passive control system and active control systems were implemented on several asymmetric building models.

Parametric studies were conducted using a model of a single story building with an asymmetric stiffness distribution along one axis. The results showed that increasing asymmetry results in an increase in torsional response and a decrease in translational response, which concentrates the deformation at some columns and amplifies the maximum acceleration of the floors.

In controlling the responses of asymmetric buildings, active control systems were found to reduce the responses more than passive control systems. This effect was more pronounced as the number of stories in the building increased and as the eccentricity increased. The application of active control clearly has advantages over passive here.

Chapter 5

Experimental Verification of Torsional Response Control of Asymmetric Buildings

In this chapter, the performance of the proposed method to control torsional responses is studied experimentally using a 2-story building model with an asymmetric stiffness distribution. An automated system identification methodology is developed and implemented to form a control-oriented model which has the natural frequencies observed in the experimental system. The parameters for the MR damper model are identified using experimental data to develop an integrated model of the structure and MR dampers. This model is found to be effective for control design. To demonstrate the performance of the control system, a shake table is used to reproduce an El Centro 1940 N-S earthquake acceleration as well as a broadband random excitation. The responses for the proposed control system are also compared to those of passive control cases in which a constant voltage is applied to the MR damper [63–65].

5.1 Experimental Setup

An experimental model has been designed and constructed for this study. The model is a 2-story frame building with an asymmetric column distribution (see Figs. 5-1 and 5-2). The mass of each story is simulated by two steel plates, 30.48×50.8×0.95 cm (12×20×3/8 in) and 30.48×38.1×1.27 cm (12×15×1/2 in), and has a weight of 23.3 kg

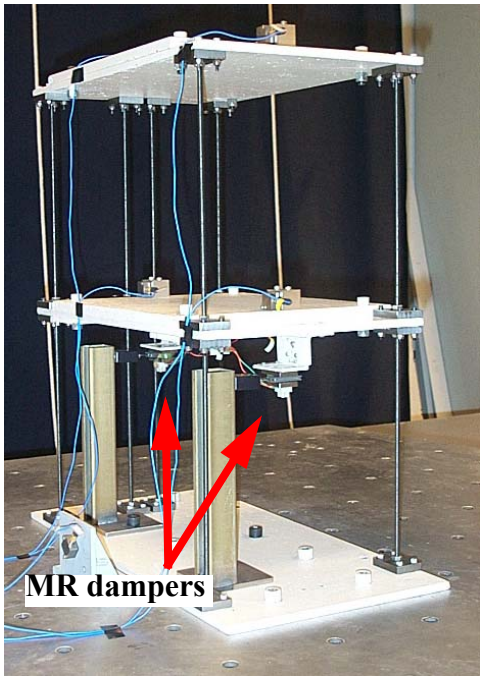

FIGURE 5-1. Photo of Experiment.

(51.12 lb). This mass is supported by a total of six columns, one at each corner plus two additional columns along one side of the building to create asymmetry. These columns are threaded steel rods with an outer diameter of 0.64 cm (1/4 in) and a length of 30.48 cm (12 in). Two MR dampers are installed between the first floor and the ground and equally spaced from the center of mass. Four accelerometers (two on each floor) are installed as shown in Figure 5-2. Control actions are computed using a DSP-based, real-time controller manufactured by dSpace, Inc.

5.2 Identification of Experimental Structure

The first step in the experiment is to obtain a model of the structural system that is appropriate for control design purposes. Herein we implement an automated approach that was developed here specifically for control-oriented structural modeling [25]. The method is based on the Eigensystem Realization Algorithm (ERA) [27] and integrates

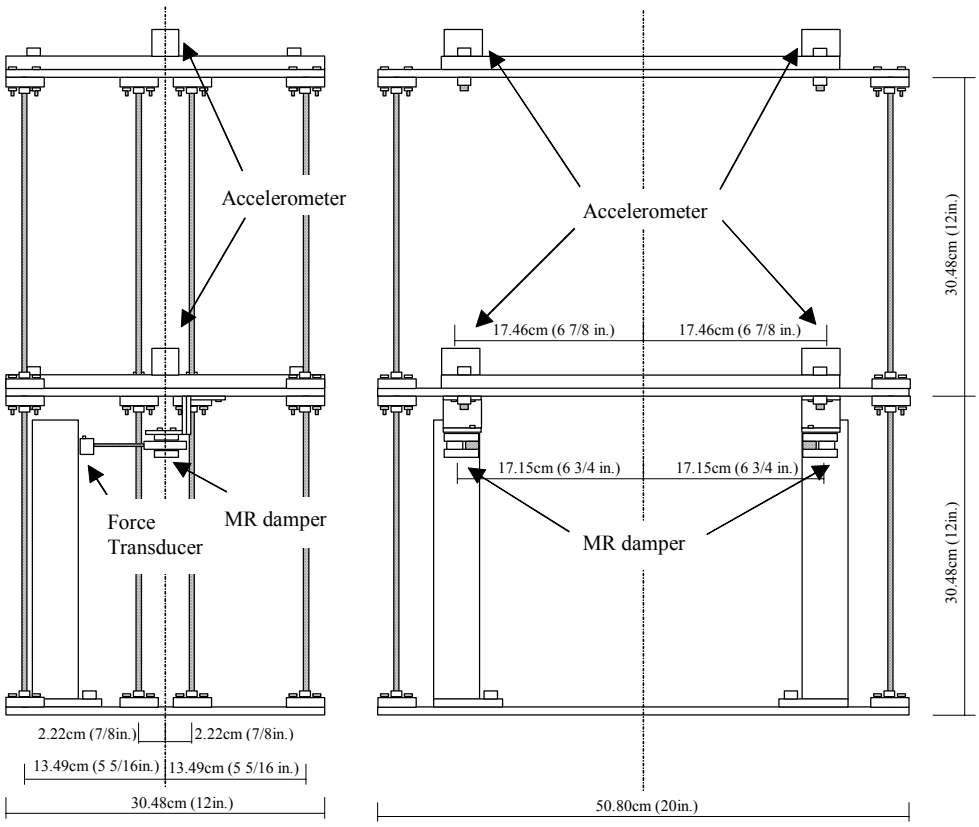

FIGURE 5-2. Schematic View of Test Structure.

the results of this automated system identification technique with an analytical model of the structural system.

A block diagram of the system to be identified is shown in Figure 5-3. The three inputs to the system include the ground acceleration $\ddot{x}_g$ and the two control force inputs, f_1 and f_2 at the weak and strong sides of the structure where the MR devices will be placed. Four outputs to the system include the accelerations of weak and strong side on 1FL, $\ddot{x}_{11}$ and $\ddot{x}_{12}$, and the accelerations of weak and strong side on 2FL, $\ddot{x}_{21}$ and $\ddot{x}_{22}$.

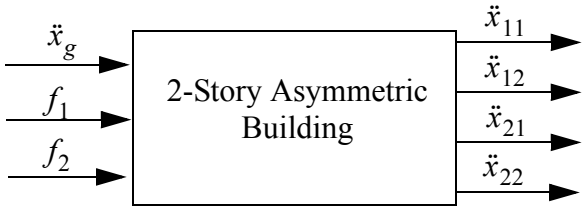

FIGURE 5-3. Block Diagram of System to be Identified.

To obtain a realization of the structure which has the frequencies observed in the experimental system, an analytical model of the system is developed based on the structure, and this model is modified [25,61]. The parameters used for this analytical model are based on the physical dimensions of the members and the materials. Fixed connections are assumed at column-beam joints. The lumped parameter model takes the form

$$\mathbf{M}_s\ddot{\mathrm{x}} + \mathbf{C}_s\dot{\mathrm{x}} + \mathbf{K}_s\mathrm{x} = -\mathbf{M}_s\Gamma\ddot{x}_g + \Lambda\mathbf{f} \tag{5-1}$$

where $\mathbf{x} = \left[x_1\ x_2\ \theta_1\ \theta_2\right]^T$, where x_1 and x_2 are the relative displacements of the mass center of the 1st floor and 2nd floor, respectively, θ_1 and θ_2 are the rotation about vertical axis of the 1st floor and 2nd floor, respectively, $\ddot{x}_g$ is a one-dimensional ground acceleration, $\mathbf{f}$ is the vector of control forces, Γ is a $[-1\ -1\ 0\ 0]^T$, and

$$\mathbf{M}_s = \begin{bmatrix} m_1 & 0 & 0 & 0 \\ 0 & m_2 & 0 & 0 \\ 0 & 0 & I_1 & 0 \\ 0 & 0 & 0 & I_2 \end{bmatrix}, \qquad \mathbf{K}_s = \begin{bmatrix} 2k_x & -k_x & 2k_{x\theta} & -k_{x\theta} \\ -k_x & k_x & -k_x & k_{x\theta} \\ 2k_{x\theta} & -k_{x\theta} & 2k_\theta & -k_\theta \\ -k_{x\theta} & k_{x\theta} & -k_\theta & k_\theta \end{bmatrix}, \qquad \Lambda = \begin{bmatrix} 1 & 1 \\ 0 & 0 \\ -l_1 & -l_2 \\ 0 & 0 \end{bmatrix} \tag{5-2}$$

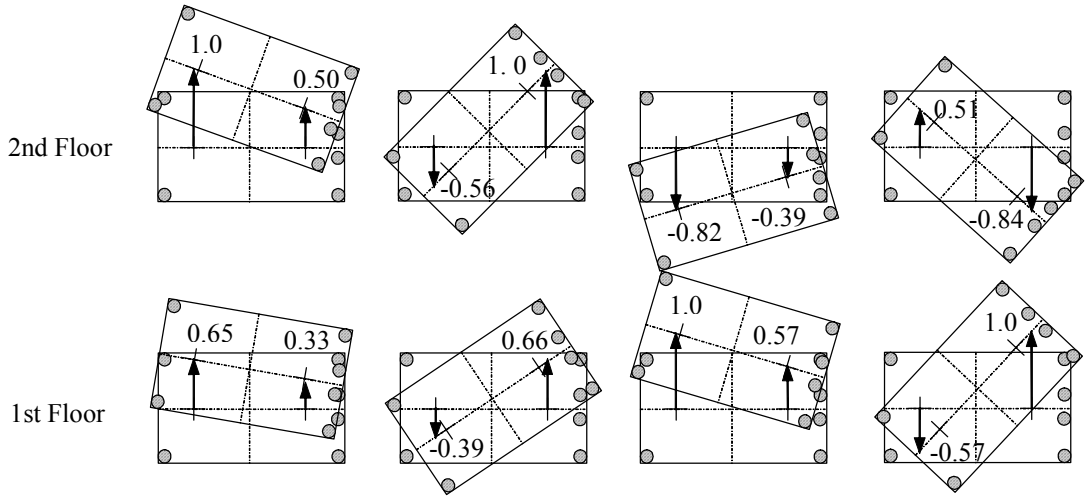

FIGURE 5-4. Mode Shapes of the Test Structure.

where $l_1 = -17.15$ cm and $l_2 = 17.15$ cm are the coordinates of the control forces input locations. From the experimental structure, $m_1 = 0.272$ N/(cm/sec^2), $m_2 = 0.241$ N/(cm/sec^2), $I_1 = 75.95$ N·cm/(rad/sec^2), $I_2 = 62.55$ N·cm/(rad/sec^2), $k_x = 212.0$ N/cm, $k_{x\theta} = 1.62 \times 10^3$ N, and $k_\theta = 1.37 \times 10^3$ N·cm. The frequencies of this lumped mass model are f_n =[2.64 4.62 6.73 11.69] (Hz).

Here the ERA [27] was applied to experimental data to determine the natural frequencies and the damping ratios of the experimental model. The identified natural frequencies and damping ratios are f_e =[2.68 4.56 7.04 11.91] (Hz), and h_e =[0.44 0.26 0.18 0.12] (%), respectively**.** Also, the identified mode shapes are shown in Figure 5-4.

To obtain a realization of the structure which has the frequencies observed in the experimental system, the analytical model is modified [61]. In this approach, the modal matrix,

$\Phi = [\phi_1\ \phi_2\ \ldots\phi_n]$, is used where ϕ_i are the eigenvectors of $\mathbf{M}_s^{-1}\mathbf{K}_s$. The new stiffness matrix is computed using

$$\mathbf{K}_r = \mathbf{M}_s\Phi diag([2\pi f_e]^2)\Phi^T \tag{5-3}$$

yielding the modified stiffness matrix, $\mathbf{K}_r$. Note that this approach results in a model of the system which maintains the mode shapes of the analytical model, but has the frequencies of the experimental system. In addition, the damping matrix $\mathbf{C}_s$ is determined to have the modal damping ratios which are identified by ERA method as follows

$$\mathbf{C}_s = \mathbf{M}_s\Phi diag(2h_e[2\pi f_e])\Phi^T \ . \tag{5-4}$$

These updated stiffness matrix and damping matrix are used to form the state space equations for this system as

$$\dot{\mathbf{z}} = \mathbf{A}\mathbf{z} + \mathbf{B}\mathbf{f} + \mathbf{E}\ddot{x}_g \qquad \mathbf{y} = \mathbf{C}\mathbf{z} + \mathbf{D}\mathbf{f} \tag{5-5}$$

where $\mathbf{z}=[\mathbf{x}^T\ \dot{\mathbf{x}}^T]^T$ is the state vector, and

$$\mathbf{A} = \begin{bmatrix} \mathbf{0} & \mathbf{I} \\ -\mathbf{M}_s^{-1}\mathbf{K}_r & -\mathbf{M}_s^{-1}\mathbf{C}_s \end{bmatrix}, \quad \mathbf{B} = \begin{bmatrix} \mathbf{0} \\ \mathbf{M}_s^{-1}\Lambda \end{bmatrix}, \quad \mathbf{E} = -\begin{bmatrix} \mathbf{0} \\ \Gamma \end{bmatrix}. \tag{5-6}$$

Here, the vector of outputs is taken as $\mathbf{y}=[\mathbf{y}_m{}^T\ \mathbf{y}_d{}^T]^T$, where $\mathbf{y}_m = \begin{bmatrix}\ddot{x}_{11}\ \ddot{x}_{12}\ \ddot{x}_{21}\ \ddot{x}_{22}\end{bmatrix}^T$ is the vector of acceleration measurements, and $\mathbf{y}_d = \begin{bmatrix}\dot{x}_{d1}\ \dot{x}_{d2}\end{bmatrix}^T$ is the vector of relative

velocities across the MR dampers. Thus the matrices for the output equation $\mathbf{C}$ and $\mathbf{D}$ have the following form:

$$\mathbf{C} = \begin{bmatrix} -\mathbf{P}_m\mathbf{M}_s^{-1}\mathbf{K}_r & -\mathbf{P}_m\mathbf{M}_s^{-1}\mathbf{C}_s \\ \mathbf{0} & \mathbf{P}_d \end{bmatrix}, \qquad \mathbf{D} = \begin{bmatrix} \mathbf{P}_m\mathbf{M}_s^{-1}\Lambda \\ \mathbf{0} \end{bmatrix}, \tag{5-7}$$

where

$$\mathbf{P}_m = \begin{bmatrix} 1 & 0 & -l_{m1} & 0 \\ 1 & 0 & -l_{m2} & 0 \\ 0 & 1 & 0 & -l_{m1} \\ 0 & 1 & 0 & -l_{m2} \end{bmatrix}, \quad \mathbf{P}_d = \begin{bmatrix} 1 & 0 & -l_1 & 0 \\ 1 & 0 & -l_2 & 0 \end{bmatrix}, \tag{5-8}$$

and $l_{m1} = -17.46$ cm and $l_{m2} = 17.46$ cm are the coordinates of the acceleration measurements.

Figure 5-5 provides a comparison of the identified model and the experimentally obtained data. The transfer functions of the model appear to match the experimental data well in general. Because the mode shapes from the analytical model are used, small errors in the zeros of the transfer functions may occur, although this is not expected to be problematic for semiactive control systems. Further examination of this control-oriented system identification method is being performed for more realistic structures that may not behave as shear buildings.

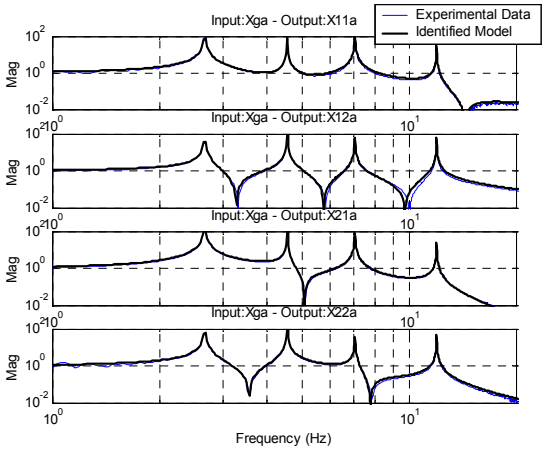

(a) Transfer Functions from Ground Acceleration

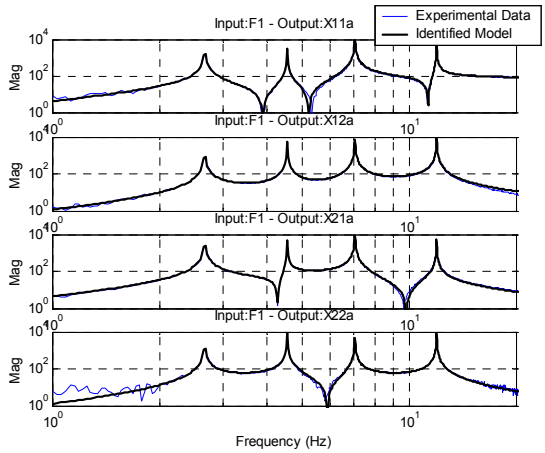

(b) Transfer Functions from Force 1

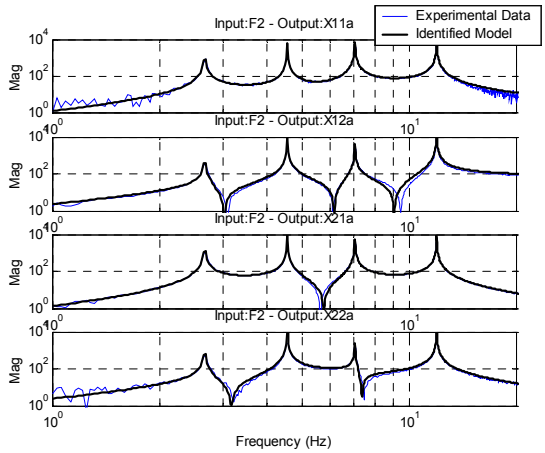

(c) Transfer Functions from Force 2

FIGURE 5-5. Transfer Functions of Test Structure.

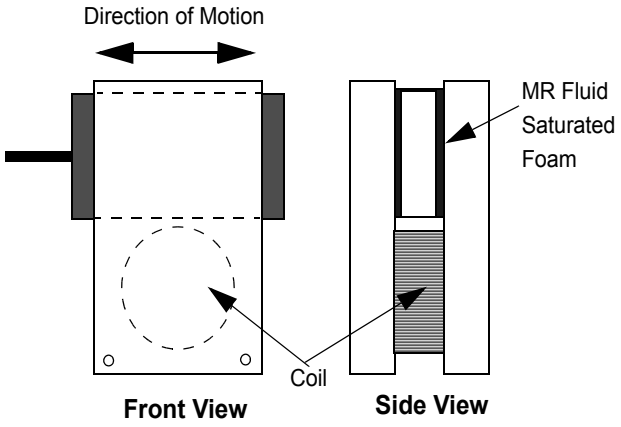

FIGURE 5-6. Schematic Diagram of a Shear Mode MR Damper.

5.3 Identification of Applied MR damper

The MR devices employed in this experiment are shear mode MR dampers, shown schematically in Figure 5-6. The experimental devices were obtained from the Lord Corporation <*http://www.mrfluid.com/*>. The device consists of two steel parallel plates. The dimensions of the device are 4.45×1.91×2.54 cm (1.75×0.75×1.0 in). The magnetic field produced in the device is generated by an electromagnet consisting of a coil at one end of the device. Forces are generated when the moving plate, coated with a thin foam saturated with MR fluid, slides between the two parallel plates.

Power is supplied to the device by a regulated voltage power supply driving a DC to pulse-width modulator (PWM). As a PWM unit, RD-3002 Rheonetic Device Controller (Load Corporation) is used in this study. This PWM unit supplies regulated current to the MR damper at a frequency of 30kHz. The maximum output current is 2 Amps with input voltage of 5 V. Although the relationship between input voltage and output current is linear, there exists a small dead zone in the input voltage, as described in the following section.

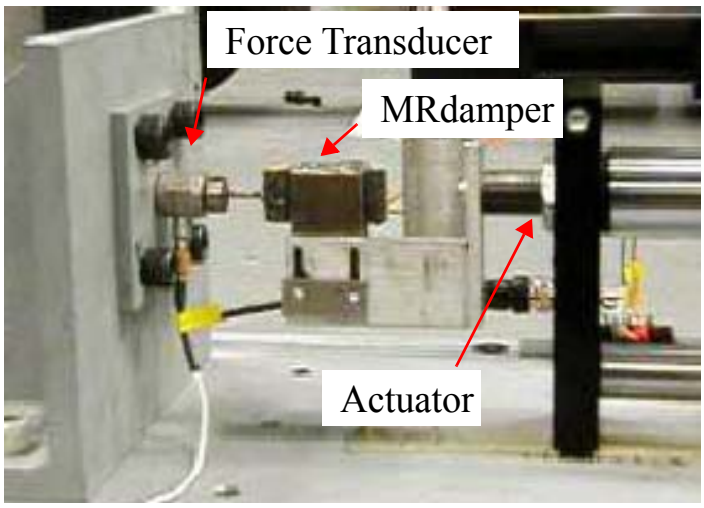

FIGURE 5-7. Photo of Load Frame Test.

The model parameters for this shear mode MR damper had been already identified in previous experiments [60,61]. However, it is necessary to update some parameters of the MR damper model because the MR damper is at a different operating point when it is employed in this study. Additionally, a new PMW unit is used in this study and the relationship between input command voltage and force generated by MR damper will change.

The first step in developing a new set of model parameters is to obtain the characteristics of the MR damper itself. The load frame shown in Figure 5-7 was used to obtain this data. The MR damper is cycled using sinusoidal displacements of 0.318 cm (1/8 in.) and 0.635 cm (1/4 in.) at 3Hz, while various command voltage levels were applied. Representative results for a sinusoidal displacement of 0.635 cm (1/4 in.) are shown in Figure 5-8, including force-displacement and force-velocity loops.

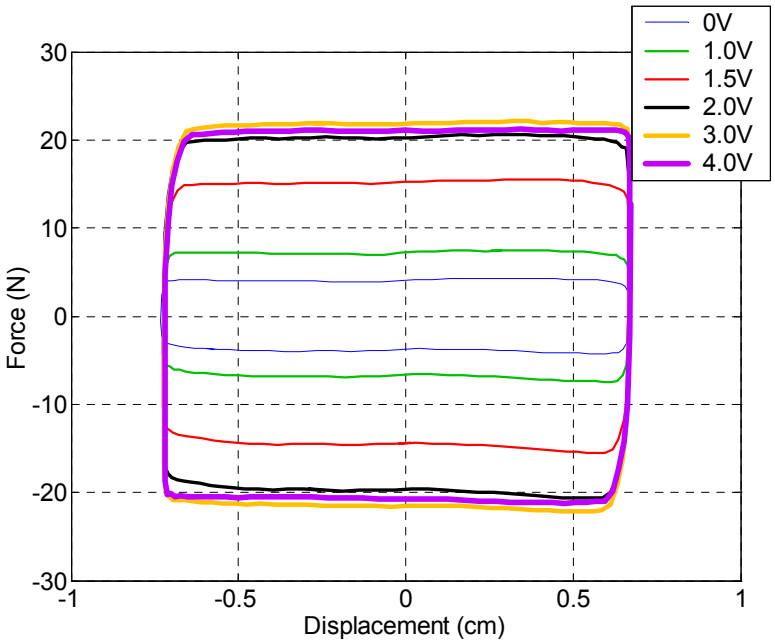

(a) Force-Displacement Hysteresis Loop

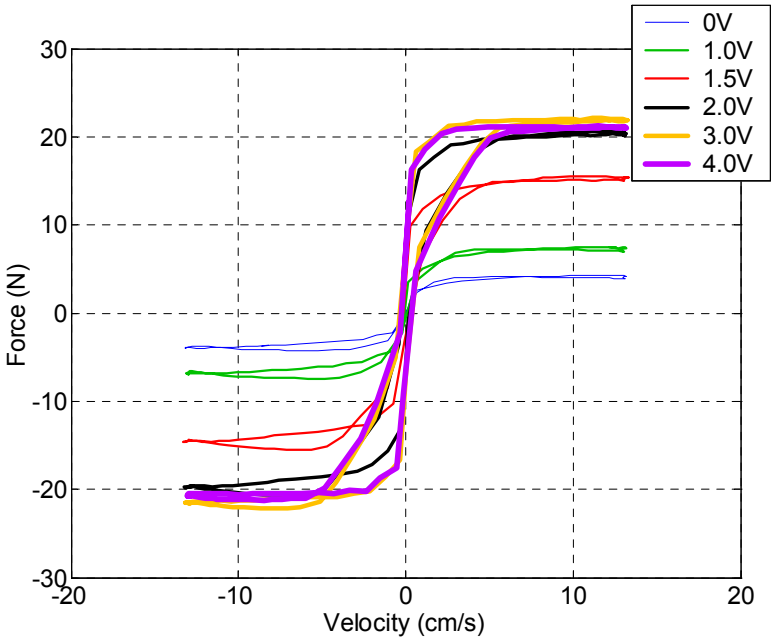

(b) Force-Velocity Hysteresis Loop

FIGURE 5-8. Characteristics of Applied MR damper.

The maximum force generated by this MR damper was found to be about 20–25 N depending on relative velocity across the MR damper with saturation voltage of 2 V. So, in this study, the range of voltage applied to the MR dampers was set to be 0–2 V, and the dynamic range, defined as the ratio of the maximum force with maximum control input of 2 V to the maximum force with minimum 0 V, is approximately 4. Also it was found that the input voltage range 0–0.8 V is determined to be a dead zone, assuming the linear relationship using the data of 1 V and 2 V. This dead zone is taken into account in the program implementing the digital controller within the dSpace environment on the computer.

To identify the new set of model parameters, a series of tests was conducted to measure the response of the system with MR dampers in the test structure due to sinusoidal excitation with the first natural frequency of the test structure and random broadband excitation, while applying voltage of 0V, 1V, and 2V to MR damper. The identified new set of parameters are as follows: $\alpha_a = 13.8$ N/cm, $\alpha_b = 62.1$ N/(cm·V), $c_{0a} = 0.454$ N·sec/cm, $c_{0b} = 0.195$ N·sec/(cm·V), $n = 1$, $A = 12$, $\gamma = 30$ cm^{-1}, $\beta = 30$ cm^{-1}, and $\eta = 80$ sec^{-1}.

The responses of the integrated system model, which is a model of the test structure combined with MR damper, are shown in Figure 5-9. The results are shown for the acceleration outputs of the weak side of the building on each floor and the force applied at the weak side of the building by the MR damper with sinusoidal input excitation at the first natural frequency of the structure (2.68 Hz) and the command voltage to MR dampers of 0 V and 2 V. The identified integrated system model is adequate to represent the experimental system for control design purposes.

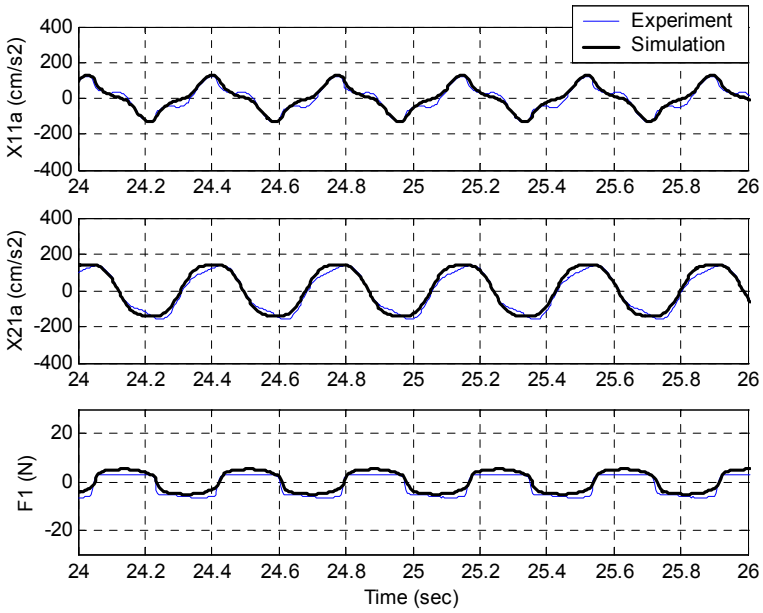

(a) Command Voltage of 0V

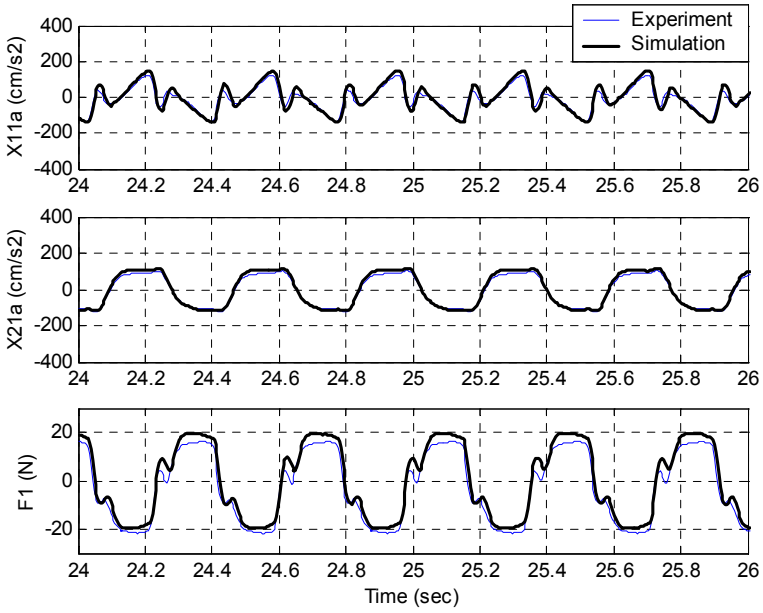

(b) Command Voltage of 2V

FIGURE 5-9. Responses of Integrated System Model (Sinusoidal Excitation at 2.68Hz).

5.4 Design of Nominal Control Algorithm

In this study a clipped-optimal control is chosen as a semiactive control algorithm where H_2/LQG controller is employed as a nominal controller. The feedback measurements included the four accelerations on the structure $\mathbf{y}_m = \left[\ddot{x}_{11}\ \ddot{x}_{12}\ \ddot{x}_{21}\ \ddot{x}_{22}\right]^T$, as well as measurements of the forces provided by the MR damper $f_m = \left[f_1\ f_2\right]^T$.

In the design of the H_2/LQG controller, the ground acceleration input, $\ddot{x}_g$, is taken to be a stationary white noise, and an infinite horizon performance index is chosen as

$$J = \lim_{\tau \to \infty} \frac{1}{\tau} E\left[\int_0^{\tau} \{\mathbf{y}_r{}^T \mathbf{Q} \mathbf{y}_r + \mathbf{f}^T \mathbf{R} \mathbf{f}\} dt\right] \tag{5-9}$$

where $\mathbf{Q}$ and $\mathbf{R}$ are weighting matrices for the vectors of regulated responses $\mathbf{y}_r = \left[\ddot{x}_{11}\ \ddot{x}_{12}\ \ddot{x}_{21}\ \ddot{x}_{22}\right]^T$ and of control forces $f = \left[f_1\ f_2\right]^T$, respectively. For design purposes, the measurement noise vector, $\mathbf{v}$, is assumed to contain identically distributed, statistically independent Gaussian white noise processes, with $S_{\ddot{x}_g \ddot{x}_g} / S_{v_i v_i} = \gamma_g = 25$.

The nominal controller is represented as

$$\dot{\hat{\mathbf{z}}} = (\mathbf{A} - \mathbf{LC})\hat{\mathbf{z}} + \mathbf{L}\mathbf{y}_m + (\mathbf{B} - \mathbf{LD})\mathbf{f}_m \tag{5-10}$$

$$\mathbf{f}_c = -\mathbf{K}\hat{\mathbf{z}} \tag{5-11}$$

where $\mathbf{L}$ is the gain matrix for state estimator and $\mathbf{K}$ is the gain matrix for linear quadratic regulator. For more information on the determination of these gain matrices, see [14] or [61]. As described in the previous chapter, the control force determined using this algorithm is compared to the measured control force, and, using Eq. (2-9), the appropriate control voltage is applied to the control devices.

To design the nominal controller, parametric studies were performed where the weighting matrix $\mathbf{Q}$ for the regulated responses are selected as $\mathbf{Q} = q_1 \cdot diag\left(\begin{bmatrix} 1 & 1 & q_2 & 1 \end{bmatrix}\right)$, while the weighting matrix $\mathbf{R}$ for control forces remains unit values as $\mathbf{R} = diag(\begin{bmatrix} 1 & 1 \end{bmatrix})$. To find the optimal values of q_1 and q_2, the maximum and *rms* acceleration responses are calculated due to both broadband white noise (0–20 Hz) and El Centro earthquake (1940N-S) ground excitations. The El Centro earthquake is scaled by 0.4 in time to cause resonance at the first natural frequency of the test structure. Because the integrated system with MR dampers is nonlinear and the responses depend highly on input excitation level, three different input levels are considered for each input. Maximum accelerations of 100, 200, and 300 (cm/s^2) are chosen for the white noise excitation, and El Centro earthquake is scaled in magnitude by 0.15, 0.3, and 0.45.

The optimal values of q_1 and q_2 are determined as follows. As a first step, q_2 is set as $q_2 = 1$, parametric studies are performed for various values of q_1. The results for the scaled El Centro earthquake are shown in Figure 5-10(a). Similar results are also obtained for the random white noise excitations. From these results, the optimal value is chosen as $q_1 = 0.001$. As a next step, parametric studies are performed for various values of q_2. The results for the scaled El Centro earthquake are shown in Figure 5-10(b)

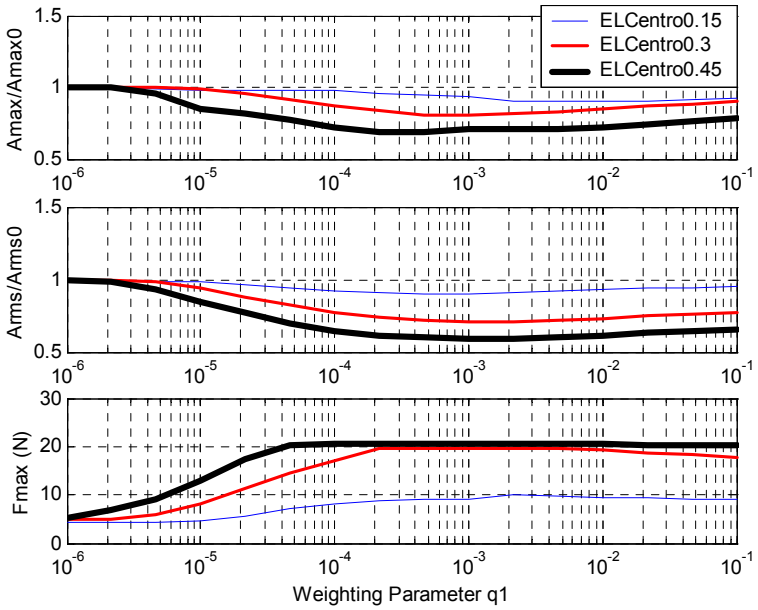

(a) For Weighting Parameter q_1 (q_2=1)

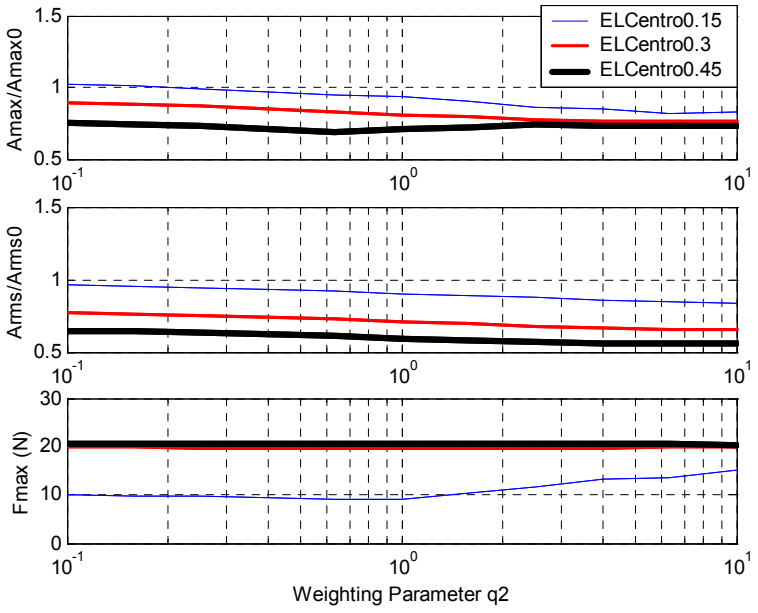

(b) For Weighting Parameter q_2 (q_1=0.001)

FIGURE 5-10. Parametric Study for Weighting Parameter q_1 and q_2 (Scaled El Centro Earthquake).

and similar results are also obtained for the broadband random excitation. Thus, the optimal value is chosen as $q_2 = 3$.

5.5 Experimental Results

To evaluate the performance of this control system on the experimental structure, the test structure was subjected to both historical earthquake inputs and broadband random ground motions. In the first set of tests the shaking table was used to reproduce an El Centro 1940 N-S earthquake. The original earthquake acceleration was scaled by factors of 0.45, 0.3, and 0.15 in magnitude and by a factor of 0.4 in time. A second set of tests was also performed in which a broadband random acceleration (0-20 Hz) with a flat power spectrum in the frequency range of interest was used as the input ground excitation. A compensation procedure was employed here to compensate for the shake table dynamics. Two input levels were considered for the random excitation with maximum acceleration of 250 and 122 cm/sec^2. Three cases were studied for each type of input, including semiactive control with the clipped-optimal controller, passive-off where a constant 0 V was applied to the MR dampers, and passive-on where a constant 2 V was applied to the MR dampers. Note that an optimal constant voltage might be determined for the controller for a given excitation amplitude, but the optimal voltage level is likely to be different for different input amplitudes and characteristics.

5.5.1 Compensation Method for Shake Table Dynamics

It is well known fact that shake tables have their own dynamics, so it is necessary to compensate the original input command to reproduce the intended shake table motion. The shake table in the Structural Control and Earthquake Engineering Laboratory at Washington University has the dynamics shown in Figure 5-11. This figure shows the transfer function from the input command voltage to the acceleration response of the shake table.

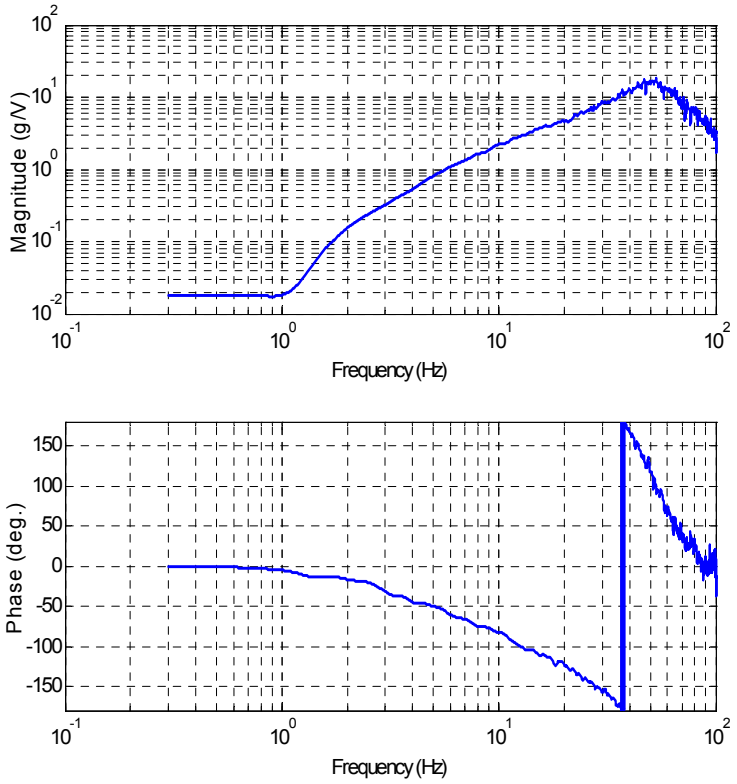

FIGURE 5-11. Dynamics of the Shaking Table.

To compensate for the dynamics of the shake table, the command signal to the shake table was developed by inverting the transfer function of the shake table and thus amplifying the power of the lower frequency signals as needed. A diagram of this procedure is provided in Figure 5-12.

The first step of this procedure is to obtain the transfer function of the shake table by exciting the shake table with the broadband random signal. The transfer function is obtained from the relation between the input signal and the output acceleration response of the shake table.

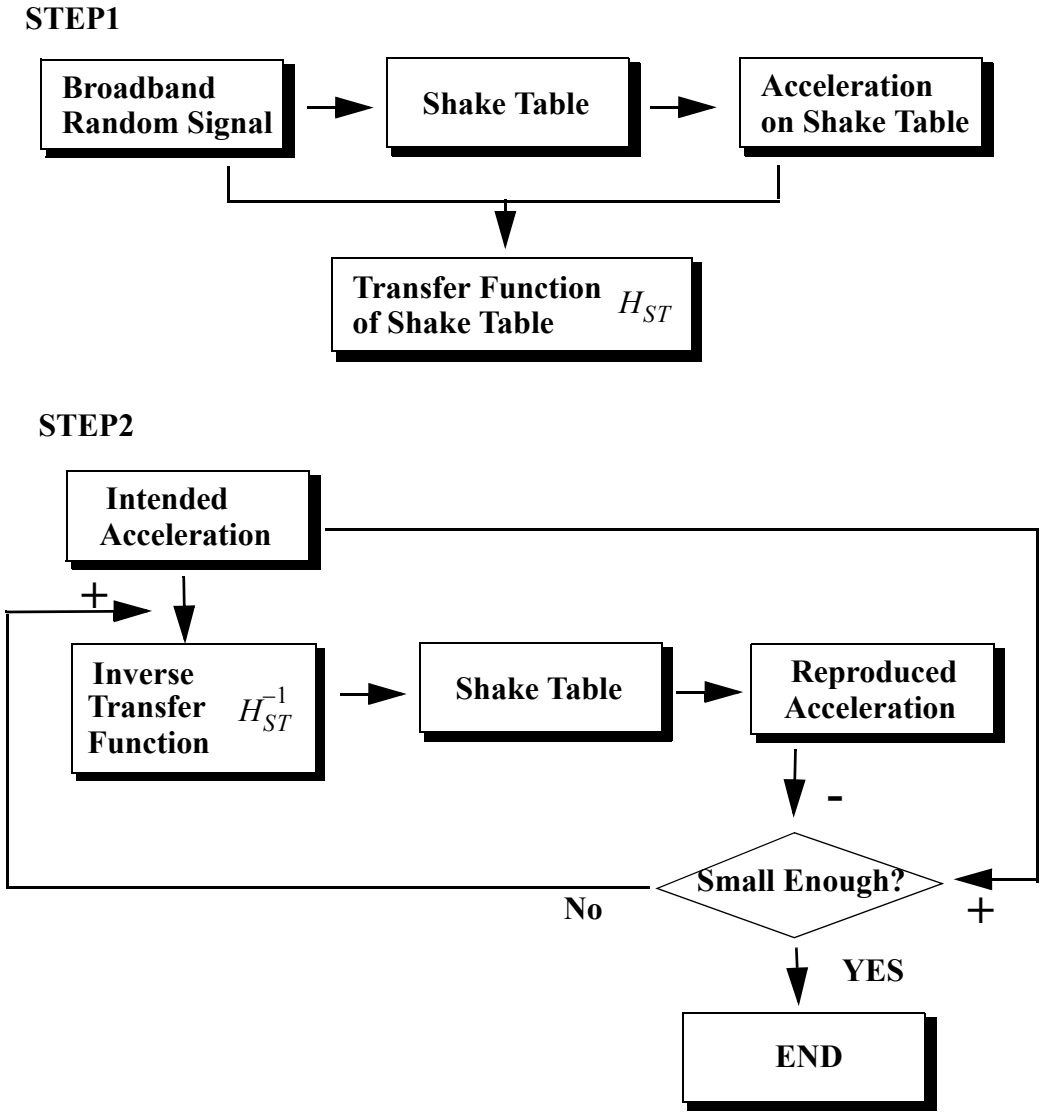

FIGURE 5-12. Flow Chart Describing Compensation Procedure.

The next step is the iteration procedure is to reproduce the intended acceleration of the shake table. The intended acceleration is fed into the inverse transfer function of the shake table, and input to the shake table as a command. The resulting acceleration response of the shake table is compared with the intended acceleration. If the error is not small enough, the difference is added to the command input. This procedure is continued until the intended acceleration is obtained within an acceptable error.

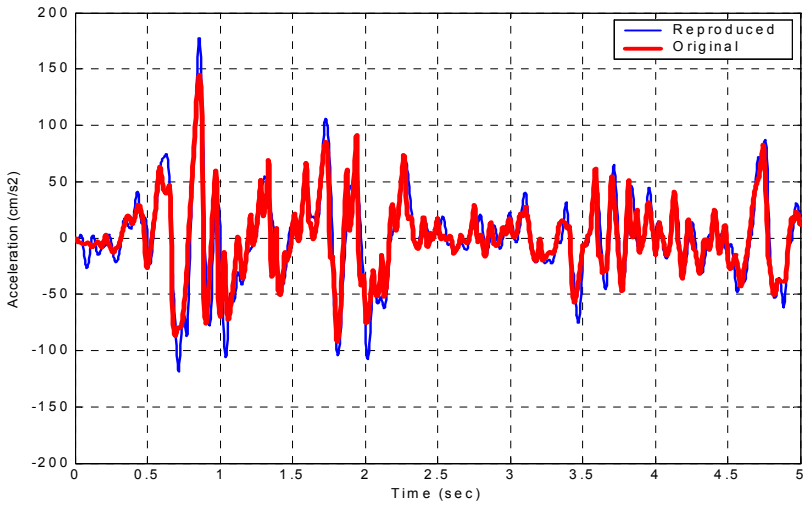

FIGURE 5-13. Typical Reproduced Scaled El Centro Earthquake.

This compensation method was applied to reproduce both a scaled El Centro earthquake and a broadband random excitation with a flat spectrum. Figure 5-13 shows the reproduced scaled El Centro earthquake, which is compared with the original. As shown this figure, good agreement is found between the two. A typical power spectrum of the resulting ground acceleration for broadband random excitation is provided in Figure 5-14. Note that after the compensation procedure is applied, the power spectrum of the ground acceleration is reasonably flat.

5.5.2 Scaled El Centro Earthquake Results

Figures 5-15 through 5-17 shows typical responses of the test structure due to the scaled El Centro earthquakes, including the acceleration response of the weak side on 2FL, which is the maximum among all of the acceleration outputs, and the control force of the MR damper attached to the weak side, which is also the maximum among all of the control forces. In these figures, the experimental results are compared with the simulation

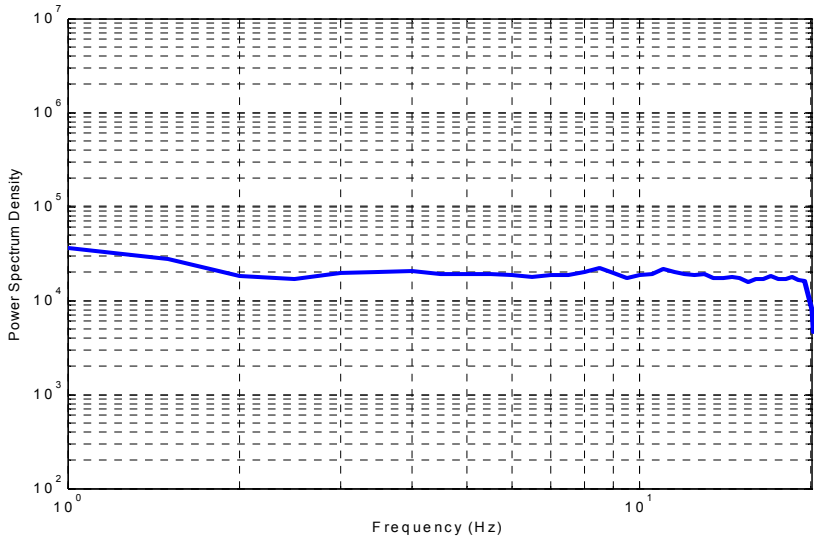

FIGURE 5-14. Typical Power Spectral Density of Broadband Random Ground Motion Using Compensation Procedure.

results for each case. Good agreement is found between the experimental and the simulation results in general.

The experimental responses are provided in Table 5-1. In the case of the large amplitude earthquake, the passive-on control reduces the maximum acceleration of the structure by 28% of the passive-off case, while reducing the *rms* acceleration responses by only 11%. This occurs because the maximum control voltage is applied to the MR dampers at all times in the passive-on tests and the control forces are quite large even after the main event of the earthquake. Thus, the first floor is rigid and the second floor can move freely. However, in the case of the clipped-optimal control, the maximum and *rms* responses can each be reduced to 60% of the passive-off results while using smaller control forces than the passive-on controller. In the case of the medium and small amplitude earthquakes, good control performance cannot be achieved using the passive-on controller and some responses are larger than the passive-off controller. Here the clipped-optimal controller can reduce the maximum accelerations by 28% and 24%, and

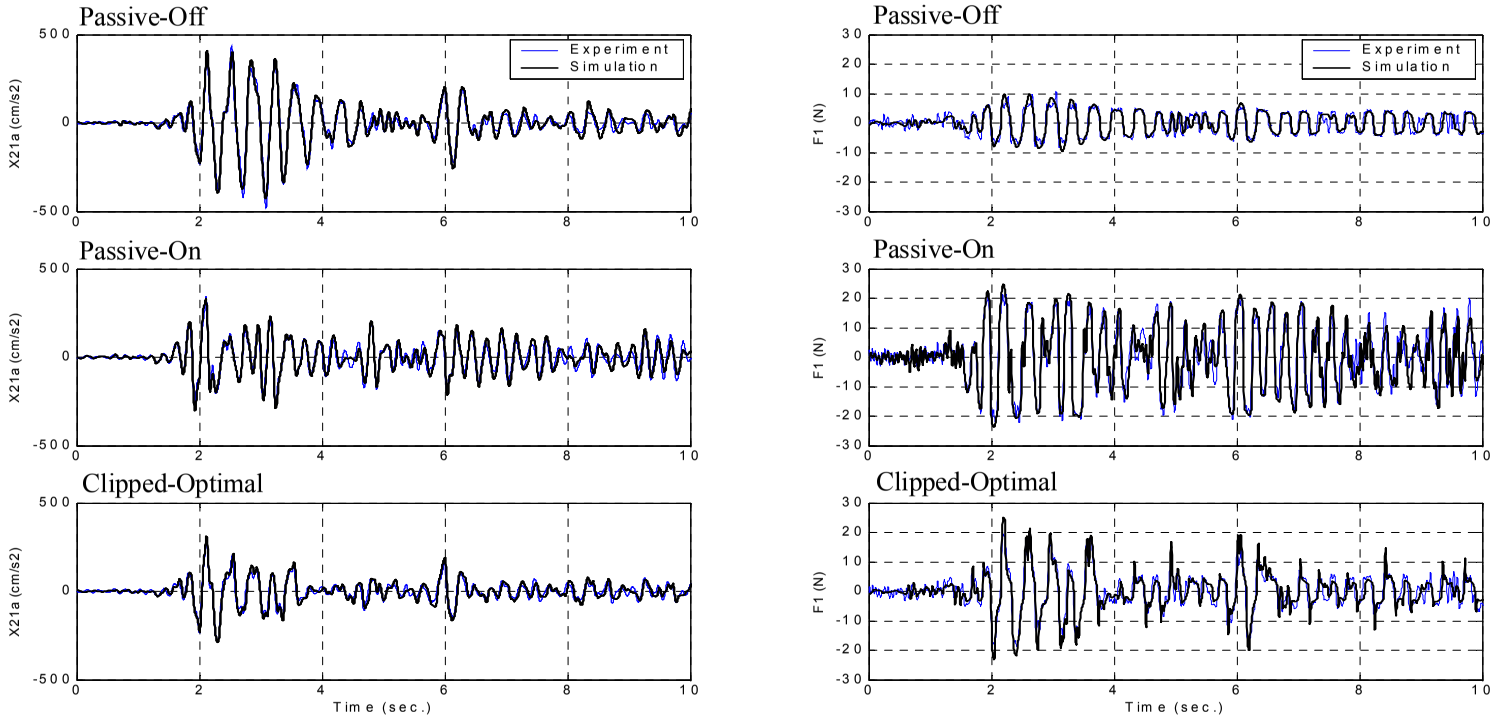

a) Acceleration Responses at Weak Side on 2FL

b) MR Damper Forces at Weak Side on 1FL

FIGURE 5-15. Typical Responses Due to Scaled El Centro Earthquake (0.45 in magnitude).

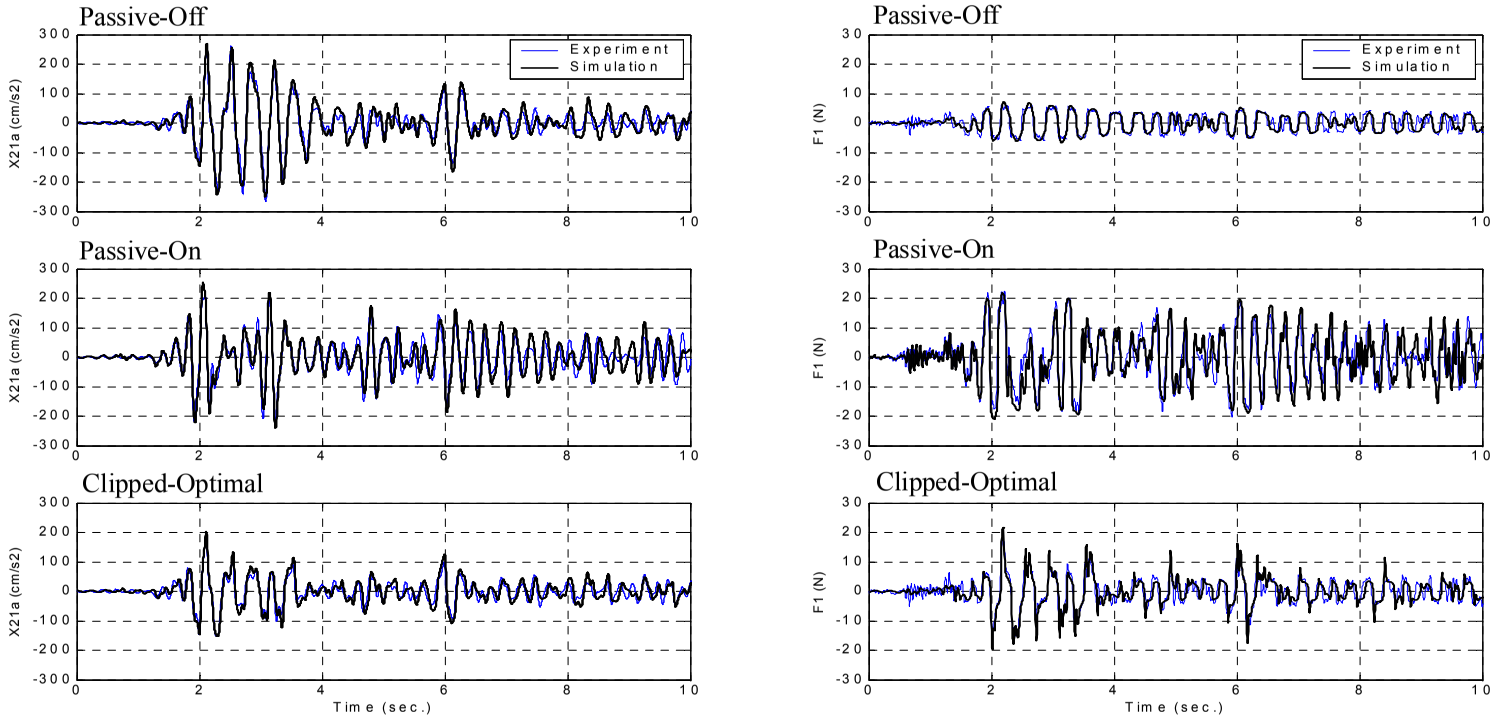

a) Acceleration Responses at Weak Side on 2FL

b) MR Damper Forces at Weak Side on 1FL

FIGURE 5-16. Typical Responses Due to Scaled El Centro Earthquake (0.3 in magnitude).

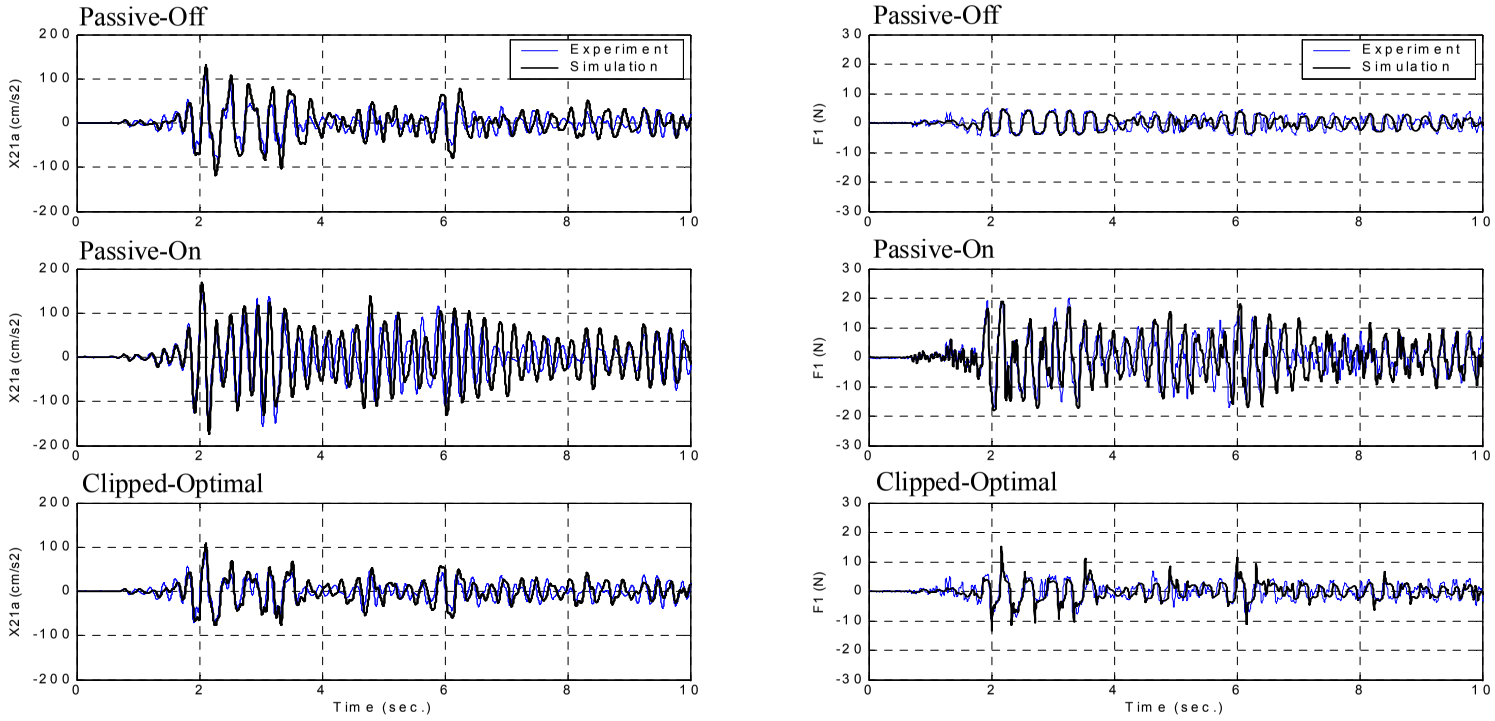

a) Acceleration Responses at Weak Side on 2FL

b) MR Damper Forces at Weak Side on 1FL

FIGURE 5-17. Typical Responses Due to Scaled El Centro Earthquake (0.15 in magnitude).

can reduce the maximum *rms* accelerations by 34% and 7% as compared to the passive-off results.

TABLE 5-1. Maximum and *rms* Responses Due to Scaled El Centro Earthquake.

	Acceleration (cm/s^2)		Control Force (N)	
	Maximum	*rms*	Maximum	*rms*
Large Amplitude Scaled El Centro Earthquake (45%)				
Passive-Off	479	78.9	10.8	3.17
Passive-On	343 (72%)	70.4 (89%)[a]	22.2	8.53
Clipped-Optimal	293 (61%)	46.3 (59%)	19.8	4.87
Medium Amplitude Scaled El Centro Earthquake (30%)				
Passive-Off	267	46.0	5.95	2.64
Passive-On	245 (92%)	54.3 (118%)	22.4	6.87
Clipped-Optimal	191 (72%)	30.5 (66%)	18.1	3.60
Small Amplitude Scaled El Centro Earthquake (15%)				
Passive-Off	123	19.1	4.97	1.98
Passive-On	157 (128%)	42.0 (220%)	19.9	5.38
Clipped-Optimal	93.4 (76%)	17.8 (93%)	9.33	2.34

a. Parenthesis indicate percent of passive-off results.

5.5.3 Broadband Random Excitation Results

Figure 5-18 provides the experimentally obtained power spectral densities of the structural responses due to broadband random acceleration input. The power spectral densities of the weak side accelerations on each floor are shown for the large and small amplitude excitations. Figure 5-18 includes results for the clipped-optimal controller as well as the passive-on and passive-off cases. With the passive-on controller, the response peaks on the first floor are reduced, while another resonant peak is produced in the second floor responses around 4Hz. This result clearly demonstrates that when the passive-on controller is applied, the first floor become rigid and the second floor moves freely. For small amplitude excitations, the magnitude of this resonant peak becomes larger than that of the first mode peak for the passive-off controller. It is also noted that

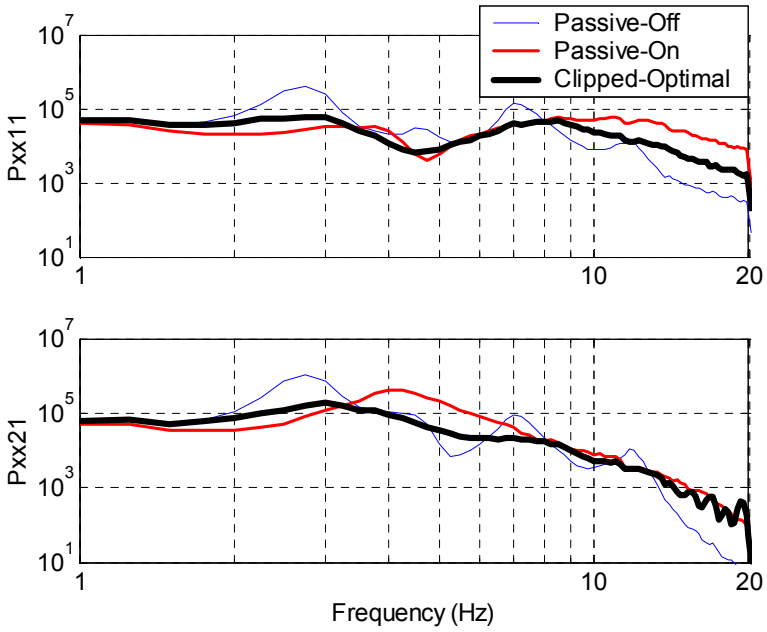

(a) Large Amplitude White Noise Excitation (max=250cm/s^2)

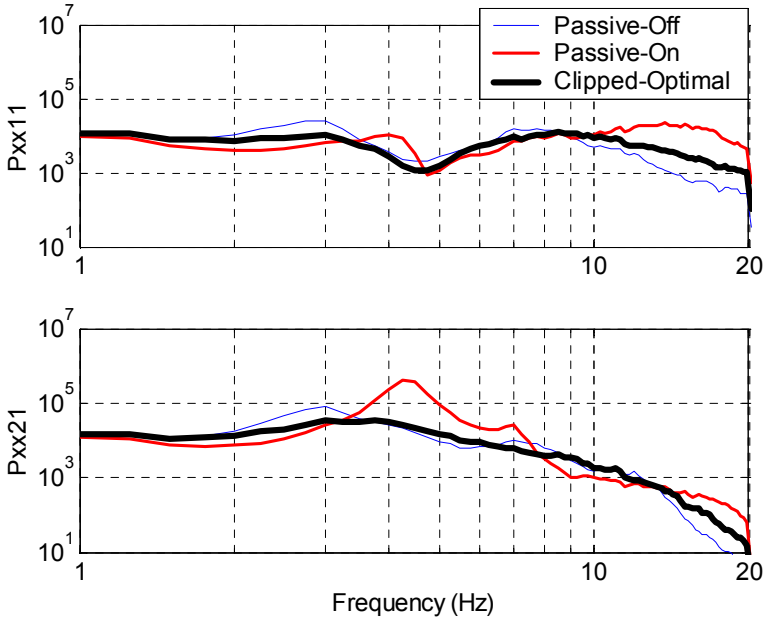

(b) Small Amplitude White Noise Excitation (max=122cm/s^2)

FIGURE 5-18. Power Spectral Densities Due to Random Acceleration Input with a Flat Power Spectrum.

the passive-on controller makes the responses in the higher frequency range larger, especially the responses at the first floor. However, the clipped-optimal controller can reduce the resonant peaks effectively without exciting other modes. This is especially true for the small amplitude excitation in which, even though the passive-off control works well, the clipped-optimal controller achieves higher performance reduction in the system.

The experimental responses due to broadband random excitations are provided in Table 5-2. With the large amplitude excitation, the passive-on control strategy reduces the maximum and *rms* acceleration of the structure by 19% and 9%, respectively. However, with the clipped-optimal controller, the maximum and *rms* responses can each be reduced to 35–37% of the passive-off case. In the case of the smaller amplitude, the clipped-optimal control can reduce the maximum and *rms* responses by 20% and 11% compared to the passive-off case, while the passive-on control increases these responses to 144% and 170% of the passive-off case.

TABLE 5-2. Maximum and *rms* Responses Due to Random White Noise.

	Acceleration (cm/s^2)		Control Force (N)	
	Maximum	*rms*	Maximum	*rms*
Large Amplitude Random White Noise (max=250cm/s^2 *rms*=54cm/s^2)				
Passive-Off	426	95.4	10.6	3.55
Passive-On	347 (81%)	86.4 (91%)[a]	25.3	12.1
Clipped-Optimal	270 (63%)	62.4 (65%)	19.4	6.99
Small Amplitude Random White Noise (max=122cm/s^2 *rms*=26cm/s^2)				
Passive-Off	152	35.7	5.67	2.92
Passive-On	219 (144%)	60.8 (170%)	22.2	8.79
Clipped-Optimal	122 (80%)	31.6 (89%)	12.8	4.16

a. Parenthesis indicate percent of passive-off results.

5.6 Summary

In this chapter, experimental studies were conducted using a 2-story, asymmetric building model with four degrees of freedom. To obtain a control-oriented model of this experimental structure, a new automated procedure was developed to identify a control-oriented model of the system to be controlled. The analytical model of the system was developed based on the structural parameters, and this model was modified to have the frequencies observed in the experimental system. The ERA technique was used to experimentally identify frequencies and mode shapes of the test structure. The parameters for the MR damper model were identified for the integrated system model, which considers the test structure combined with the MR dampers. The obtained integrated system model was found to represent the experimental system well.

The optimal nominal controller was designed through a series of parametric studies. High performance controllers were designed by placing a higher weighting on the acceleration responses of the weak side on the 2nd floor. The experimental results demonstrate that the performance of a semiactive controller using MR dampers is significantly better than passive control system where constant voltages are applied to the MR dampers. When the large constant voltage is applied to the MR damper, the first floor becomes rigid and the second floor can move freely with its own natural frequency, resulting in an increase in the maximum response, especially for small ground excitations. However, when the proposed semiactive controller is applied, all responses of the structure can be effectively reduced at all input amplitudes.

Chapter 6

Application to Full Scale Asymmetric Buildings

This chapter considers the performance of the proposed control system when applied to models of full scale asymmetric buildings. Two full scale buildings are studied. The first case considers a 9-story building with an asymmetric structural plan (denoted Case I). The footprint of this building is rectangular, and the asymmetry is due to the distribution of shear walls. The second case considers an L-shaped, 8-story building with additional vertical irregularity due to setbacks (denoted Case II). Linear, lumped-parameter models of the buildings are employed to evaluate the potential of the control systems to effectively reduce the responses.

In each case a device placement scheme based on genetic algorithms (GA) is used to place the control devices effectively. Each of the proposed control systems is evaluated by simulating the responses of the model due to the El Centro 1940 and the Kobe 1995 earthquake excitations. In Case II, simulations are conducted using a two-dimensional ground motion (North-South and East-West components aligned with the coordinate axes). The performance of the proposed semiactive control systems are compared to that of the ideal active control systems and to that of the passive control systems in which constant voltages are applied to the MR dampers. Multiple earthquake intensities are considered for each case due to the nonlinear nature of the controlled systems.

6.1 Equation of Motion

In general, the equation of motion for an *n*-story, asymmetric building is written

$$\mathbf{M}_s\ddot{\mathbf{x}} + \mathbf{C}_s\dot{\mathbf{x}} + \mathbf{K}_s\mathbf{x} = -\mathbf{M}_s\Gamma\ddot{X}_g + \Lambda\mathbf{f} \tag{6-1}$$

where $\mathbf{x} = \begin{bmatrix} X\ Y\ \Theta \end{bmatrix}^T$. The terms $X = \begin{bmatrix} x_1 \ \ldots \ x_n \end{bmatrix}$ and $Y = \begin{bmatrix} y_1 \ \ldots \ y_n \end{bmatrix}$ are row vectors of the relative displacements of the center of mass of each floor in the x- and y-directions, respectively, and $\Theta = \begin{bmatrix} \theta_1 \ \ldots \ \theta_n \end{bmatrix}$ is the vector of the rotations of each floor about the vertical axis. The disturbance, $\ddot{X}_g = \begin{bmatrix} \ddot{x}_g\ \ddot{y}_g \end{bmatrix}^T$, is a vector of the ground accelerations, and the coefficient matrix is

$$\Gamma = \begin{bmatrix} -1_{n\times 1} & 0_{n\times 1} \\ 0_n & -1_{n\times 1} \\ 0_{n\times 1} & 0_{n\times 1} \end{bmatrix}. \tag{6-2}$$

Also, $\mathbf{f}$ is the vector of control forces, where its coefficient matrix, Λ, is the matrix determined due to the location of control devices.

The mass matrix takes the form

$$\mathbf{M}_s = \begin{bmatrix} \mathbf{M} & 0 & \mathbf{M}_{x\theta} \\ 0 & \mathbf{M} & \mathbf{M}_{y\theta} \\ \mathbf{M}_{x\theta} & \mathbf{M}_{y\theta} & I \end{bmatrix}, \tag{6-3}$$

where $\mathbf{M} = diag\left(\begin{bmatrix} m_1 \ \ldots \ m_n \end{bmatrix}\right)$ is the diagonal $n \times n$ matrix of the masses of each floor, and

$$I = diag\left(\left[I_1 + m_1(L_{CMx1}^2 + L_{CMy1}^2) \ \ldots \ I_n + m_n(L_{CMxn}^2 + L_{CMyn}^2)\right]\right), \tag{6-4}$$

where I_i is the moment of inertia of the *i*th floor, and (L_{CMxi}, L_{CMyi}) are the coordinates of the center of the mass of *i*th floor. The coupling terms in the mass matrix are given by

$$\mathbf{M}_{x\theta} = diag\left(\left[-m_1 L_{CMy1} \ \ldots \ -m_n L_{CMyn}\right]\right), \tag{6-5}$$

$$\mathbf{M}_{y\theta} = diag\left(\left[m_1 L_{CMx1} \ \ldots \ m_n L_{CMxn}\right]\right). \tag{6-6}$$

The stiffness matrix takes the form

$$\mathbf{K}_s = \begin{bmatrix} \mathbf{K}_x & 0 & \mathbf{K}_{x\theta} \\ 0 & \mathbf{K}_y & \mathbf{K}_{y\theta} \\ \mathbf{K}_{x\theta} & \mathbf{K}_{y\theta} & \mathbf{K}_{\theta} \end{bmatrix}, \tag{6-7}$$

where

$$\mathbf{K}_x = \begin{bmatrix} k_{x1} + k_{x2} & -k_{x2} & 0 & 0 \\ -k_{x2} & \ldots & \ldots & 0 \\ 0 & \ldots & \ldots & -k_{xn} \\ 0 & 0 & -k_{xn} & k_{xn} \end{bmatrix}, \tag{6-8}$$

$$\mathbf{K}_y = \begin{bmatrix} k_{y1}+k_{y2} & -k_{y2} & 0 & 0 \\ -k_{y2} & \cdots & \cdots & 0 \\ 0 & \cdots & \cdots & -k_{yn} \\ 0 & 0 & -k_{yn} & k_{yn} \end{bmatrix}, \tag{6-9}$$

and

$$\mathbf{K}_\theta = \begin{bmatrix} k_{\theta 1}+k_{\theta 2} & -k_{\theta 2} & 0 & 0 \\ -k_{\theta 2} & \cdots & \cdots & 0 \\ 0 & \cdots & \cdots & -k_{\theta n} \\ 0 & 0 & -k_{\theta n} & k_{\theta n} \end{bmatrix}. \tag{6-10}$$

Here k_{xi}, k_{yi}, and $k_{\theta i}$ correspond to the stiffnesses of the *i*th floor in the x-, y-, and θ-directions, respectively. The coupling terms in the stiffness matrices are written

$$\mathbf{K}_{x\theta} = \begin{bmatrix} k_{x\theta 1}+k_{x\theta 2} & -k_{x\theta 2} & 0 & 0 \\ -k_{x\theta 2} & \cdots & \cdots & 0 \\ 0 & \cdots & \cdots & -k_{x\theta n} \\ 0 & 0 & -k_{x\theta n} & k_{x\theta n} \end{bmatrix} \tag{6-11}$$

and

$$\mathbf{K}_{y\theta} = \begin{bmatrix} k_{y\theta 1}+k_{y\theta 2} & -k_{y\theta 2} & 0 & 0 \\ -k_{y\theta 2} & \cdots & \cdots & 0 \\ 0 & \cdots & \cdots & -k_{y\theta n} \\ 0 & 0 & -k_{y\theta n} & k_{y\theta n} \end{bmatrix} \tag{6-12}$$

where $k_{x\theta i} = -k_{xi}L_{yi}$, $k_{y\theta i} = k_{yi}L_{xi}$, where (L_{xi} , L_{yi}) are the coordinates of the center of rigidity in the *i*th floor.

6.2 Design of the Nominal Controller

Two types of semiactive control algorithms are employed in this study. The original clipped-optimal controller and the modified clipped-optimal controller, are used for controlling the MR dampers. An H_2/LQG control algorithm is employed for design of the nominal controller in both algorithms.

The H_2/LQG controller is designed by selecting a vector of regulated responses, $\mathbf{y}_r$, containing both x- and y-components of the acceleration on each floor *i.e.*,

$$\mathbf{y}_r = \left[\ddot{x}_{a11} \ \ldots \ \ddot{x}_{aij} \ \ldots \ \ddot{x}_{an2} \ \ddot{y}_{a11} \ \ldots \ \ddot{y}_{aij} \ \ldots \ \ddot{y}_{an2}\right]^T \tag{6-13}$$

for $i = 1 \ldots n$, and $j = 1, 2$, where $\ddot{x}_{ai1}$ is the x-component of the acceleration at one side on *i*th floor, $\ddot{x}_{ai2}$ is the acceleration at the other side on *i*th floor, $\ddot{y}_{ai1}$ is the y-component of the acceleration at one side on *i*th floor, and $\ddot{y}_{ai2}$ is the acceleration at the other side on *i*th floor. The weighting matrix $\mathbf{Q}$ corresponding to the regulated output vector, $\mathbf{y}_r$, is $\mathbf{Q} = a \cdot diag([\mathbf{1}_{1\times nm}])$, while the weighting matrix $\mathbf{R}$ corresponding to the control force vector $\mathbf{f}$ remained as $\mathbf{R} = diag\left(\left[n_{11}{}^2 \ \ldots \ n_{ij}{}^2 \ \ldots \ n_{n2}{}^2\right]\right)$, where n_{ij} is number of devices employed at *j*th location on *i*th floor. This approach will result in equal weighting on the forces of each control device location.

6.3 Optimal Placement of Control Devices

One important and challenging issue in controlling the coupled lateral and torsional responses of an asymmetric structure is the placement of control devices. In the case of a symmetric building, the control performance is primarily dependent on the floor at

which the control device is placed, and the specific location within the floor is not a critical parameter for control design. That is, the building is symmetric and the center of mass and rigidity coincide, so the control devices should be distributed symmetrically about this point (with due consideration to both the load capacity at the attachment points and the intended purpose of the area within the floor). However, in the case of asymmetric buildings, not only the floor but also the placement within the floor is fundamental to the control system performance. Thus, the number of the combinations of device placement is significantly larger than for symmetric buildings.

In recent years in the field of optimization, evolutionary techniques such as genetic algorithms (GA) have become popular for complex, discrete optimization problems that involve, and have the potential for a large number of local minima. GAs function by simulating the process of natural selection ("survival of the fittest"). They have shown promise in determining the optimal sensor and actuator placement in the civil structures [1,32,42,43].

In GAs, the parameters to be optimized are coded into a genetic string known as a chromosome. Each of these chromosomes has an associated fitness value, which is based, in general, on an appropriate mathematical combination of the performance criteria that the designer is interested in. The designer sets the population size, which is comprised of different chromosomes. In each generation, the fitness of each chromosome is determined, and a new generation is developed by combining features of chromosomes with the highest fitness values. The GA proceeds by reproducing only the fittest chromosomes in the next generation. The goal is to find new chromosomes with increasing fitness, resulting in increasing the average fitness of each successive generation. GAs use three basic operations to produce the next generation, selection, cross-over, and mutation. Selection is the process of choosing the fittest chromosome from the current population. Cross-over is the process by which new chromosomes are generated from individual strings in the current generation by cutting each chromosome at a random

location and replacing the tail with that of another chromosome. Mutation is the random process by which values of elements in a chromosome are changed randomly.

In this study, each chromosome has *n* integer elements, where *n* is the number of control devices installed in a building, and the element represents the location of each control device. For example if 9 control devices are placed in the structure, the chromosomes would have 9 elements. If there are a total of 45 possible locations for the control devices to be installed, each element in the chromosome (vector) has an integer value between 1 and 45, such as

$$Chromosome = \left[6\ 11\ 16\ 20\ 21\ 22\ 26\ 30\ 31\right]. \tag{6-14}$$

Herein, the fitness of each chromosome is determined based on a mathematical combination of the actively controlled responses of the structure for a white noise disturbance. Specifically, in this study, the response of interest is selected to be the maximum of the *rms* absolute acceleration of the structure, determined using the Lyapunov equation. The fitness function is

$$A_{max} = \max_{i,j} \left(\left|\ddot{x}_{aij}\right|\right) \qquad i = 1 \ldots n, \quad j = 1, 2 \tag{6-15}$$

where $\ddot{x}_{aij}$ is the *j*th absolute acceleration on *i*th floor. Also, the maximum interstory drift D_{max} is observed to ensure that this response is not adversely effected while reducing the accelerations. This performance function is given by

$$D_{max} = \max_{i,j} \left(\left|d_{ij}\right|\right) \qquad i = 1 \ldots n, \quad j = 1, 2 \ . \tag{6-16}$$

where d_{ij}, is the *j*th interstory drift on *i*th floor.

The GA codes using in this analysis are implemented in MATLAB ([38]; See *http://www.geatbx.com/*).

6.4 Evaluation Criteria

In each of the two cases to be considered herein, the performance of the proposed semiactive control system applied to the full scale building models is evaluated by calculating the responses due to earthquake excitations. Because application of the semiactive control system results in a nonlinear system, the amplitude of the earthquakes are varied. The El Centro earthquake (1940) and the Kobe earthquake (1995) are used. The El Centro earthquake is scaled in magnitude by factors of 0.5, 1.0 and 1.5, and are denoted El Centro 0.5, El Centro 1.0, and El Centro 1.5, respectively. The Kobe earthquake is scaled in magnitude by factors of 0.5 and 1.0, and are denoted Kobe 0.5 and Kobe 1.0, respectively. A total of five earthquake records are employed.

Five separate control systems are studied: passive-off, passive-on, original clipped-optimal control, modified clipped-optimal control, and ideal active control. The passive-off and the passive-on controllers correspond to the situations in which a constant zero voltage or a maximum voltage is applied to the MR dampers, respectively. The clipped-optimal and the modified clipped-optimal controllers correspond to the semiactive control systems using MR dampers, denoted MR-OCO and MR-MCO, respectively. The ideal active controller employs an active control system which can apply ideal control forces to the building. Note that the nominal H_2/LQG controller for the semiactive control systems and the ideal active control system are identical.

To evaluate the control performance quantitatively, five nondimensional evaluation criteria are defined as follows:

- Maximum Interstory Drift: $J_1 = \dfrac{\max\limits_{t,i,j} |d_{ij}(t)|}{d^{\max}}$
- Maximum Acceleration: $J_2 = \dfrac{\max\limits_{t,i,j} |\ddot{x}_{aij}(t)|}{\ddot{x}_a{}^{\max}}$
- Normed Interstory Drift: $J_3 = \dfrac{\max\limits_{t,i,j} \|d_{ij}(t)\|}{\|d^{\max}\|}$
- Normed Acceleration: $J_4 = \dfrac{\max\limits_{t,i,j} \|\ddot{x}_{aij}(t)\|}{\|\ddot{x}_a{}^{\max}\|}$
- Maximum Control Force: $J_5 = \dfrac{\max\limits_{t,i} |f_i(t)|}{W}$

Note that the first four evaluation criteria are normalized by the corresponding uncontrolled responses of the structure, and the fifth evaluation criteria corresponding to the maximum control force is normalized by the total weight of the building.

6.5 Case I: 9-Story, Plan-Irregular Building

6.5.1 Description of the Building

Case I of this dissertation considers a 9-story building subjected to one dimensional seismic excitation. This building is a office building designed and constructed in Japan before the new building code in Japan has been enforced. A project for retrofitting this building to agree with the new building code has been planned and successfully completed. The building is 34.4 m (113 ft) by 25.6 m (84 ft) in plan and 40.25 m (132 ft) in elevation. The main structural system of this building is steel reinforced concrete (SRC). The plan of this structure is shown in Figure 6-1. Dimensions are given in millimeters.

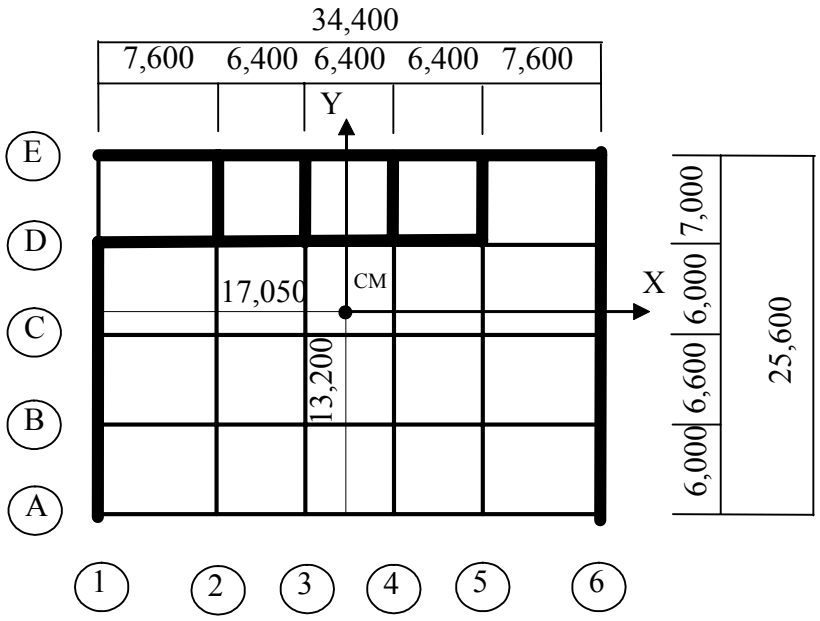

FIGURE 6-1. Plan of 9-Story Asymmetric Building.

On each floor there are five bays in the x-direction and four bays in the y-direction. The important feature of this building is that the distribution of shear walls makes this structure behave asymmetrically, coupling the lateral and torsional motions.

A linear, lumped-parameter model of this building is developed. The columns and beams of this building are modeled as reinforced concrete (RC), where the contribution of the steel members is taken into account as equivalent steel bars. Each shear wall is modeled as three RC columns, where the center column resists moments and shear forces and the two side columns resist only the vertical loads assuming pin connections at the ends. A nonlinear analysis of this structure was performed by Obayashi Corporation, Technical Research Institute [35]. Here a bilinear hysteresis model was used for the RC members and a static pushover analysis was performed to obtain the shear force-story drift diagrams for each frame. The three-dimensional model of this structure is shown in Figure 6-2. From the results of that analysis, a linear stiffness coefficient of

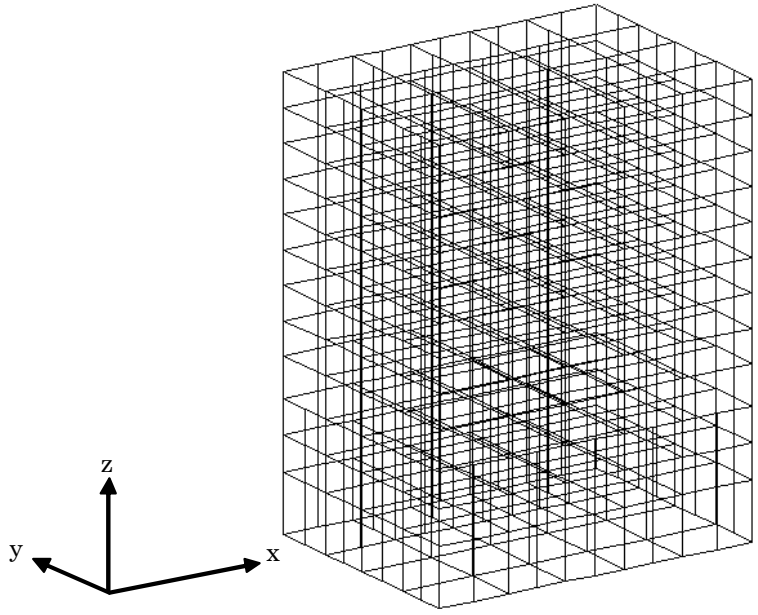

FIGURE 6-2. Three-Dimensional Model of the 9-Story Asymmetric Building.

each frame is estimated assuming linearity between the origin and the yielding point. The stiffness of each frame obtained using this approach is provided in Table 6-1 and 6-2 along with the mass and moment of inertia of each floor. The first two calculated natural frequencies are 0.83 Hz (translation), and 1.29 Hz (torsion). The damping is assumed to be 2% for all modes of the structural model.

TABLE 6-1. Structural Parameters (x-direction).

Story i	Weight W_i (kN)	Inertia I_i (kNcm^2)	Radius of Gyration r_i (cm)	Initial Stiffness k_{xij} (kN/cm)				
				Frame A	B	C	D	E
				Coordinate L_y = -1320(cm)	-720	-60	540	1240
9	15556	2.50E+10	1268.1	833.3	783.8	677.0	3163	3749
8	10198	1.64E+10	1268.1	863.3	859.6	807.5	3794	5192
7	10118	1.63E+10	1268.1	901.2	802.6	750.1	3527	5428
6	10205	1.64E+10	1268.1	976.9	932.7	905.1	3530	5387
5	10295	1.66E+10	1268.1	1053	1021	984.9	3677	5521
4	10294	1.66E+10	1268.1	1208	1122	1092	3895	5866
3	10382	1.67E+10	1268.1	1208	1257	1255	4028	7425
2	10470	1.68E+10	1268.1	1485	1478	1443	4240	7655
1	10983	1.77E+10	1268.1	1852	1886	1792	4651	8128

Story i	Total Stiffness k_{xi} (kN/cm)	Torsional Stiffness $k_{\theta i}$ (kNcm/rad)	Natural Frequency Ratio $\omega_{\theta i}/\omega_{xi}$	Eccentricity e_{yi} (cm)	Eccentricity ratio e_{yi}/r_i	Eccentricity ratio e_{yi}/L
9	9206	2.65E+10	1.337	505.3	0.398	0.197
8	11516	3.07E+10	1.288	580.0	0.457	0.227
7	11408	3.25E+10	1.333	598.0	0.472	0.234
6	11731	3.32E+10	1.328	560.0	0.442	0.219
5	12257	3.48E+10	1.329	542.3	0.428	0.212
4	13182	3.83E+10	1.344	524.1	0.413	0.205
3	15172	4.35E+10	1.335	580.6	0.458	0.227
2	16301	4.63E+10	1.328	531.9	0.419	0.208
1	18309	5.34E+10	1.347	474.1	0.374	0.185

TABLE 6-2. Structural Parameters (y-direction).

Story i	Weight W_i (kN)	Inertia I_i (kNcm^2)	Radius of Gyration r_i (cm)	Initial Stiffness k_{yij} (kN/cm)					
				Frame 1	2	3	4	5	6
				Coordinate L_x = -1705 (cm)	-945	-305	335	975	1735
9	15556	2.50E+10	1268.1	2768	1308	1233	1129	905.9	2520
8	10198	1.64E+10	1268.1	2370	1327	1278	1185	1137	3408
7	10118	1.63E+10	1268.1	2554	1305	1268	1211	1097	3770
6	10205	1.64E+10	1268.1	2622	1313	1281	1242	1157	3859
5	10295	1.66E+10	1268.1	2784	1358	1337	1296	1230	4036
4	10294	1.66E+10	1268.1	3127	1444	1420	1390	1332	4481
3	10382	1.67E+10	1268.1	3428	1650	1631	1604	1539	4949
2	10470	1.68E+10	1268.1	3662	1857	1799	1773	1716	5179
1	10983	1.77E+10	1268.1	4899	2107	2071	2404	2324	5495

Story i	Total Stiffness k_{yi} (kN/cm)	Torsional Stiffness $k_{\theta i}$ (kNcm/rad)	Natural Frequency Ratio $\omega_{\theta i}/\omega_{yi}$	Eccentricity e_{xi} (cm)	Eccentricity ratio e_{xi}/r_i	Eccentricity ratio e_{xi}/L
9	9863	2.65E+10	1.291	-70.73	-0.056	-0.0206
8	10706	3.07E+10	1.336	161.9	0.128	0.0471
7	11205	3.25E+10	1.345	182.2	0.144	0.0530
6	11473	3.32E+10	1.343	186.2	0.147	0.0541
5	12041	3.48E+10	1.341	182.6	0.144	0.0531
4	13193	3.83E+10	1.343	182.6	0.144	0.0531
3	14801	4.35E+10	1.352	184.0	0.145	0.0535
2	15985	4.63E+10	1.341	169.3	0.134	0.0492
1	19299	5.34E+10	1.312	84.41	0.067	0.0245

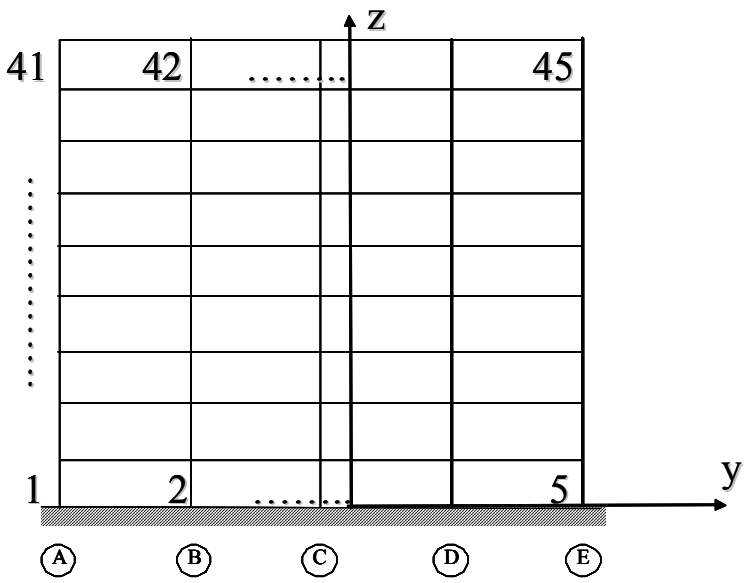

FIGURE 6-3. Potential Locations for Control Devices.

6.5.2 Optimal Control Device Placement and Design of Controller

The next step in the design of the controllers for this structure is to optimally place control devices using genetic algorithms. The acceleration responses at Frame A and Frame E on 3FL, 6FL, and 9FL, total 6 acceleration responses, are used as feedback signal for the controller. Potential locations for control devices to be installed are within each frame on each floor, for a total of 45 possible locations in the structure, as shown in Figure 6-3. A maximum of 9 control device locations are to be selected from these 45. Thus, to perform the optimization, the chromosome is defined as a vector with 9 elements. Each element is associated with a potential control device location and has an integer value between 1 and 45. The population size in each generation is selected to be 120.

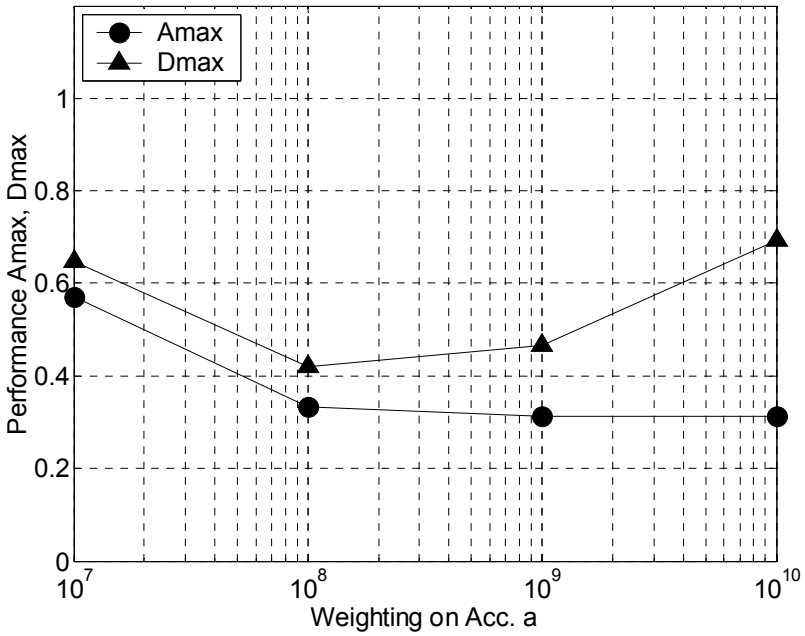

FIGURE 6-4. Performance of the GA Results.

Genetic algorithms are applied to find the optimal control device location for a range of constant weighting values, a , that are found to be appropriate for this structure. The performance of each weighting case is shown in Figure 6-4. The corresponding optimal placements for the actuators are schematically shown in Figure 6-5. Note that there is a trade-off between reducing the maximum *rms* absolute acceleration and reducing the maximum *rms* interstory displacement. As the weighting increases, the acceleration continues to decrease, while the displacements tend to increase above a value of $a = 10^8$. From these results, a weighting of $a = 10^8$ is found to be optimal to reduce both absolute acceleration and interstory drift, and is used to design the subsequent controllers for this structure. The corresponding optimal control device locations are shown in Figure 6-5.

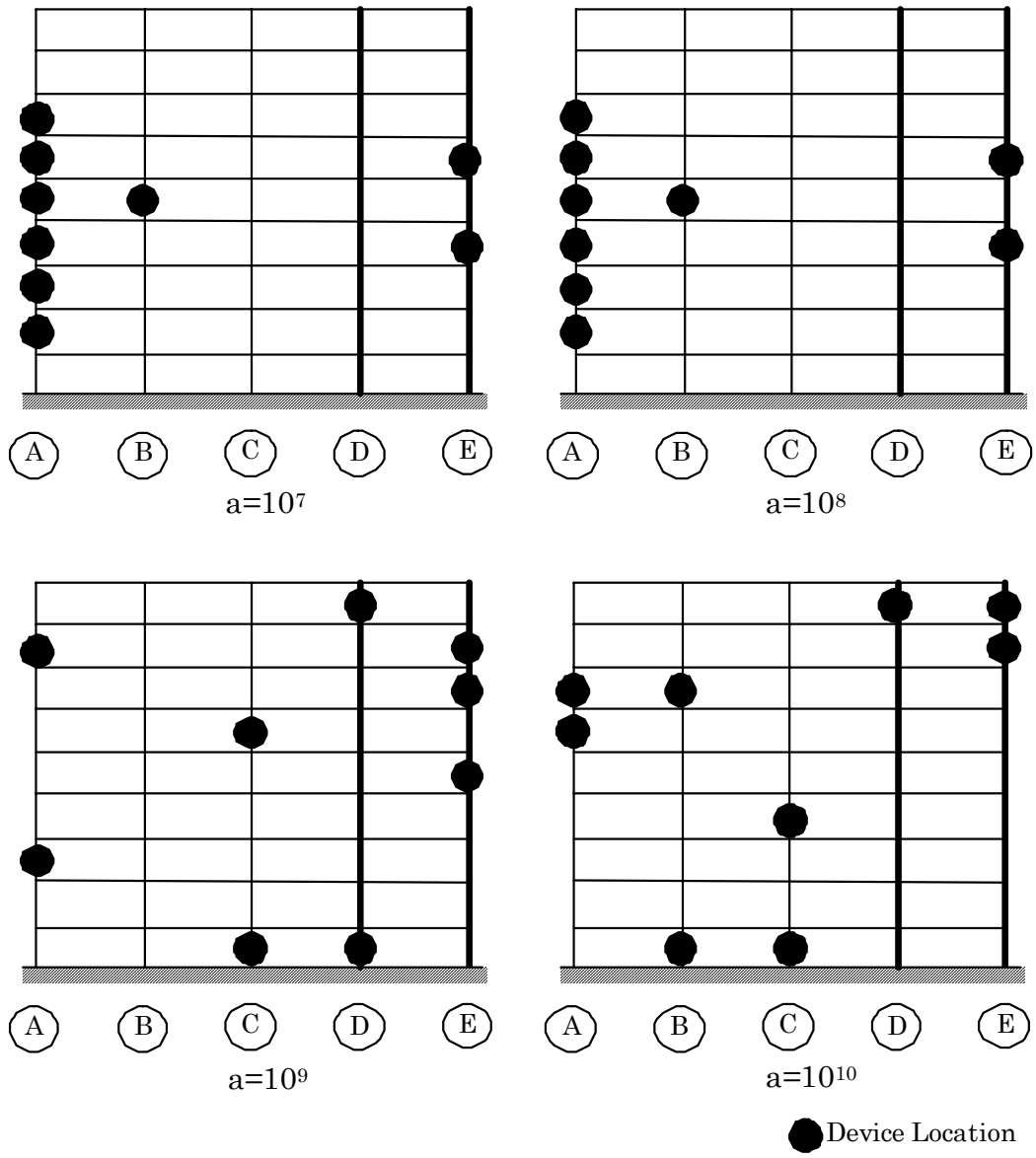

FIGURE 6-5. Optimal Device Locations.

Representative transfer functions from the input ground acceleration to the absolute accelerations of the structure for the ideal active control system with this optimal design are shown in Figure 6-6. The transfer functions corresponding to each side of 3FL, 6FL, and 9FL are provided. The damping ratios are increased to 13%, 9%, and 28% for the first three natural modes, respectively.

To determine the control forces required to realize this control design, earthquake responses are simulated. Among the earthquakes used in this study, the Kobe 1995 N-S is selected because this earthquake requires the largest forces. Using the total control force required at each control device location to realize the performance, the number of control devices which have a capacity of 1,000kN are determined. The results are shown in Table 6-3. A total of 110 devices are used.

TABLE 6-3. Location and Number of Control Devices.

Floor	2	3	4	4	5	5	6	6	7
Frame	A	A	A	E	A	B	A	E	A
No.	11	11	11	13	12	11	13	14	14

6.5.3 Response Due to Earthquake Excitation

To demonstrate the performance of the proposed semiactive control system on the real scale asymmetric building, the responses due to earthquake exactions are calculated. North-South component is used for both El Centro and Kobe earthquake. Representative time history responses are shown in Figure 6-7 through 6-16. These plots correspond to the absolute acceleration responses of the weak side (at Frame A) and the strong side (at Frame E) on 9FL as well as control forces of the weak side (at Frame A) and the strong side (at Frame E) on 6FL. The results for the uncontrolled system, passive-on controller,

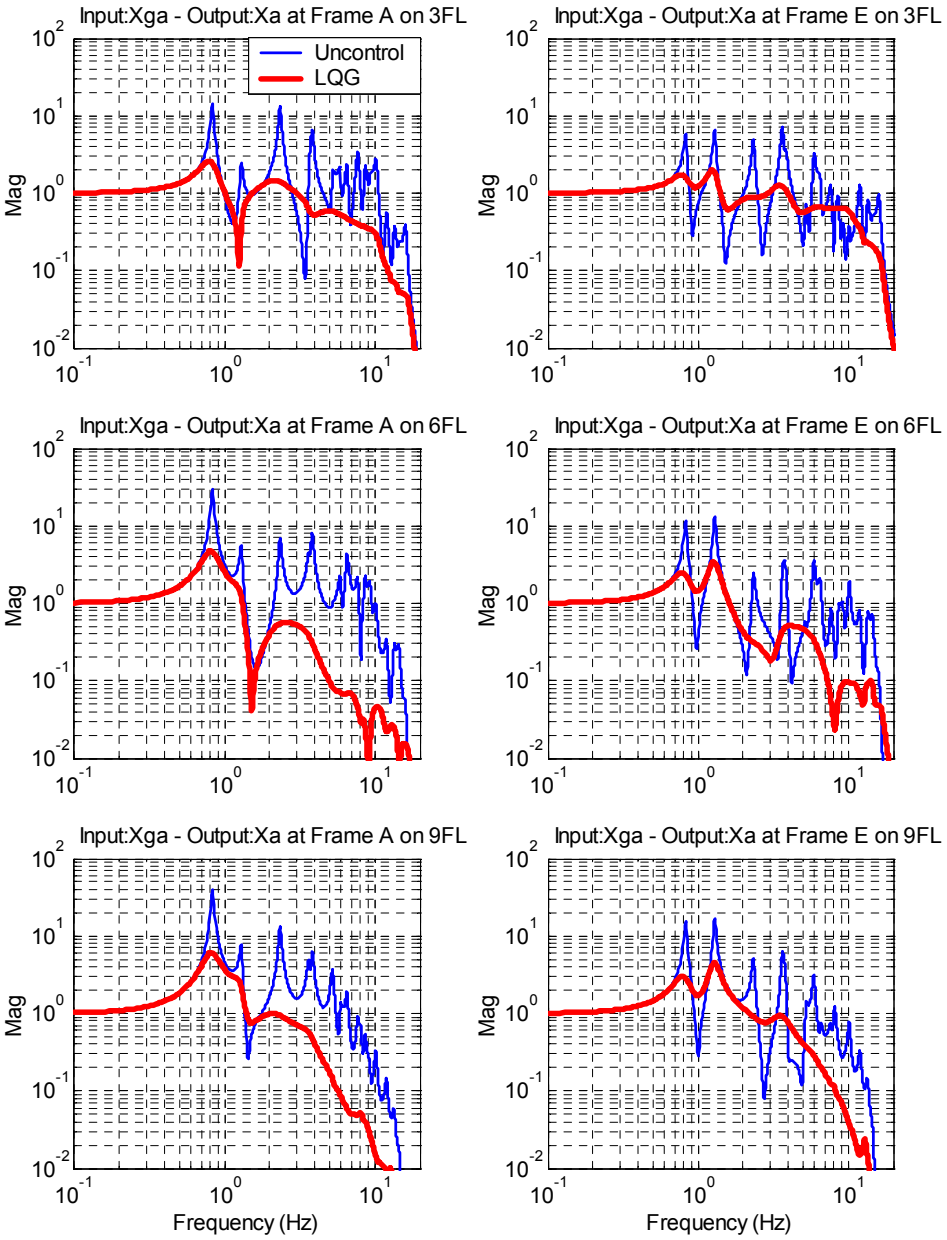

FIGURE 6-6. Representative Transfer Functions.

ideal active controller, and semiactive clipped-optimal controller (with MR dampers) are shown.

According to these time history results, the passive-on system can only reduce the acceleration of the weak side (Frame A) on 9FL, while the acceleration of the strong side (Frame E) is not effectively reduced or even increased in some cased such as El Centro 0.5, 1.0 and Kobe 0.5. However, with the ideal active and the semiactive control systems, the acceleration of both sides on 9FL is effectively reduced. The results of the semiactive controller are as good as the ideal active controller. It is also noted that the control force used for the passive-on controller is clearly larger than those used for the semiactive and the ideal active controller. So, it is concluded that the semiactive and ideal active controller can reduce the responses due to various earthquake excitations with appropriate control forces.

Numerical values corresponding to the five evaluation criteria defined for this problem are shown in Table 6-4 for all control designs considered. From these results, it is observed that the passive-off system does not achieve significant response reduction, and the modified clipped-optimal control performs similarly to the original clipped-optimal control.

To more easily examine the performance of the other three control systems, passive-on, ideal active control, and original clipped-optimal control, in detail, the graphical representation of evaluated responses are shown in Figure 6-17. First note the comparison between the semiactive clipped-optimal controller and the ideal active controller. In general, the clipped-optimal control system achieves a performance similar to that of the ideal active controller. The clipped-optimal controller reduces both the maximum interstory drift and the maximum acceleration by 40–45% for the 1940 N-S El Centro earthquakes, and by 35–40% for 1995 N-S Kobe earthquakes. In most cases, the ideal active controller achieves a modest improvement over the clipped-optimal

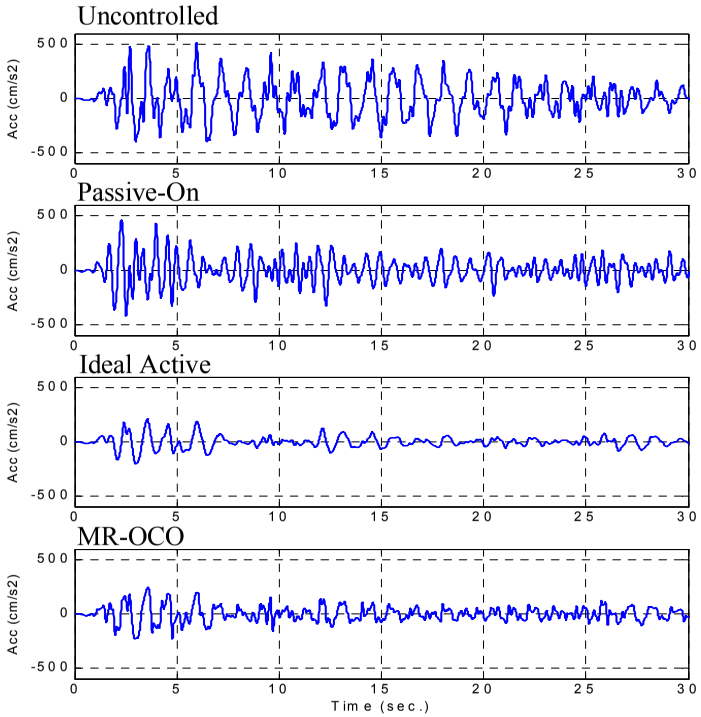

a) Acceleration Responses at Frame A on 9FL

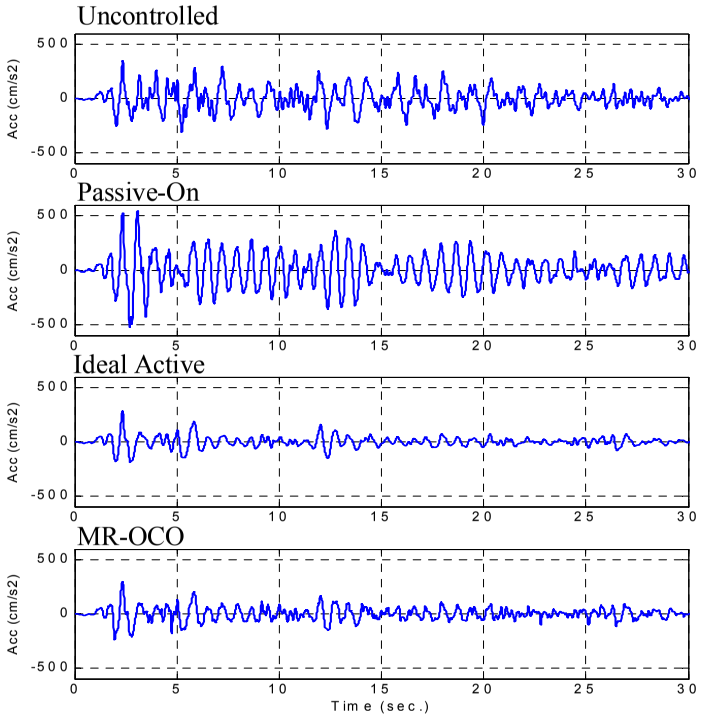

b) Acceleration Responses at Frame E on 9FL

FIGURE 6-7. Representative Acceleration Responses (El Centro 0.5).

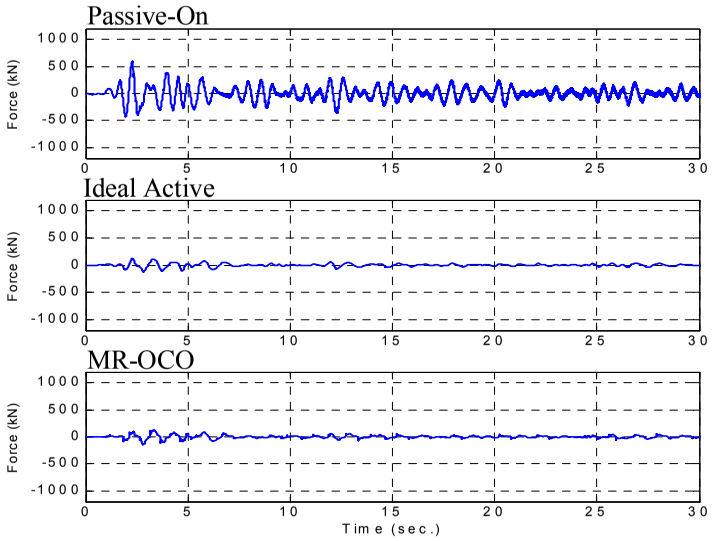

a) Control Forces at Frame A on 6FL

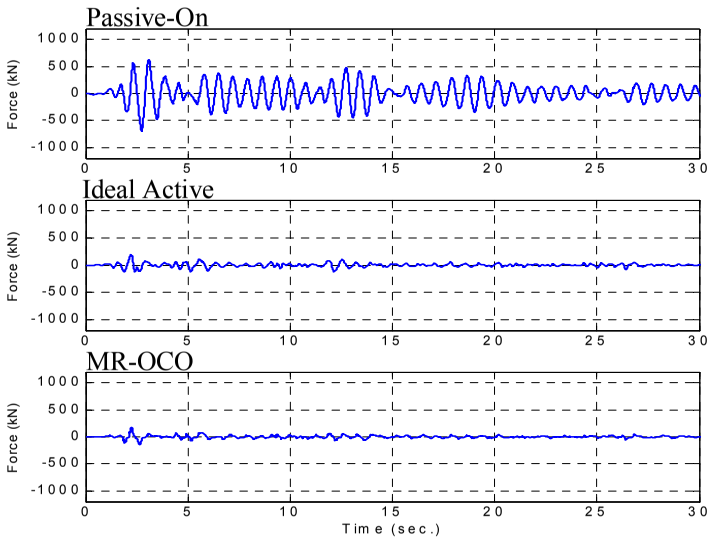

b) Control Forces at Frame E on 6FL

FIGURE 6-8. Representative Control Forces (El Centro 0.5).

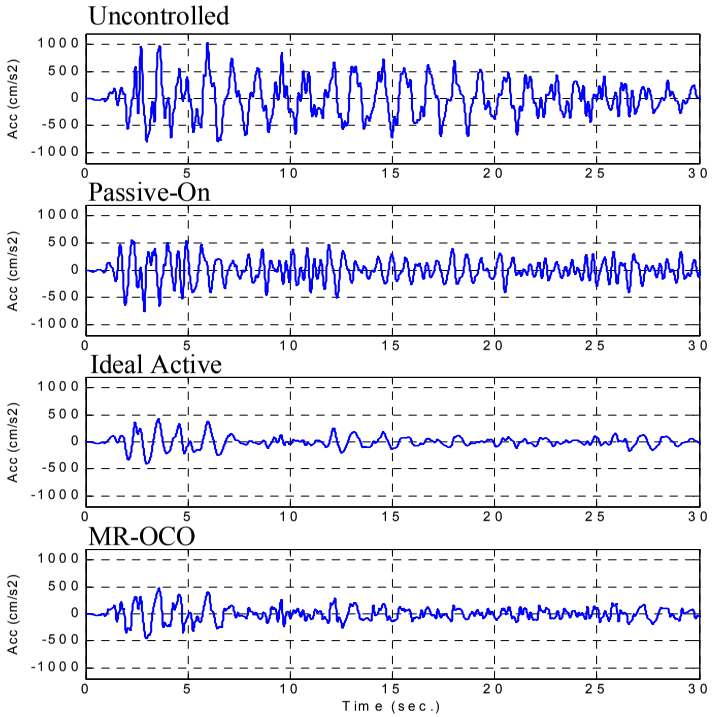

a) Acceleration Responses at Frame A on 9FL

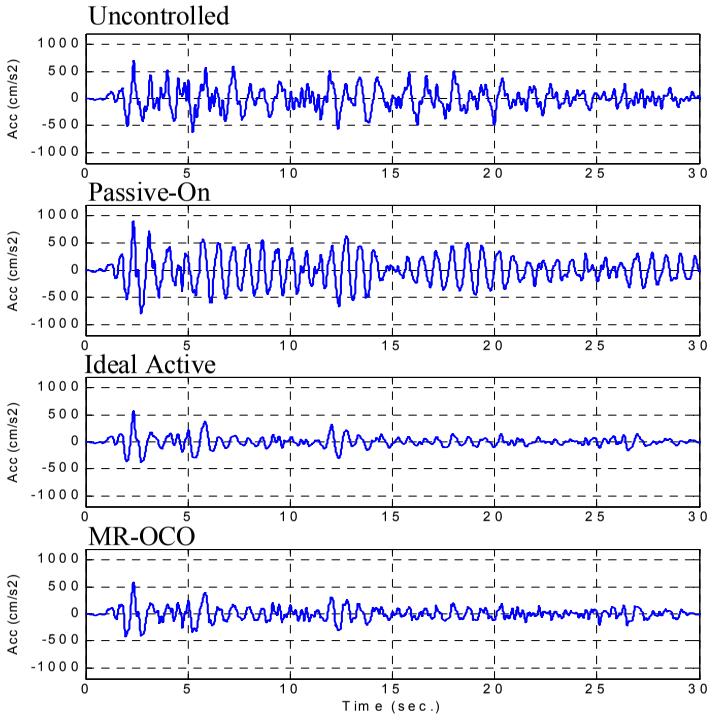

b) Acceleration Responses at Frame E on 9FL

FIGURE 6-9. Representative Acceleration Responses (El Centro 1.0).

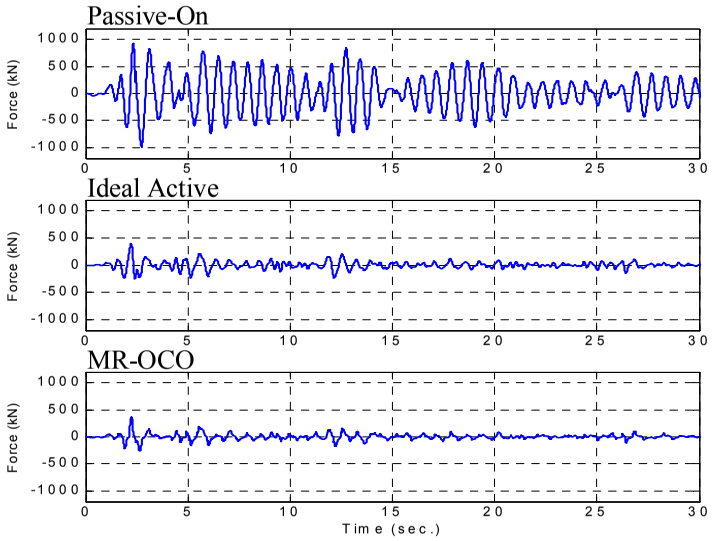

a) Control Forces at Frame A on 6FL

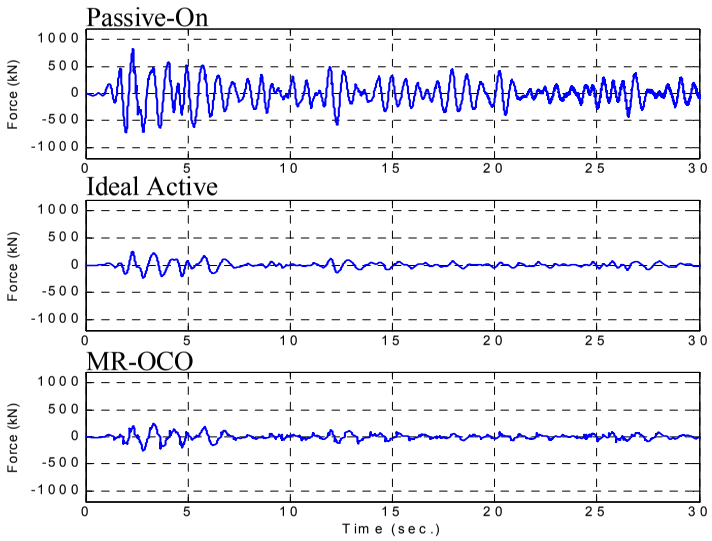

b) Control Forces at Frame E on 6FL

FIGURE 6-10. Representative Control Forces (El Centro 1.0).

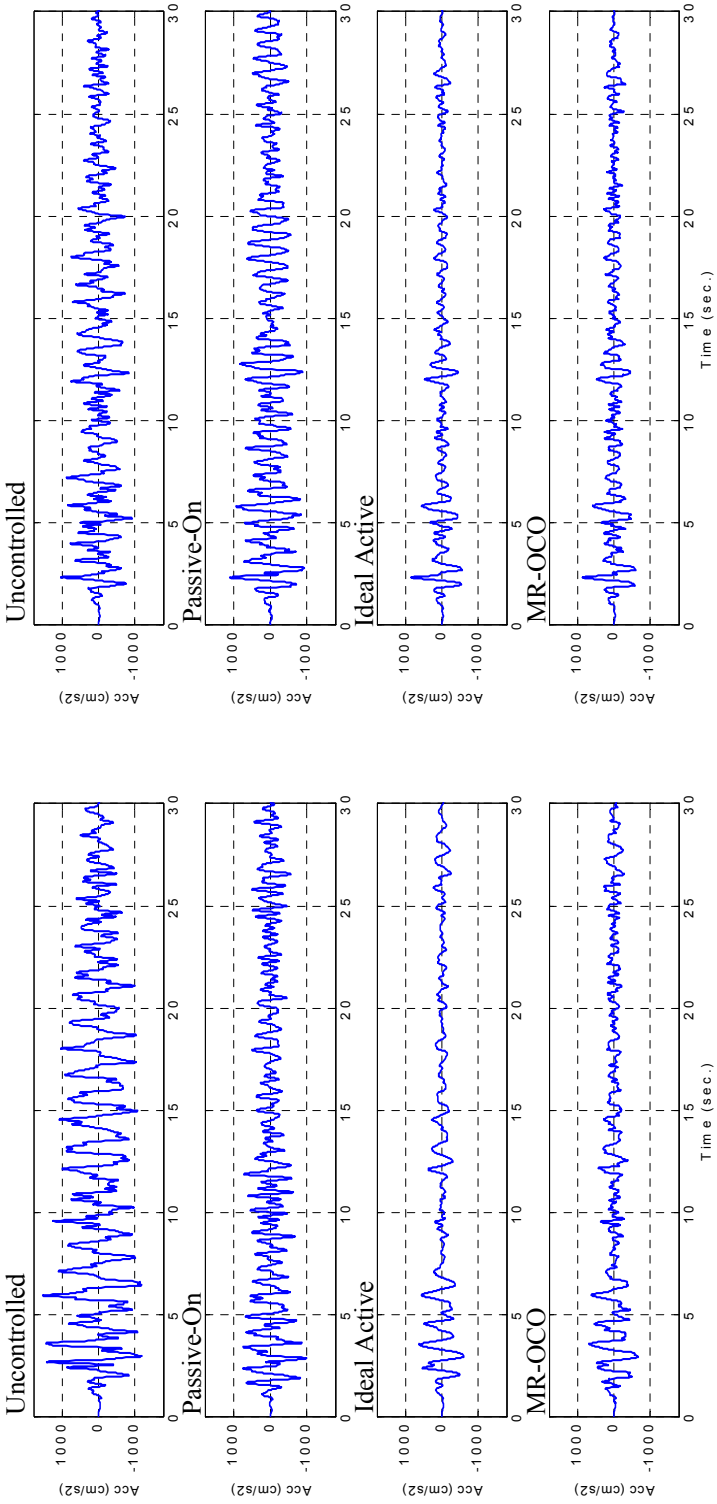

a) Acceleration Responses at Frame A on 9FL

b) Acceleration Responses at Frame E on 9FL

FIGURE 6-11. Representative Acceleration Responses (El Centro 1.5).

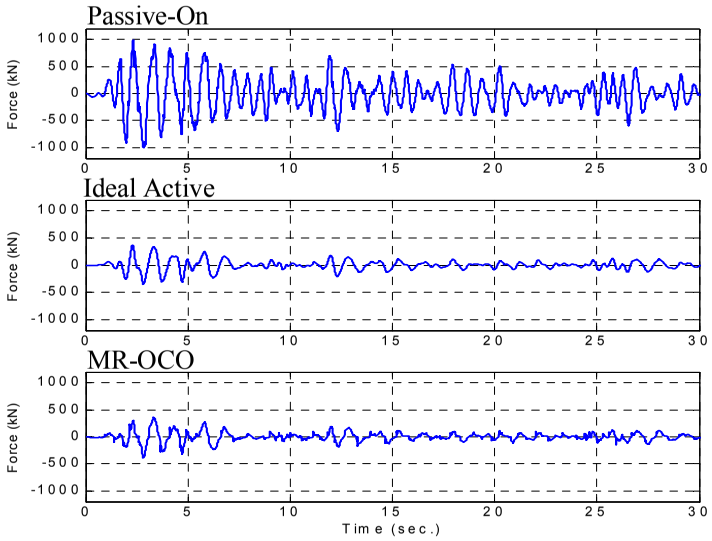

a) Control Forces at Frame A on 6FL

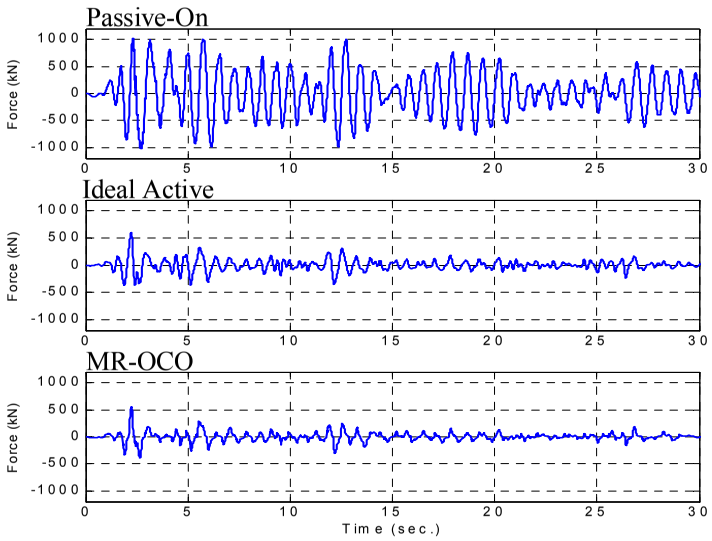

b) Control Forces at Frame E on 6FL

FIGURE 6-12. Representative Control Forces (El Centro 1.5).

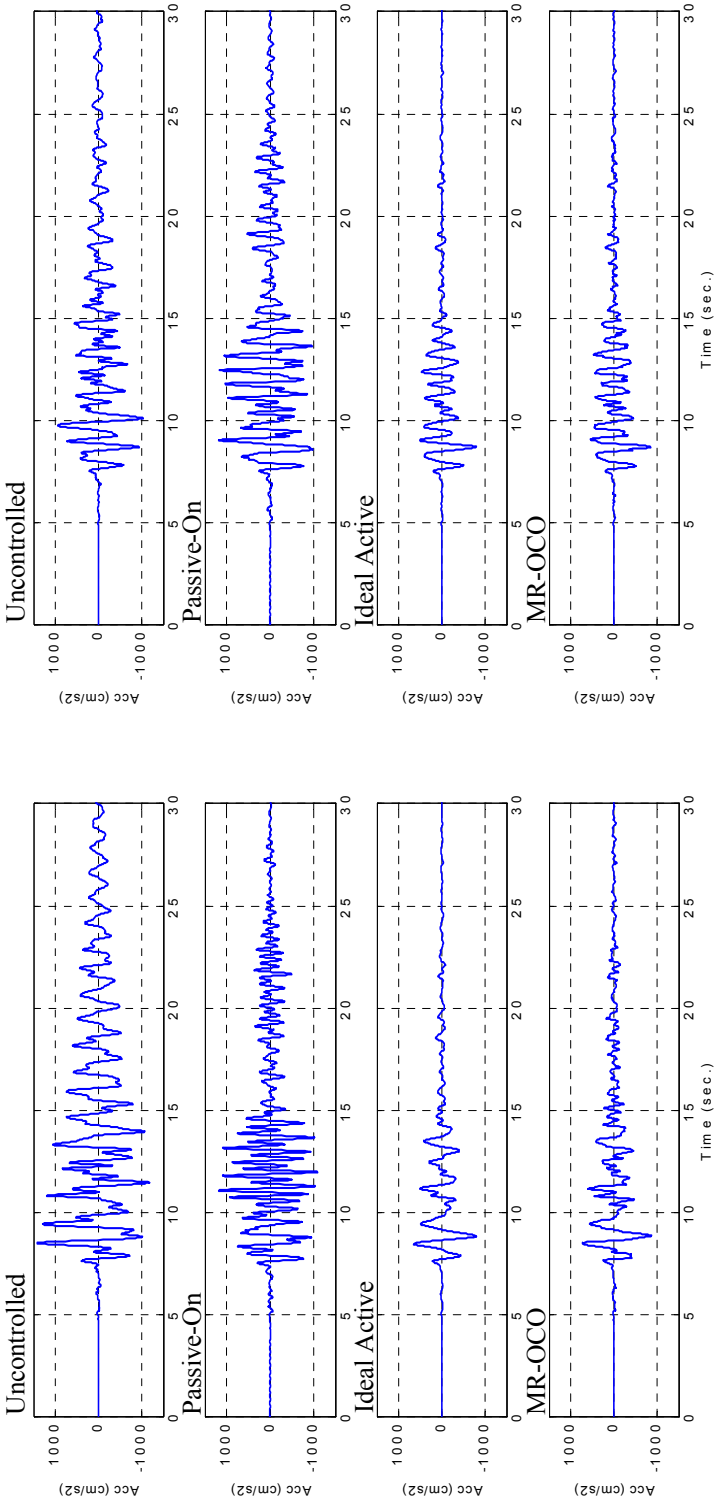

a) Acceleration Responses at Frame A on 9FL

b) Acceleration Responses at Frame E on 9FL

FIGURE 6-13. Representative Acceleration Responses (Kobe 0.5).

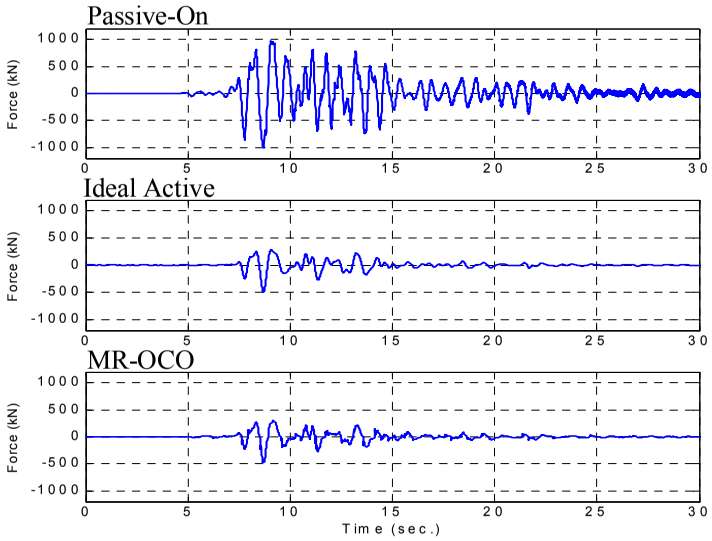

a) Control Forces at Frame A on 6FL

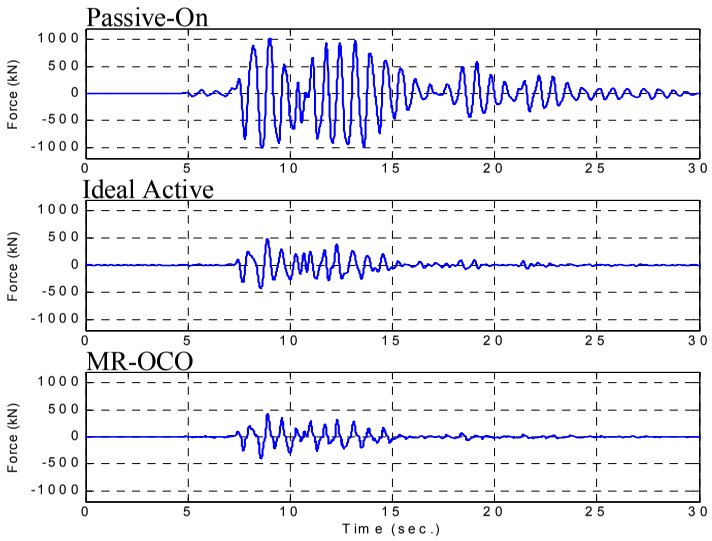

b) Control Forces at Frame E on 6FL

FIGURE 6-14. Representative Control Forces (Kobe 0.5).

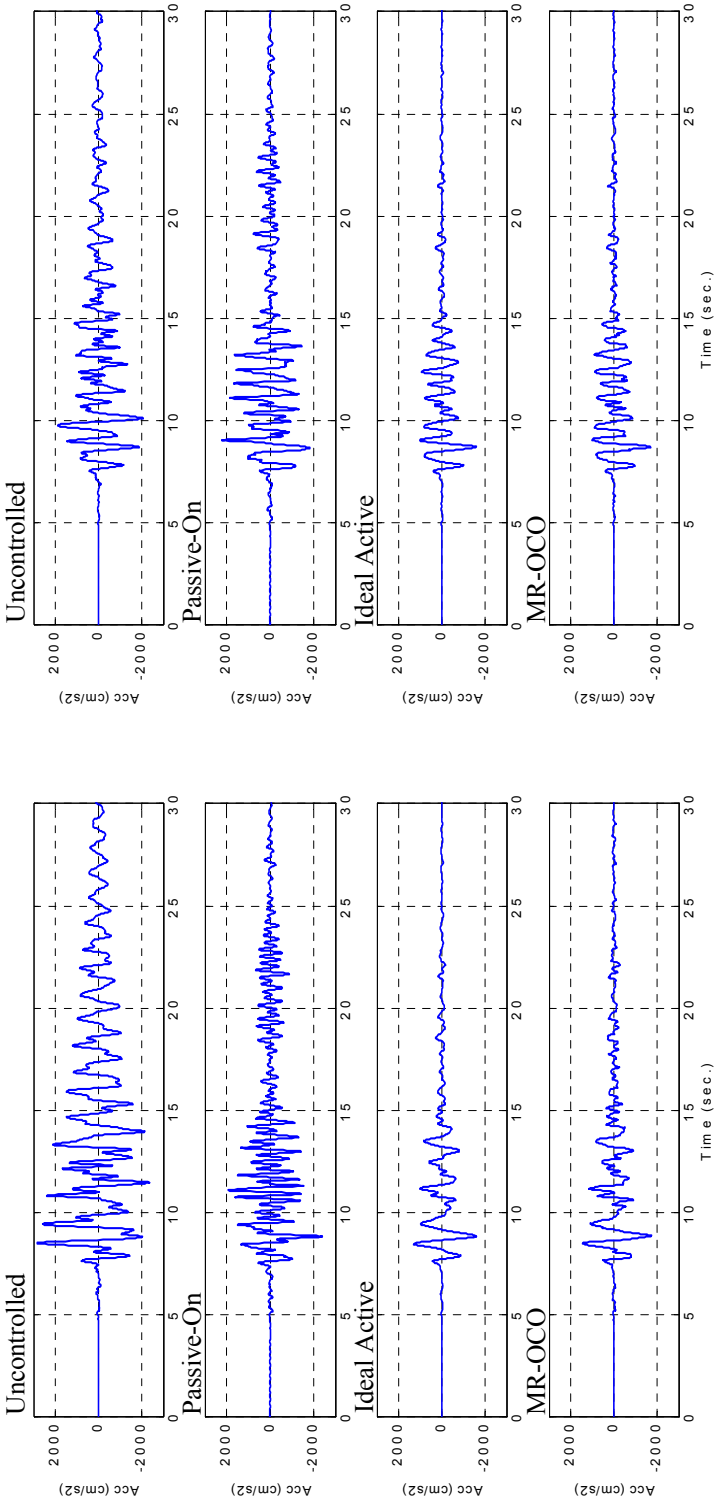

a) Acceleration Responses at Frame A on 9FL

b) Acceleration Responses at Frame E on 9FL

FIGURE 6-15. Representative Acceleration Responses (Kobe 1.0).

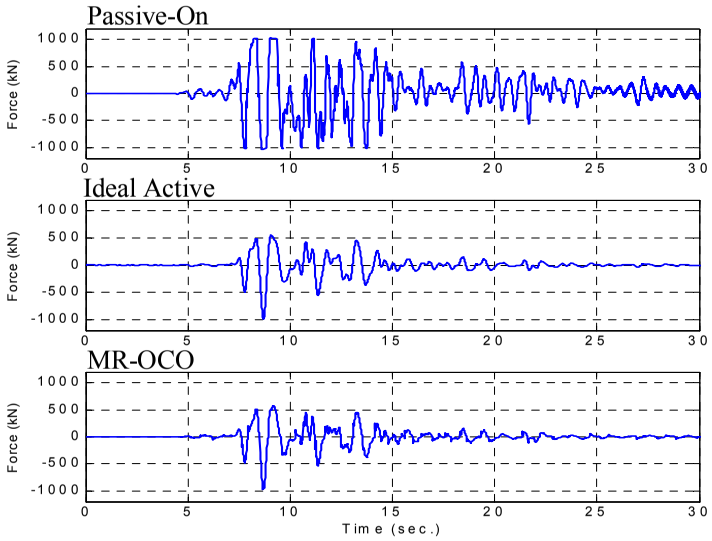

a) Control Forces at Frame A on 6FL

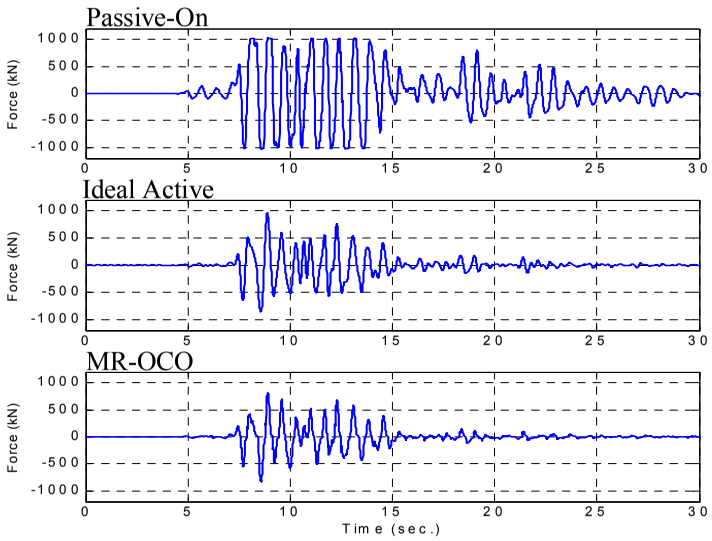

b) Control Forces at Frame E on 6FL

FIGURE 6-16. Representative Control Forces (Kobe 1.0).

controller. However, in some cases, in reducing the normed interstory drift, the clipped-optimal performs slightly better than the ideal active control system.

In comparing the performance of the clipped-optimal controller and the passive-on controller, it is clearly shown that the clipped-optimal controller is significantly better than the passive-on in reducing the acceleration responses of both maximum and normed values. Note that the acceleration responses using the passive-on controller for the El Centro 0.5 is increased compared to those of the uncontrolled building, while the clipped-optimal can reduce this response effectively. It is also noted that, in most cases, the maximum and normed interstory drift responses with the clipped-optimal controller are better than those of the passive-on controller (except the maximum value for the Kobe 0.5 and the maximum and normed values for the Kobe 1.0). Also note that the passive-on controller applies larger control forces than the ideal active and the clipped-optimal controller, while achieving a much lower performance level. So, it is concluded that the passive control forces are not always effectively used to reduce the building responses.

TABLE 6-4. Results for Evaluation Criteria.

	J_1	J_2	J_3	J_4	J_5
El Centro 1940 N-S 0.5					
Passive-Off	0.8715	0.9468	0.6162	0.7007	0.000221
Passive-On	0.9920	1.0956	0.5987	1.7983	0.010016
Ideal Active	0.5493	0.5403	0.3570	0.3303	0.002023
Original Clipped-Optimal	0.6042	0.6698	0.3508	0.4315	0.001850
Modified Clipped-Optimal	0.6369	0.6440	0.3895	0.4901	0.001966
El Centro 1940 N-S 1.0					
Passive-Off	0.8871	0.9753	0.7406	0.7860	0.000222
Passive-On	0.6663	0.8586	0.5502	0.8085	0.010400
Ideal Active	0.5493	0.5403	0.3570	0.3303	0.004046
Original Clipped-Optimal	0.5755	0.5584	0.3426	0.3924	0.003747
Modified Clipped-Optimal	0.6051	0.5797	0.3681	0.4379	0.003543
El Centro 1940 N-S 1.5					
Passive-Off	0.9139	0.9899	0.8076	0.8364	0.000223
Passive-On	0.5664	0.7559	0.4897	0.6863	0.010472
Ideal Active	0.5493	0.5403	0.3570	0.3303	0.006070
Original Clipped-Optimal	0.5698	0.5538	0.3420	0.3772	0.005678
Modified Clipped-Optimal	0.5944	0.5705	0.3623	0.4162	0.005110
Kobe 1995 N-S 0.5					
Passive-Off	0.9559	0.9013	0.8063	0.8335	0.000222
Passive-On	0.8125	0.8325	0.5613	0.9143	0.010446
Ideal Active	0.6591	0.5568	0.4434	0.3978	0.005072
Original Clipped-Optimal	0.6842	0.6172	0.4267	0.4482	0.005521
Modified Clipped-Optimal	0.7066	0.6047	0.4447	0.4926	0.005598
Kobe 1995 N-S 1.0					
Passive-Off	0.9719	0.9445	0.8817	0.8961	0.000224
Passive-On	0.5973	0.8424	0.3927	0.6252	0.010570
Ideal Active	0.6591	0.5568	0.4434	0.3978	0.010143
Original Clipped-Optimal	0.6811	0.6097	0.4288	0.4335	0.010481
Modified Clipped-Optimal	0.6979	0.6008	0.4438	0.4678	0.010456

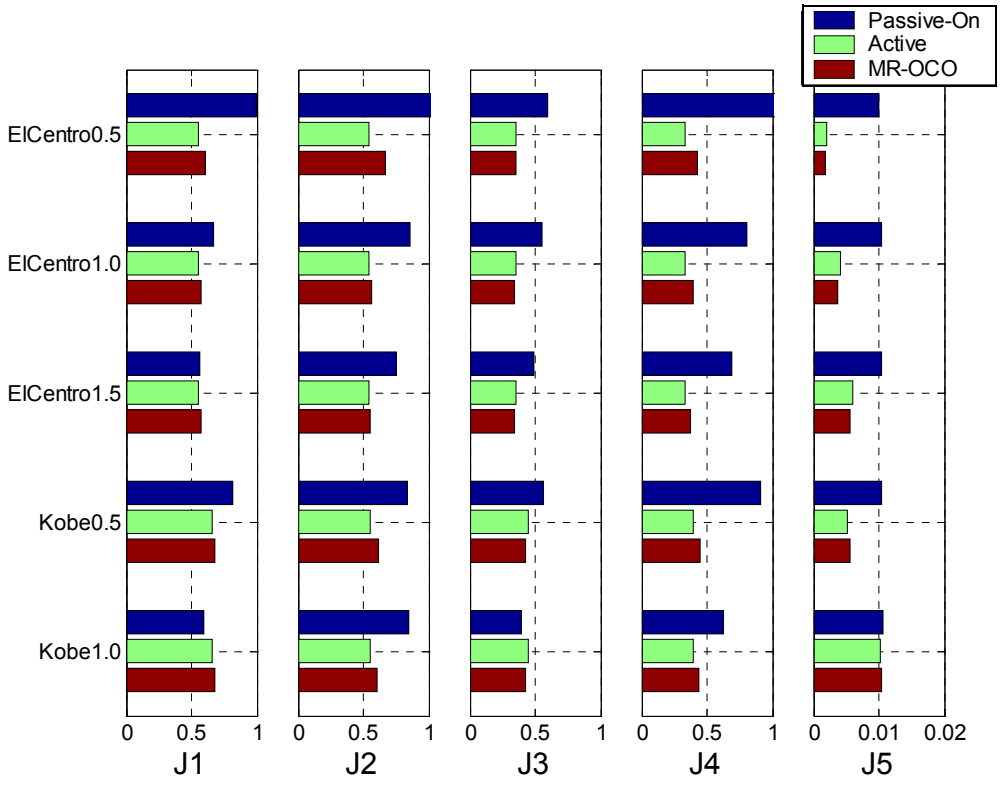

FIGURE 6-17. Evaluation Criteria for Case I.

6.6 Case II: L-Shaped, 8-Story Building

6.6.1 Description of the Building

The full scale, asymmetric building considered herein is based on the superstructure of the benchmark problem on base isolation systems for buildings [34]. The benchmark structure is similar to existing buildings in Los Angeles. This building is a 8-story, steel-braced frame building, 270.4 ft (81.9 m) by 178 ft (53.9 m) in plan and 116 ft (35.1 m) in

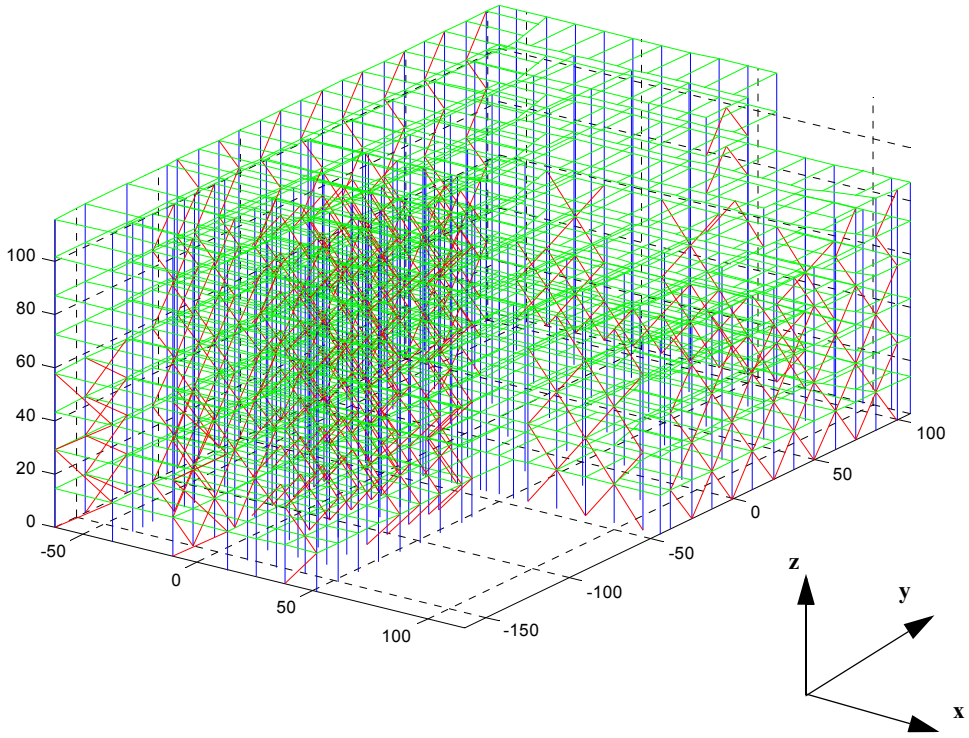

FIGURE 6-18. Structural Diagram of the 8-story L-shaped Building.

elevation. The structural details are shown in Figure 6-18. The floor plan is L-shaped and has setbacks above the fifth floor. The floor plan for each floor is shown in Figure 6-19. The distribution of steel bracing is located at the building perimeter and is shown in Figure 6-20 and 6-21.

For control studies, this building is modeled as a linear elastic system with a rigid floor slab assumption. The parameters of the model including mass, inertia, stiffness eccentricity are shown in Table 6-5 and 6-6. The first three calculated natural frequencies are 1.26 Hz (x-direction), 1.33 Hz (y-direction), 1.71 Hz (torsion). The damping ratio is assumed to be 2% in all modes.

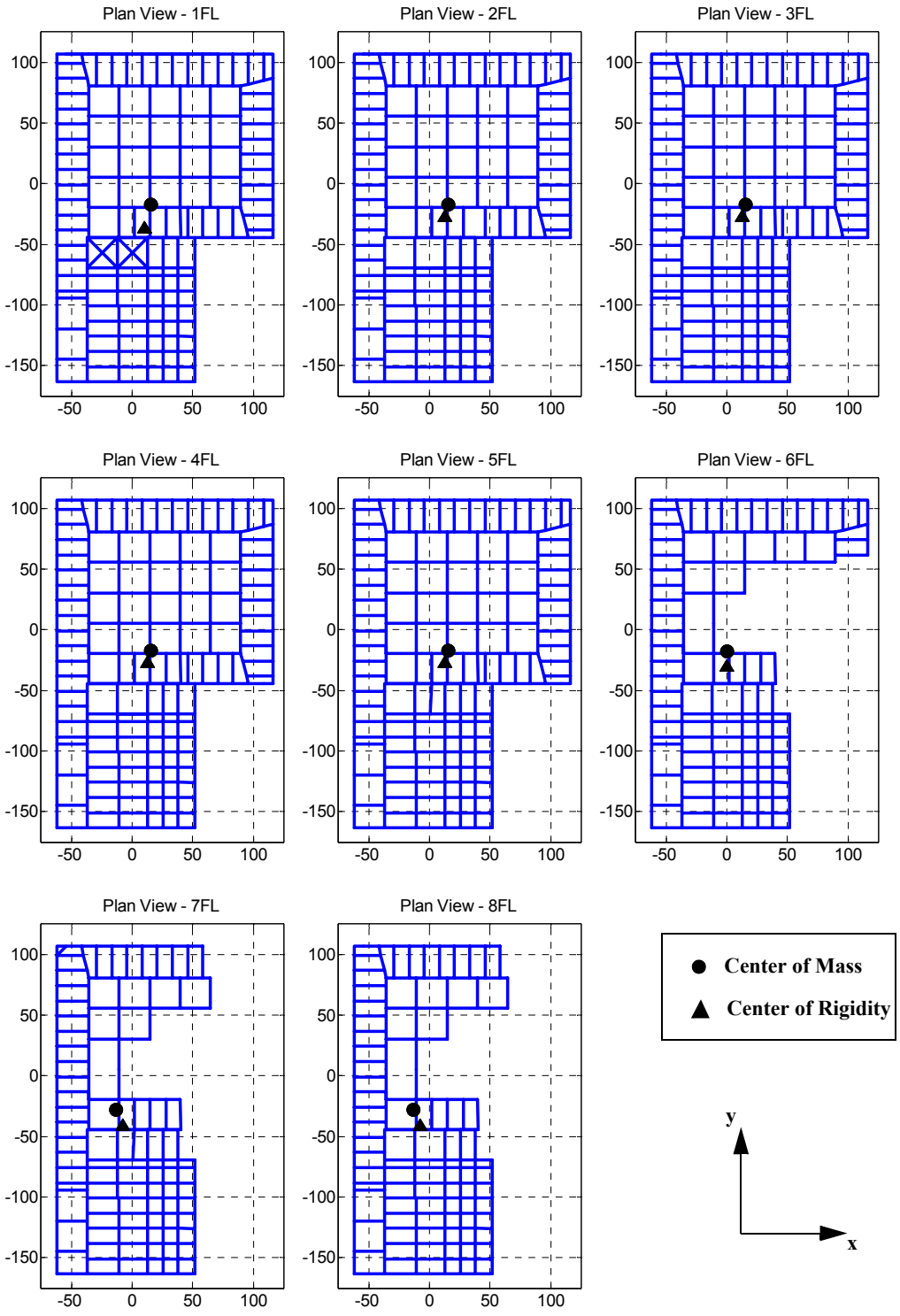

FIGURE 6-19. Plan View of the 8-story L-shaped Building.

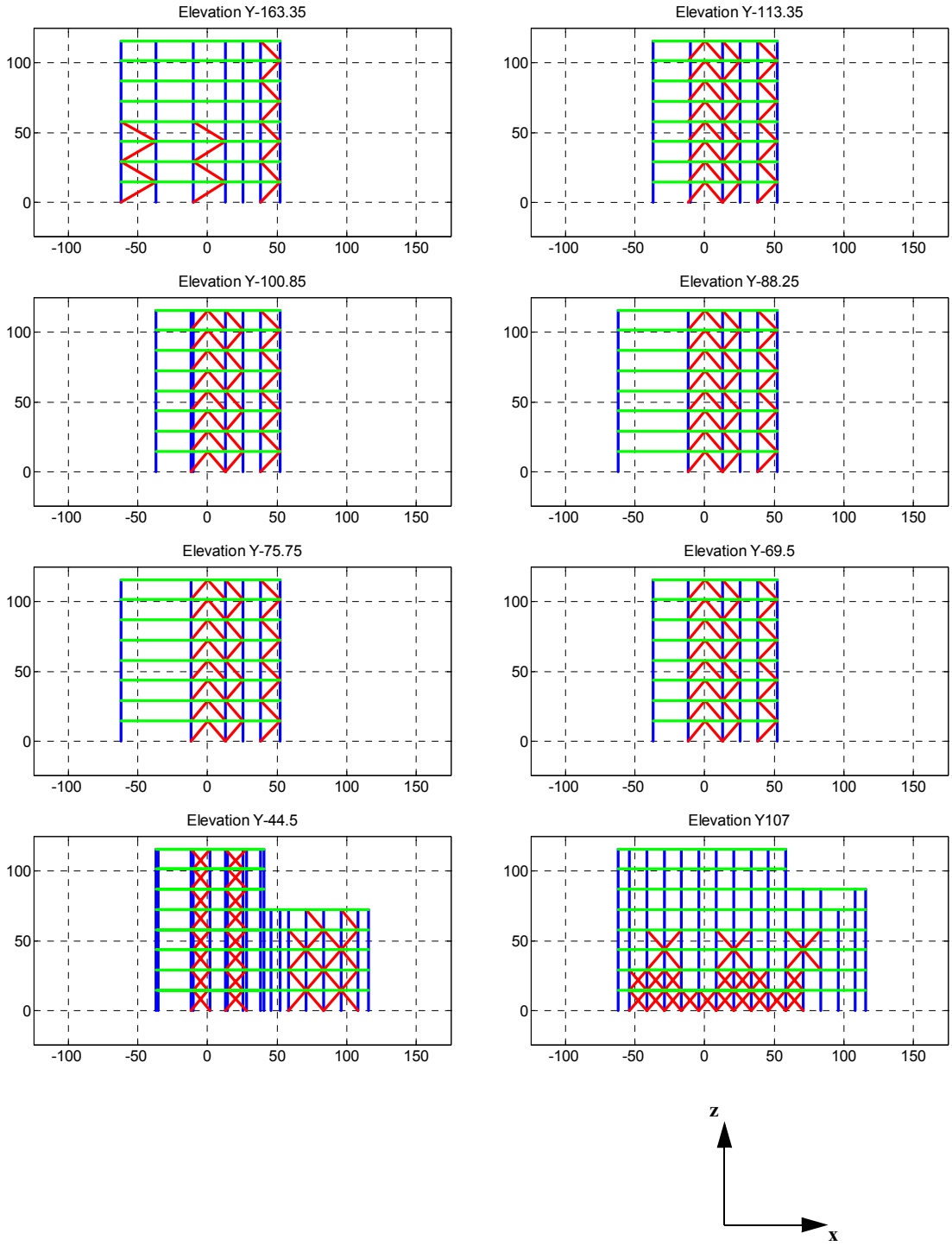

FIGURE 6-20. Elevation View along x-direction.

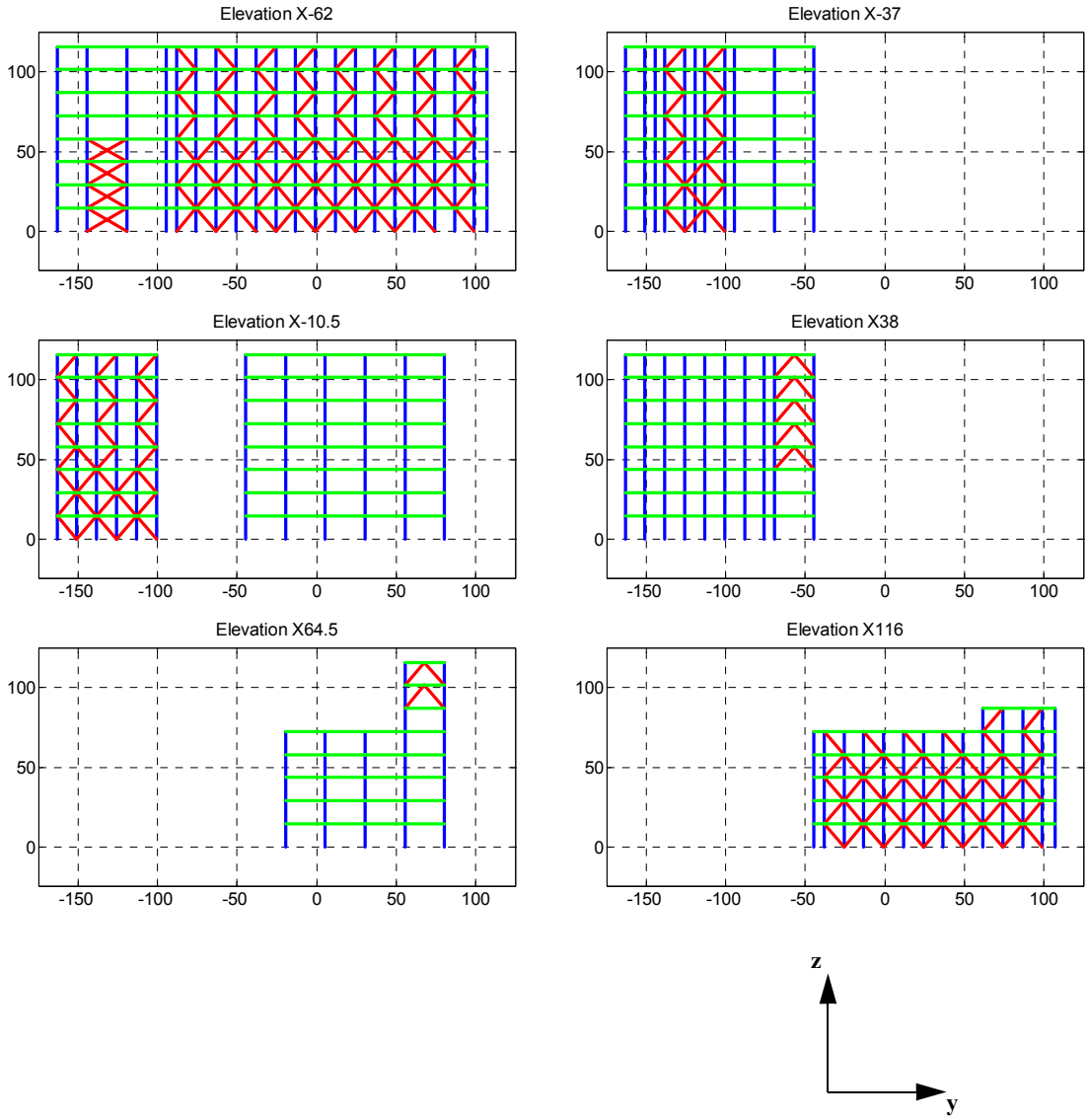

FIGURE 6-21. Elevation View along y-direction.

TABLE 6-5. Structural Parameters (x-direction).

Story i	Weight W_i (kN)	Inertia I_i (kNcm^2)	Radius of Gyration r_i (cm)	Total Stiffness k_{xi} (kN/cm)	Torsional Stiffness $k_{\theta i}$ (kNcm/rad)	Natural Frequency Ratio $\omega_{\theta i}/\omega_{xi}$	Eccentricity e_{yi} (cm)	Eccentricity ratio e_{yi}/r_i
8	10435	0.76E+11	2698.3	24902	2.37E+11	1.145	1446.3	0.536
7	13949	1.02E+11	2698.5	24558	2.34E+11	1.144	1448.7	0.537
6	14935	1.21E+11	2853.1	26190	2.59E+11	1.101	1480.8	0.519
5	19803	1.53E+11	2778.4	27904	3.02E+11	1.185	1520.9	0.547
4	20081	1.53E+11	2759.2	37249	4.77E+11	1.296	945.2	0.343
3	20136	1.53E+11	2755.3	36929	4.72E+11	1.298	986.2	0.358
2	21994	1.67E+11	2755.3	41564	5.26E+11	1.291	365.2	0.133
1	25253	1.92E+11	2755.2	46216	5.69E+11	1.274	176.5	0.064

TABLE 6-6. Structural Parameters (y-direction).

Story i	Weight W_i (kN)	Inertia I_i (kNcm^2)	Radius of Gyration r_i (cm)	Total Stiffness k_{yi} (kN/cm)	Torsional Stiffness $k_{\theta i}$ (kNcm/rad)	Natural Frequency Ratio $\omega_{\theta i}/\omega_{yi}$	Eccentricity e_{xi} (cm)	Eccentricity ratio e_{xi}/r_i
8	10435	0.76E+11	2698.3	18920	2.37E+11	1.313	66.1	0.025
7	13949	1.02E+11	2698.5	18612	2.34E+11	1.314	67.1	0.025
6	14935	1.21E+11	2853.1	19349	2.59E+11	1.281	248.0	0.087
5	19803	1.53E+11	2778.4	23587	3.02E+11	1.288	137.5	0.050
4	20081	1.53E+11	2759.2	37124	4.77E+11	1.299	244.3	0.089
3	20136	1.53E+11	2755.3	37124	4.72E+11	1.295	313.7	0.114
2	21994	1.67E+11	2755.3	37124	5.26E+11	1.366	313.7	0.114
1	25253	1.92E+11	2755.2	35411	5.69E+11	1.455	309.4	0.112

6.6.2 Optimal Control Device Placement and Design of Controller

As in the previous example, the optimal placement of control devices is determined using GAs. The study is conducted independently for the x- and y- directions. In the x-direction, the acceleration responses at Frame Y-163.25 and Frame Y107 on both 4FL and 8FL, for a total of 4 acceleration responses, are used as feedback for the control systems. In the y-direction, the acceleration responses at Frame X-62 and Frame X115 on 4FL, and at Frame X-62 and Frame X52.05 on 8FL, total 4 acceleration responses, are used as feedback for the control systems.

The potential locations for control devices to be installed are within three specific frames on each floor in each direction. These include Y-163.25, Y-44.5, and Y107 in the x-direction, and X-62, X52.05, and X115 in the y-direction, as shown in Figure 6-22. Here, it is noted that in the y-direction on the 7th and 8th floors, control devices can be installed in only two frames, X-62 and X52.05, due to the setbacks. Studies are conducted to find eight optimal locations in each direction out of 24 and 22 possible locations in the x and y-direction, respectively. Thus, to perform the optimization (independently for the x- and y-directions), the chromosome is defined as a vector with 8 elements. Each element is associated with a potential control device location and has integer value between 1 and 24 for x-direction and between 1 and 22 for y-direction. The population size for each generation is selected to be 40.

Genetic algorithms are applied to find the optimal control device location for each constant weighting a. The performance of each weighting case is shown in Figure 6-23. The corresponding optimal placements of the actuators are schematically shown in Figure 6-24. As is described in the previous case study, there is a trade-off between reducing the maximum *rms* absolute acceleration and reducing the maximum *rms* interstory displacement. As the weighting increases, the acceleration continues to decrease, while

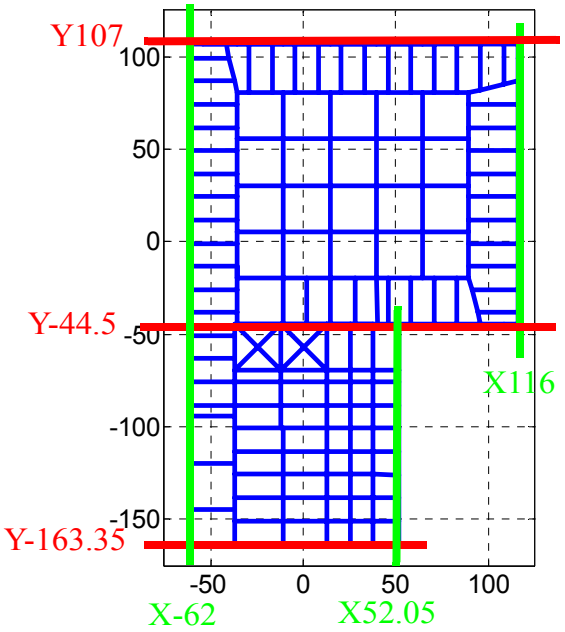

FIGURE 6-22. Potential Control Device Locations.

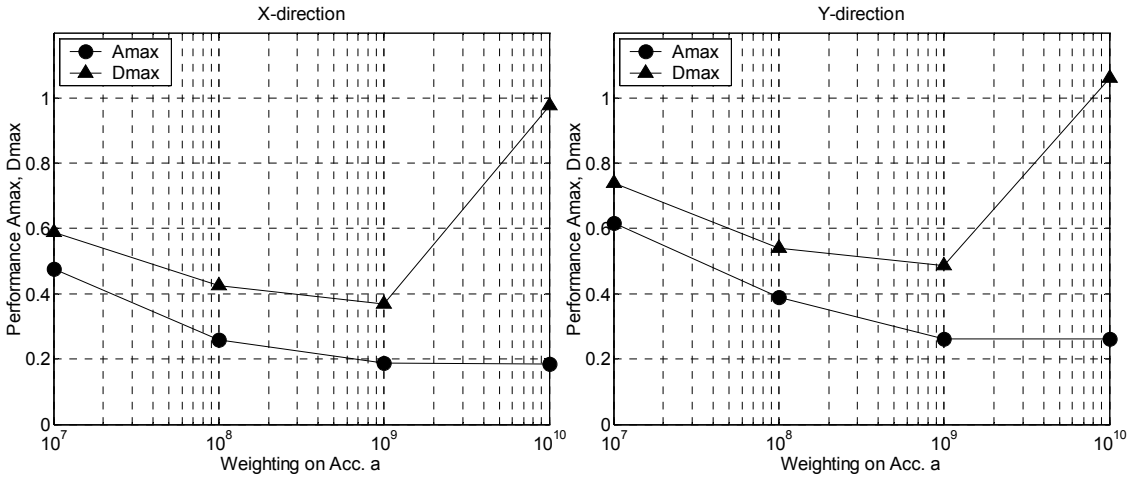

FIGURE 6-23. Results of Optimal GA Control Designs.

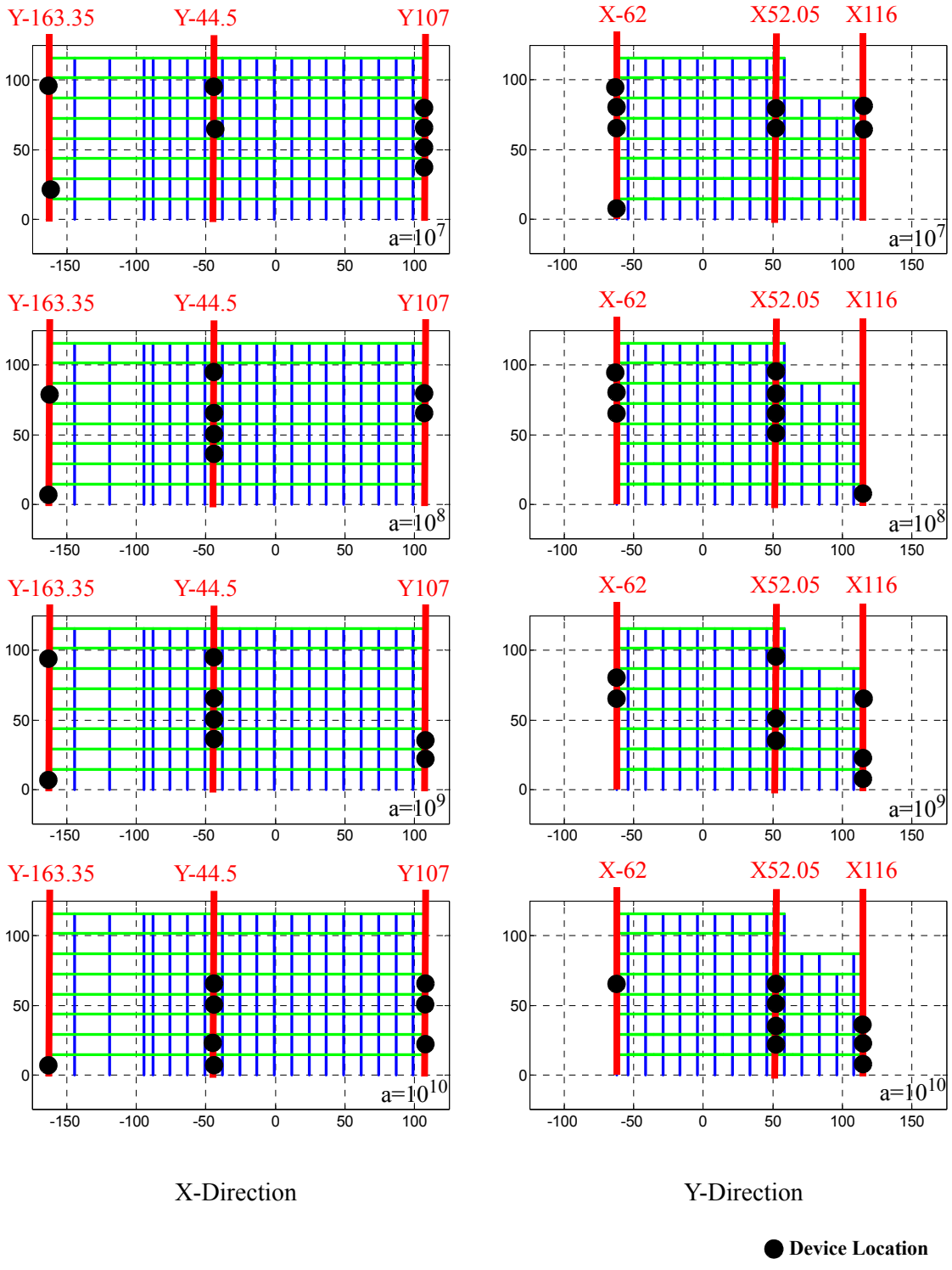

FIGURE 6-24. Optimal Device Locations.

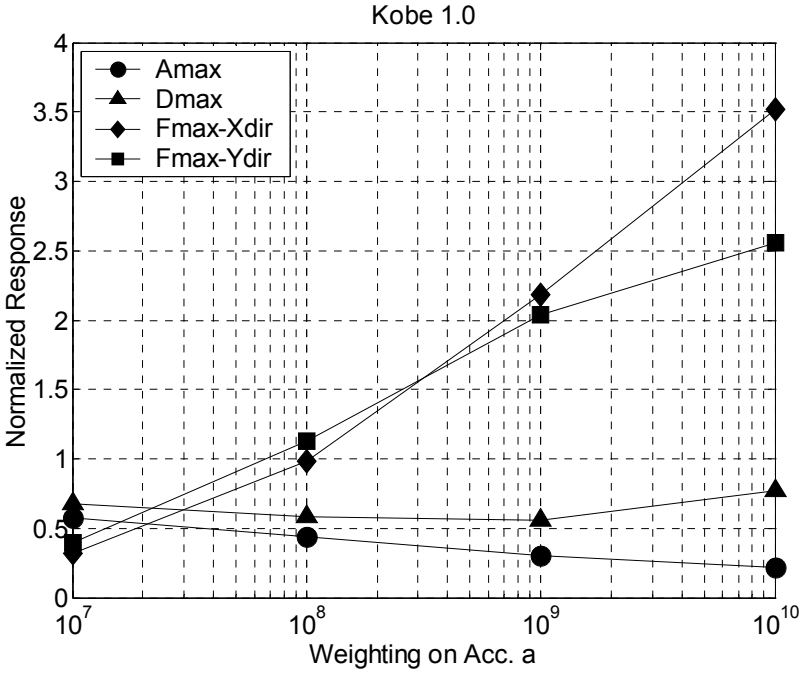

FIGURE 6-25. Responses Due to the Kobe 1.0 Earthquake.

the displacements tend to increase above a value of $a = 10^9$. From these results, the case with weighting $a = 10^9$ looks like the optimal case reducing both acceleration and interstory drift effectively. However, there is another factor to be considered, that is, the control force required to realize the control design.

To study the control force required to realize the each control design, earthquake responses are calculated. In this study, Kobe 1995 N-S is used as the input in the x-direction and Kobe 1995 E-W is used as the input in the y-direction. Maximum acceleration response and maximum interstory drift responses, normalized by those of the uncontrolled building, are shown in Figure 6-25 as well as required total control force for each direction, which is normalized by total weight of the building 147×10^3 kN (15,000 ton).

From these results, the required control force to realize the control design with weighting $a = 10^9$ is twice the total weight of the building in each direction, which is well beyond acceptable force capacity in practical case. So, for this structure, the control design with weighting $a = 10^8$ is chosen.

The optimal control device location for weighting $a = 10^8$ and the required number of devices assuming that actuators with maximum capacity of 1,000 kN are used is shown in Tables 6-7 and 6-8 for each direction. As shown in these tables, 146 control devices are used in the x-direction and 168 devices are used in the y-direction, for a total of of 314 devices.

TABLE 6-7. Location and Number of Control Devices for x-direction.

Floor	1	3	4	5	5	6	6	7
Frame	Y-163.35	Y-44.5	Y-44.5	Y-44.5	Y107	Y-163.35	Y107	Y-44.5
No.	22	18	17	18	21	16	21	13

TABLE 6-8. Location and Number of Control Devices for y-direction.

Floor	1	4	5	5	6	6	7	7
Frame	X116	X52.05	X-62	X52.05	X-62	X52.05	X-62	X52.05
No.	20	17	28	23	25	22	18	15

The transfer function of from the ground accelerations to the 4th and 8th floor acceleration responses for the selected LQG design are shown in Figures 6-26 and 6-27 and compared to those of uncontrolled building. From these results, it is shown that the responses in x-direction are excited even by the ground motion in y-direction and the responses in y-direction are excited by the ground motion in x-direction without control. Applying control, the responses in each direction due to ground excitation in each

direction are reduced and the damping ratio of the first three modes are increased to 18%, 10%, and 19%.

6.6.3 Response Due to Earthquake Excitations

To demonstrate the performance of proposed semiactive control system on the full scale asymmetric building, the responses due to earthquake excitations are calculated. In this case study, bi-directional excitations are considered.

Before discussing the results of proposed semiactive control system, the effect of bi-directional earthquake excitations is demonstrated herein. Two earthquakes, El Centro 1940 and Kobe 1995 are considered. Both North-South and East-West components are used as earthquake excitations for x- and y-direction of the corresponding building, respectively. The time history of each components of those earthquakes is shown in Figure 6-28 and the maximum accelerations are summarized in Table 6-9.

TABLE 6-9. Maximum Accelerations of Earthquakes.

	N-S Component	E-W Component
El Centro 1940	341.7 cm/s^2	210.1 cm/s^2
Kobe 1995	818.0 cm/s^2	617.3 cm/s^2

To investigate the effect of bi-directional earthquake excitation, responses of the uncontrolled building are calculated and compared for three cases: earthquake excitation only in the x-direction; earthquake excitation only in the y-direction; and bi-directional earthquake excitation. In each case, the N-S component of each earthquake is applied in the x-direction, and the E-W component is applied in the y-direction. The representative acceleration responses are shown in Figures 6-29 and 6-30 and the maximum values are summarized in Table 6-10.

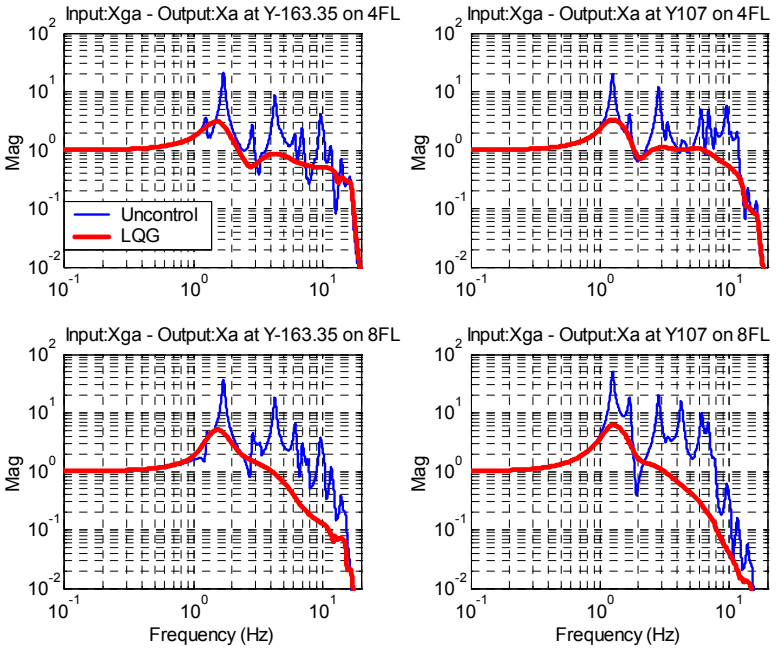

a) To Responses in x-direction

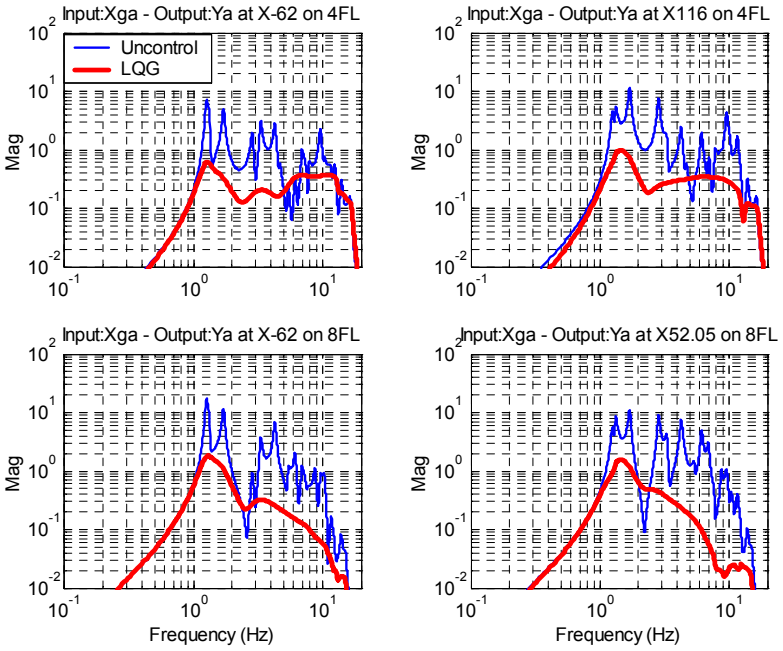

b) To Responses in y-direction

FIGURE 6-26. Transfer Functions from Ground Excitation in x-direction.

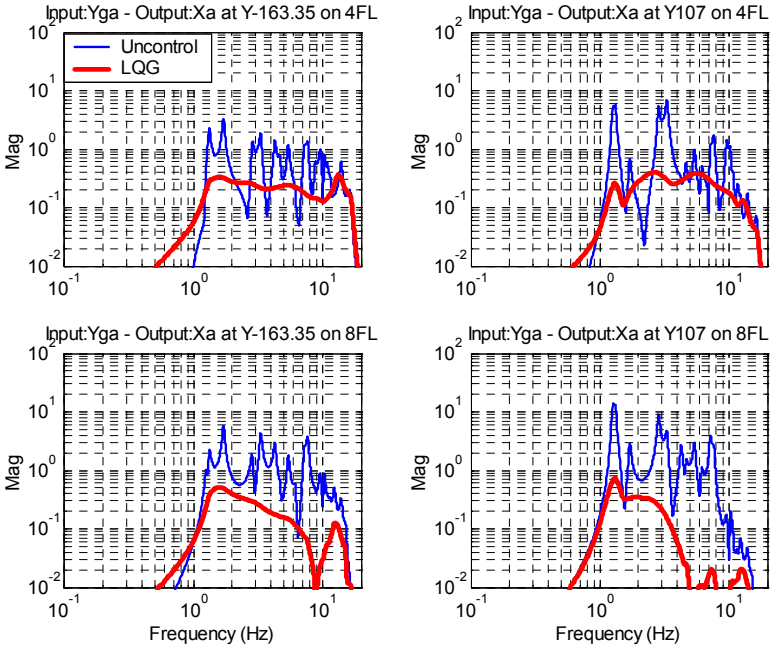

a) To Responses in x-direction

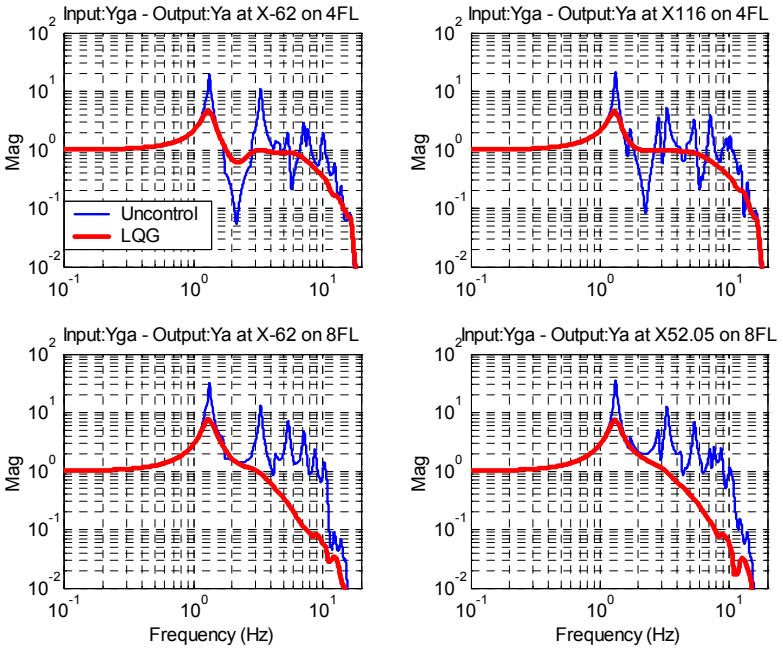

b) To Responses in y-direction

FIGURE 6-27. Transfer Functions from Ground Excitation in y-direction.

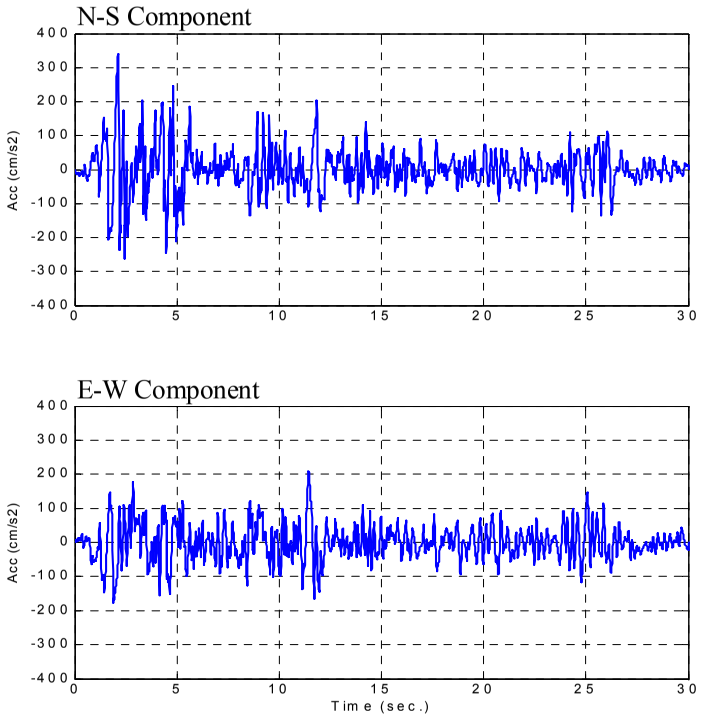

a) El Centro 1940 Earthquake

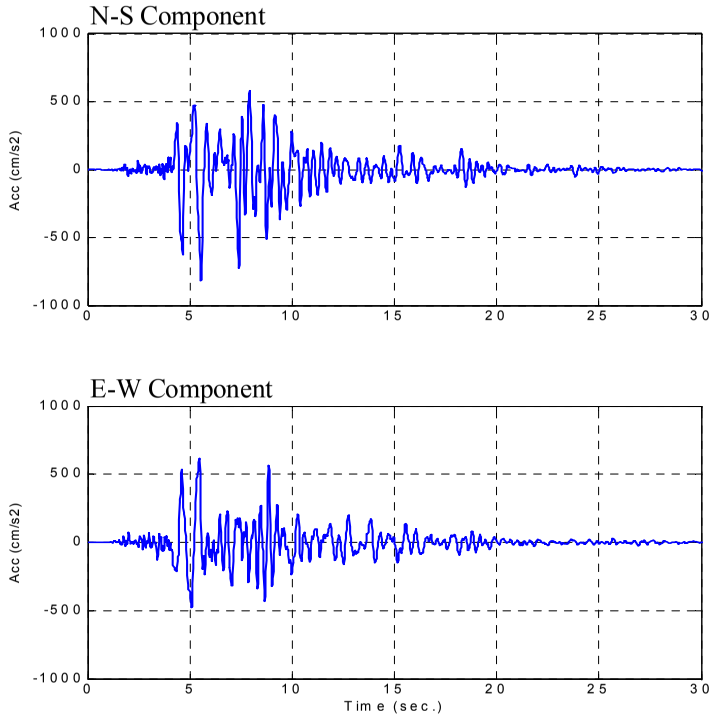

b) Kobe 1995 Earthquake

FIGURE 6-28. Time History of Earthquakes.

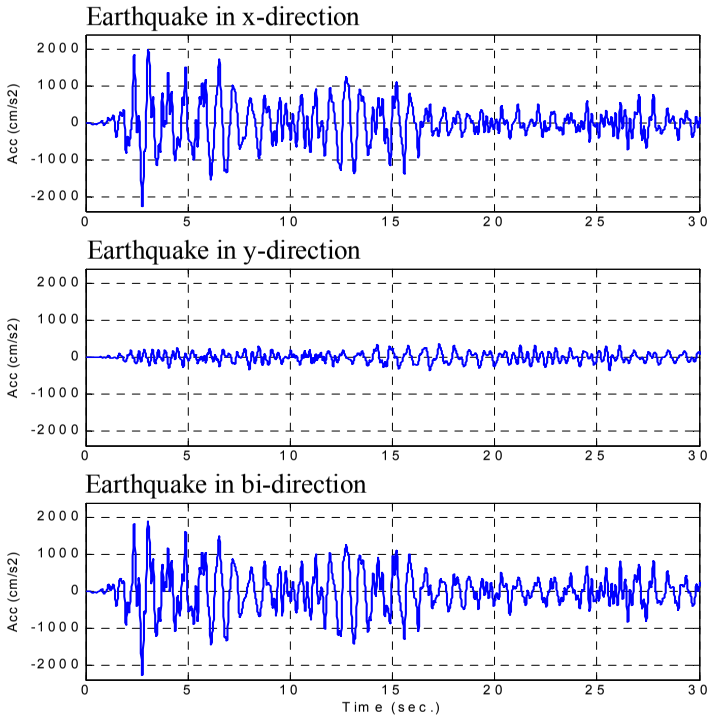

a) Acceleration Responses in x-direction at Y107 on 8FL

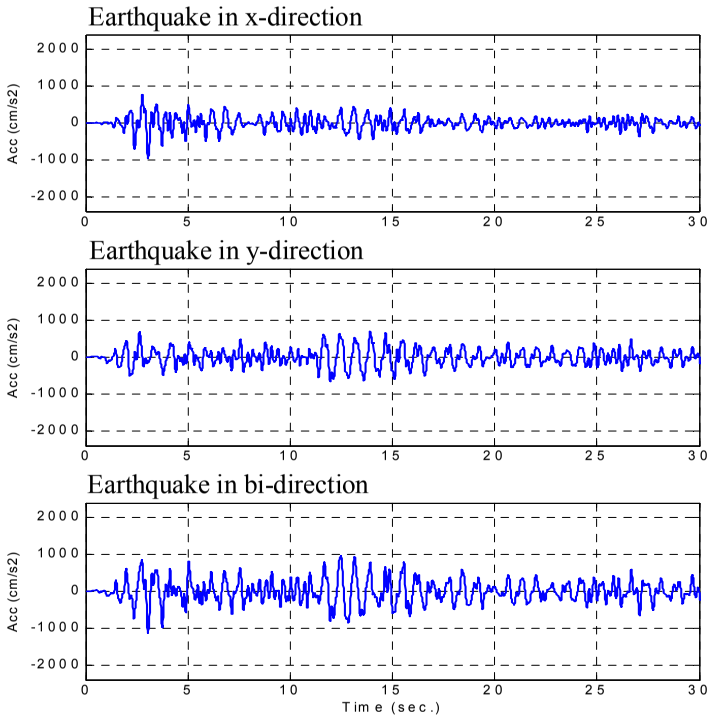

b) Acceleration Responses in y-direction at X52.05 on 8FL

FIGURE 6-29. Representative Acceleration Responses of Uncontrolled Building (El Centro 1940).

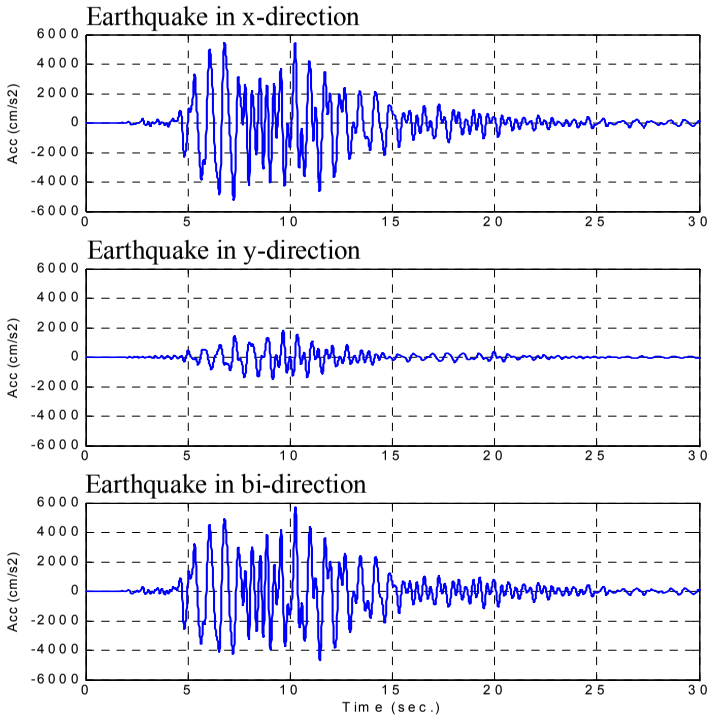

a) Acceleration Responses in x-direction at Y107 on 8FL

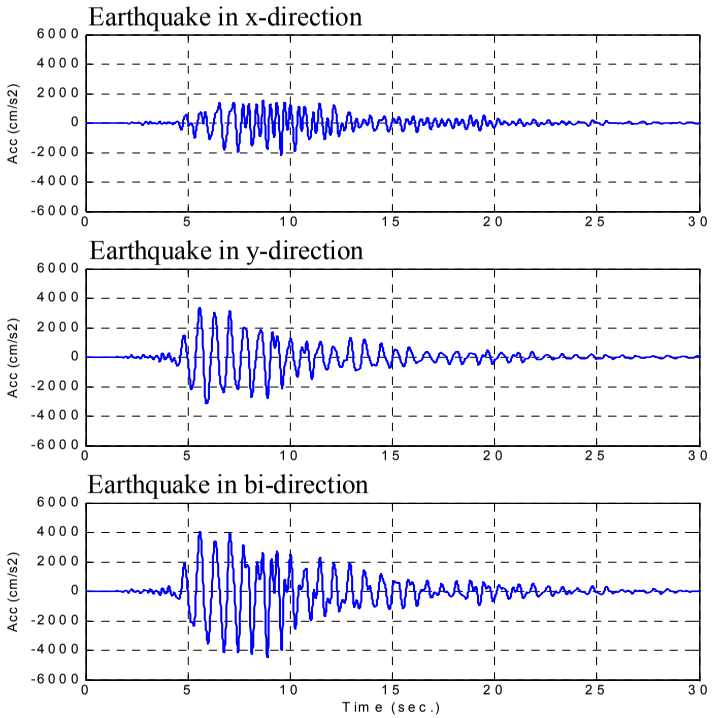

b) Acceleration Responses in y-direction at X52.05 on 8FL

FIGURE 6-30. Representative Acceleration Responses of Uncontrolled Building (Kobe 1995).

TABLE 6-10. Maximum Acceleration Responses of Uncontrolled Building.

Input Earthquake		Maximum Responses	
		x-direction	y-direction
El Centro 1940	x-direction	2269 cm/s^2	1013 cm/s^2
	y-direction	368.4 cm/s^2	772.2 cm/s^2
	bi-direction	2276 cm/s^2	1168 cm/s^2
Kobe 1995	x-direction	5440 cm/s^2	2497 cm/s^2
	y-direction	1822 cm/s^2	3385 cm/s^2
	bi-direction	5705 cm/s^2	4499 cm/s^2

According to these results, it is found that the responses in the x-direction are clearly influenced by earthquake excitation in y-direction. This observation can also be made regarding a response in the y-direction due to an excitation in the x-direction. This result is due to the fact that the translational motions in both directions are strongly coupled with the torsional motions.

For evaluation of proposed semiactive control systems, bi-directional earthquake excitations are considered. Various intensities are considered due to the nonlinear nature of the controlled system. The case studied are summarized in Table 6-11.

TABLE 6-11. Cases Studied.

CASE	x-direction		y-direction	
	Input Earthquake	Intensity	Input Earthquake	Intensity
El Centro 0.5	El Centro 1940 N-S	0.5	El Centro 1940 E-W	0.5
El Centro 1.0	El Centro 1940 N-S	1.0	El Centro 1940 E-W	1.0
El Centro 1.5	El Centro 1940 N-S	1.5	El Centro 1940 E-W	1.5
Kobe 0.5	Kobe 1995 N-S	0.5	Kobe 1995 E-W	0.5
Kobe 1.0	Kobe 1995 N-S	1.0	Kobe 1995 E-W	1.0

The representative time history responses are shown in Figures 6-31 through 6-45. These plots correspond to the acceleration responses at Frame Y-163.35 and at Frame Y107 on 8FL in the x-direction, and the acceleration responses at Frame X-62 and at Frame Y52.05 on 8FL in the y-direction, as well as control forces at Frame Y-163.35 on 1FL in the x-direction and at Frame X116 on 1FL in the y-direction. The results for the uncontrolled system, passive-on controller, ideal active controller, and clipped-optimal controller (with MR dampers) are shown.

According to these time history results, when applying the passive-on controller, modest reduction is found for the acceleration responses in the x-direction due to the El Centro earthquakes, and those in both directions due to Kobe earthquakes, while the other acceleration responses are similar or even larger than the uncontrolled values. However, the acceleration responses on both sides of 8FL in both the x- and y-directions are reduced effectively by the semiactive control system, and the performance is found to be as good as that of the ideal active control system. It is also noted that the control force used for the passive-on controller is clearly larger than those used for the semiactive and the ideal active controller. So, it is concluded that the semiactive and ideal active controller can reduce the responses due to various earthquake excitations with appropriate control forces.

Numerical values corresponding to the five earthquake criteria defined for this problem are shown in Table 6-12 for all designs considered. From these results, it is observed that the passive-off controller does not achieve significant response reduction and the modified version of clipped-optimal control achieves similar performance to that of the original clipped-optimal controller.

To examine the performance of the other three control systems, the passive-on controller, the ideal active controller and the clipped-optimal controller, the graphical

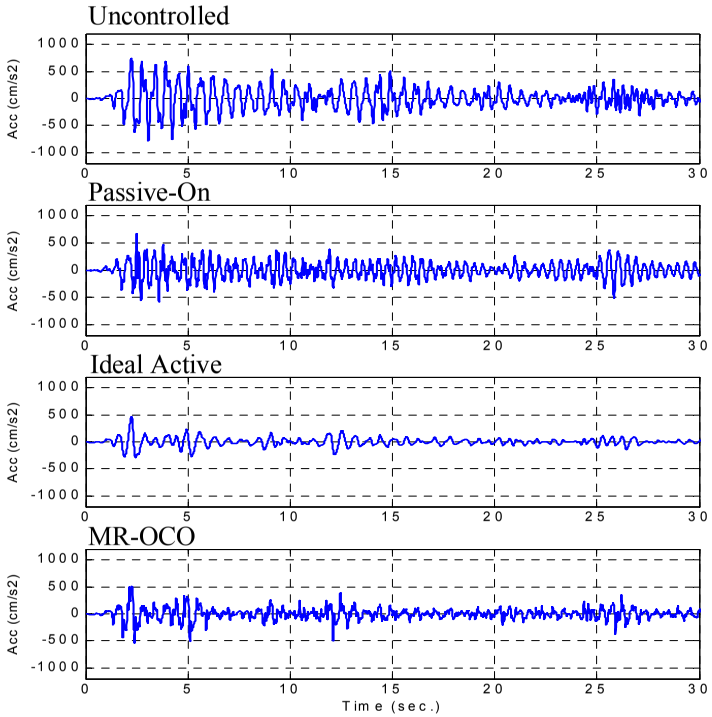

a) Acceleration Responses in x-direction at Y-163.35 on 8FL

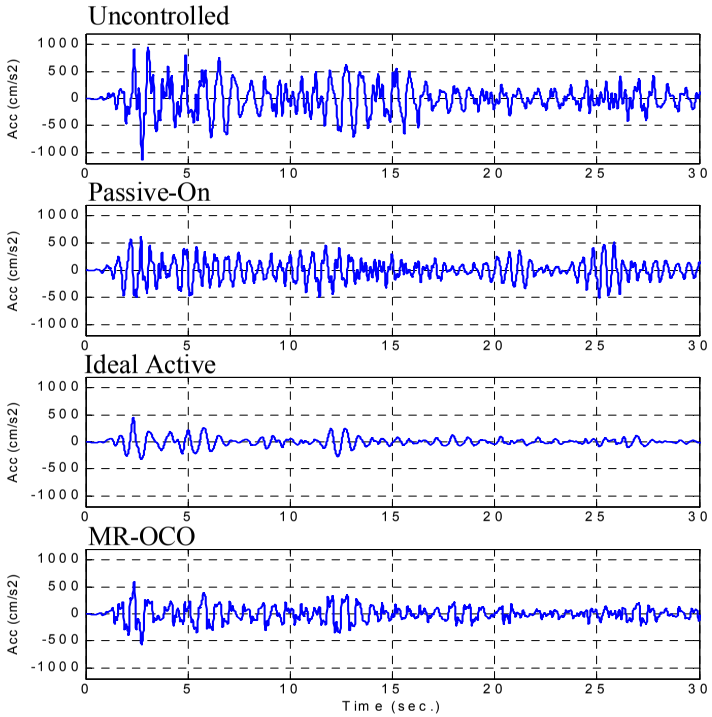

b) Acceleration Responses in x-direction at Y107 on 8FL

FIGURE 6-31. Representative Acceleration Responses in x-direction (El Centro 0.5).

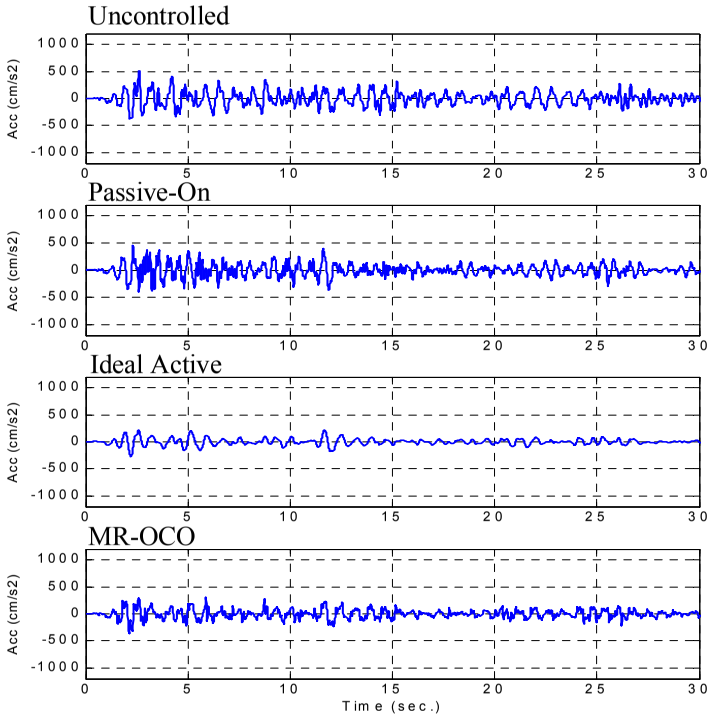

a) Acceleration Responses in y-direction at X-62 on 8FL

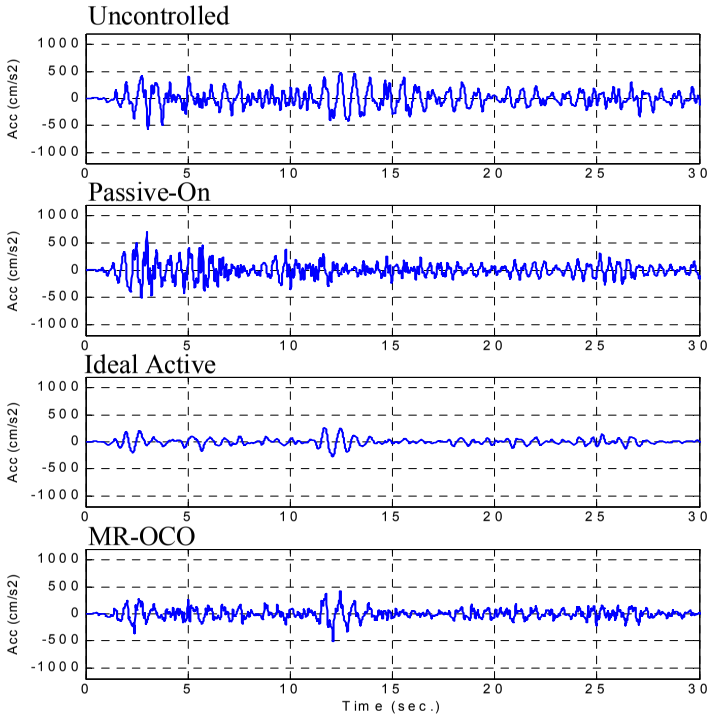

b) Acceleration Responses in y-direction at X52.05 on 8FL

FIGURE 6-32. Representative Acceleration Responses in y-direction (El Centro 0.5).

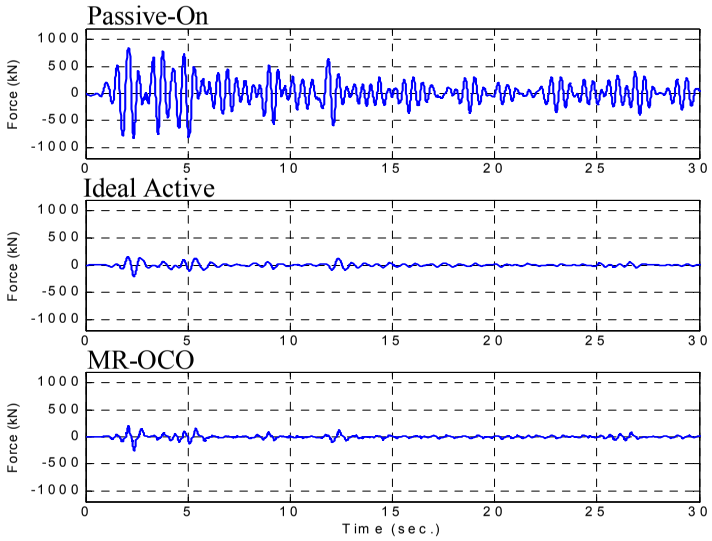

a) Control Forces in x-direction at Y-163.35 n 1FL

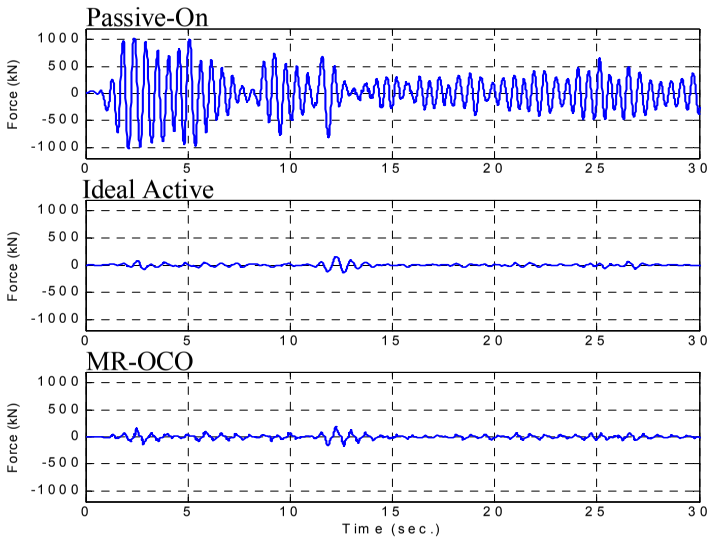

b) Control Forces in y-direction at X116 on 1FL

FIGURE 6-33. Representative Control Forces (El Centro 0.5).

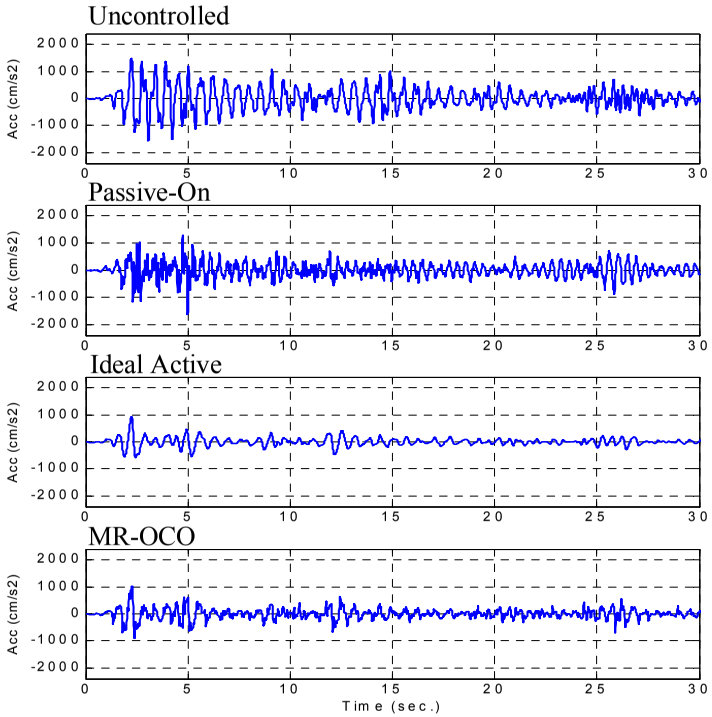

a) Acceleration Responses in x-direction at Y-163.35 on 8FL

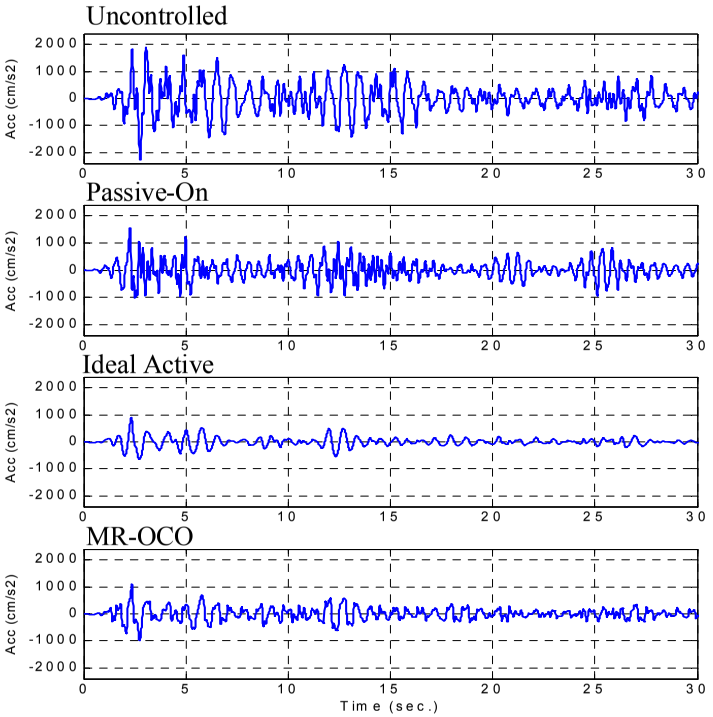

b) Acceleration Responses in x-direction at Y107 on 8FL

FIGURE 6-34. Representative Acceleration Responses in x-direction (El Centro 1.0).

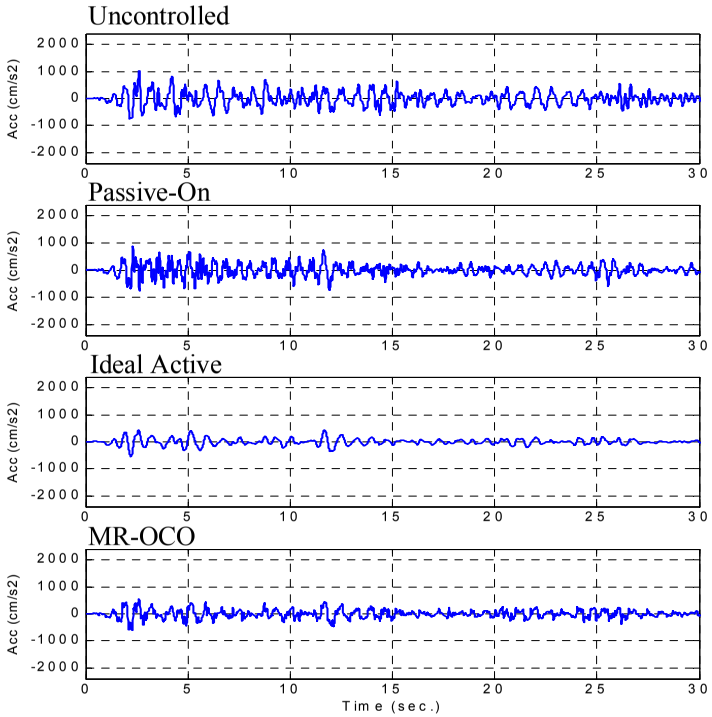

a) Acceleration Responses in y-direction at X-62 on 8FL

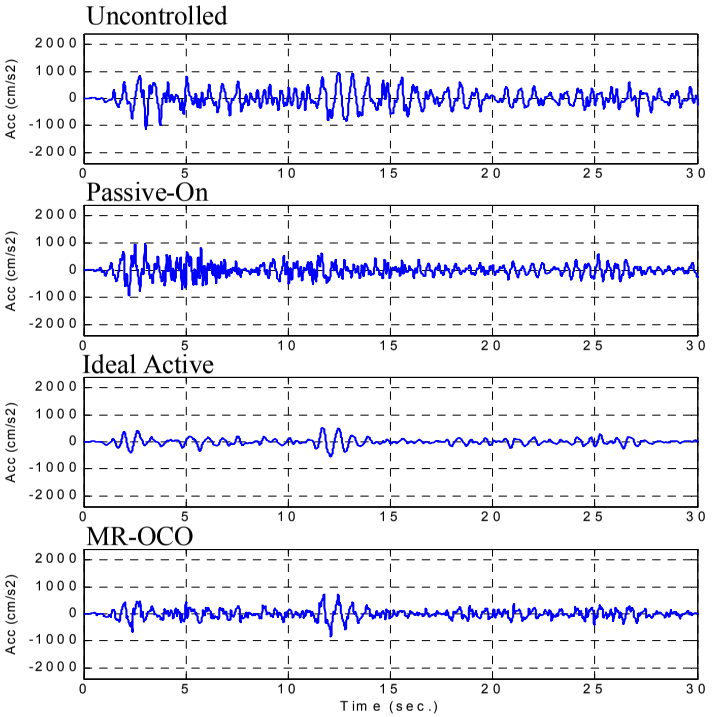

b) Acceleration Responses in y-direction at X52.05 on 8FL

FIGURE 6-35. Representative Acceleration Responses in y-direction (El Centro 1.0).

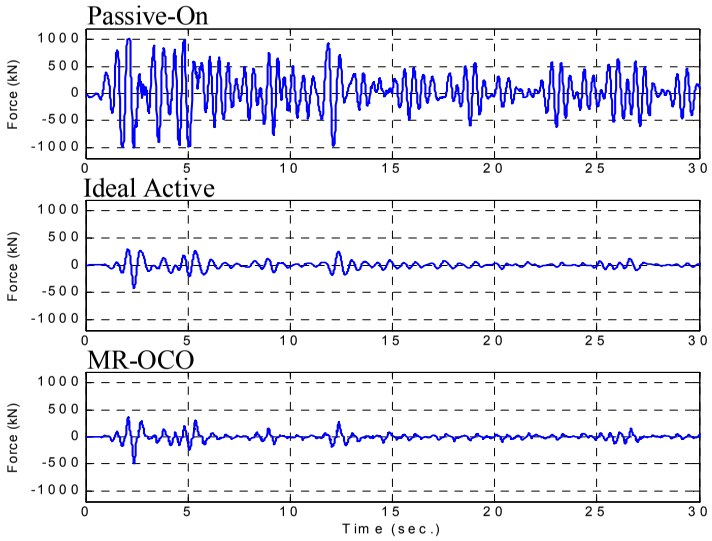

a) Control Forces in x-direction at Y-163.35 n 1FL

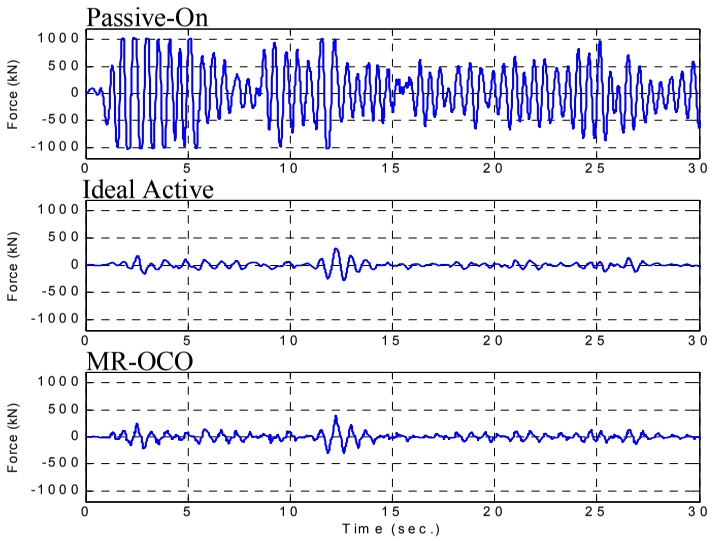

b) Control Forces in y-direction at X116 on 1FL

FIGURE 6-36. Representative Control Forces (El Centro 1.0).

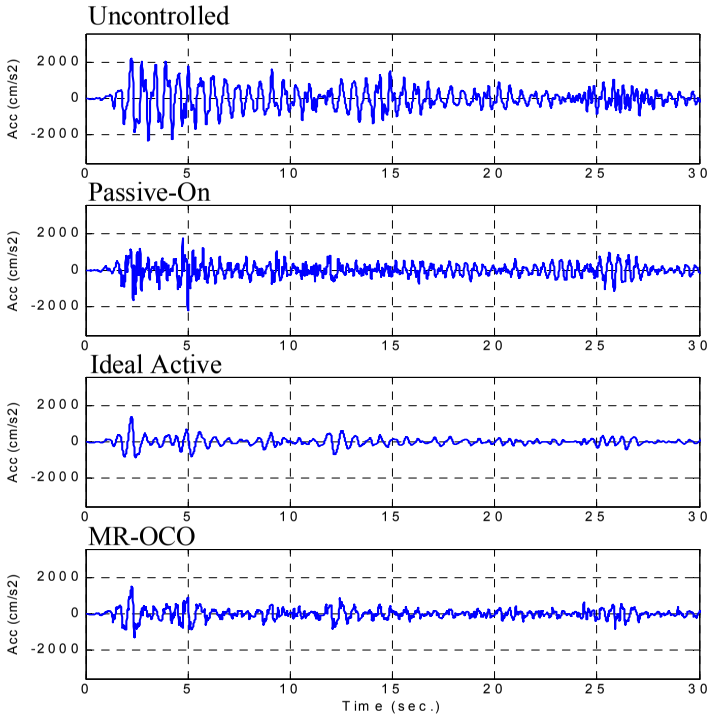

a) Acceleration Responses in x-direction at Y-163.35 on 8FL

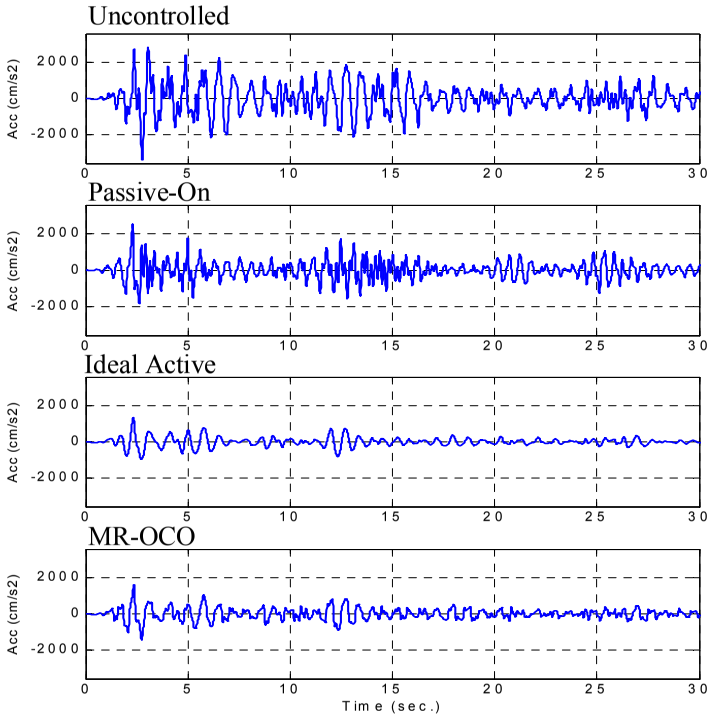

b) Acceleration Responses in x-direction at Y107 on 8FL

FIGURE 6-37. Representative Acceleration Responses in x-direction (El Centro 1.5).

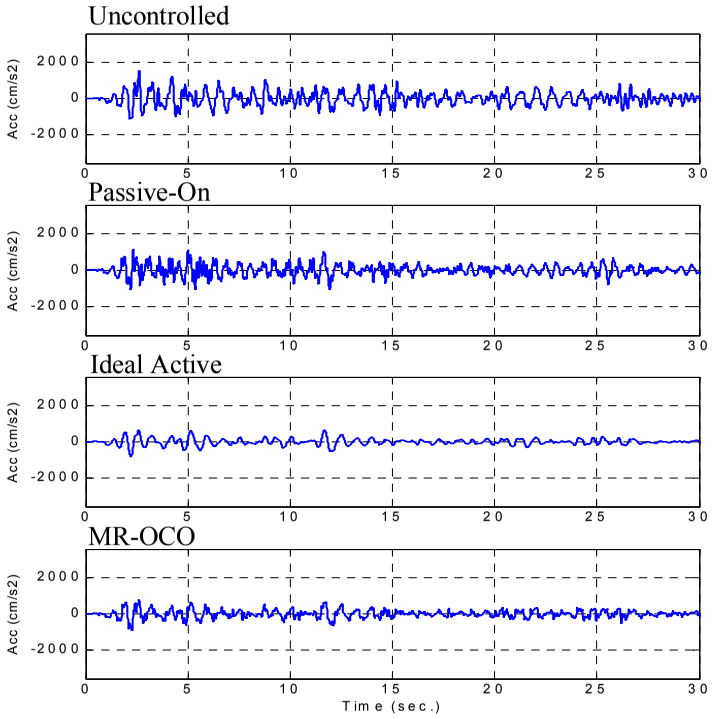

a) Acceleration Responses in y-direction at X-62 on 8FL

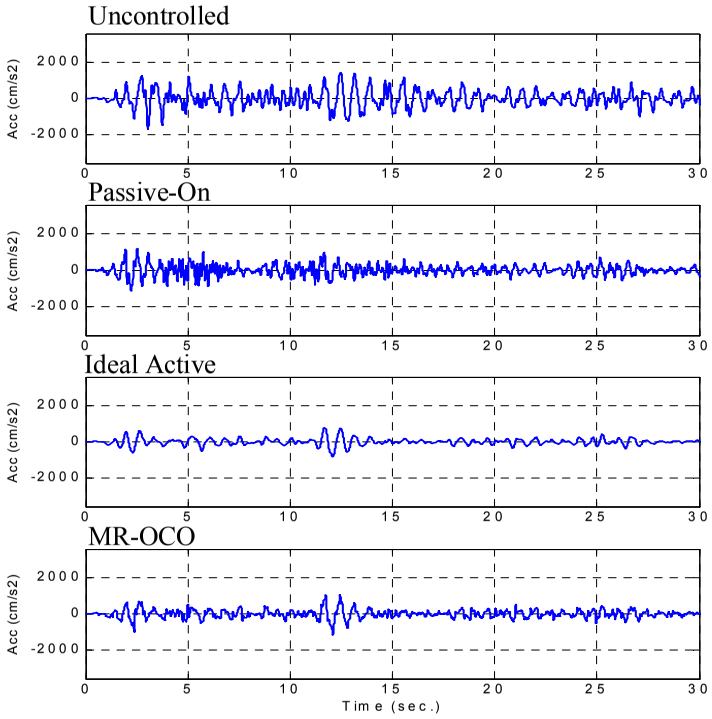

b) Acceleration Responses in y-direction at X52.05 on 8FL

FIGURE 6-38. Representative Acceleration Responses in y-direction (El Centro 1.5).

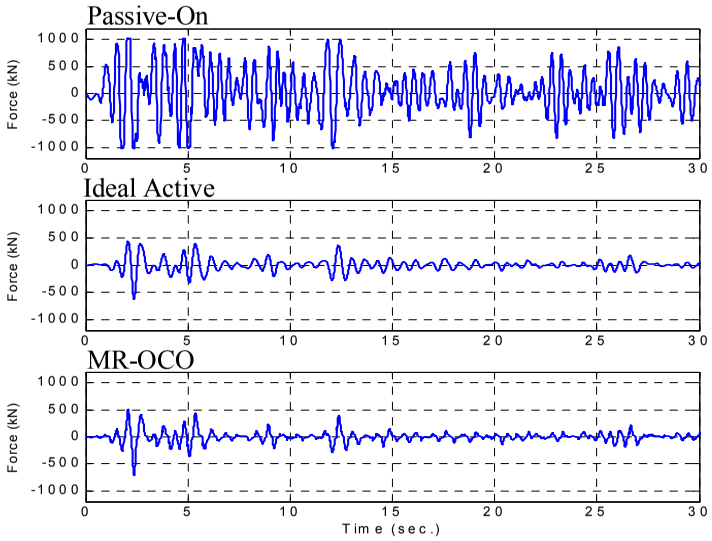

a) Control Forces in x-direction at Y-163.35 n 1FL

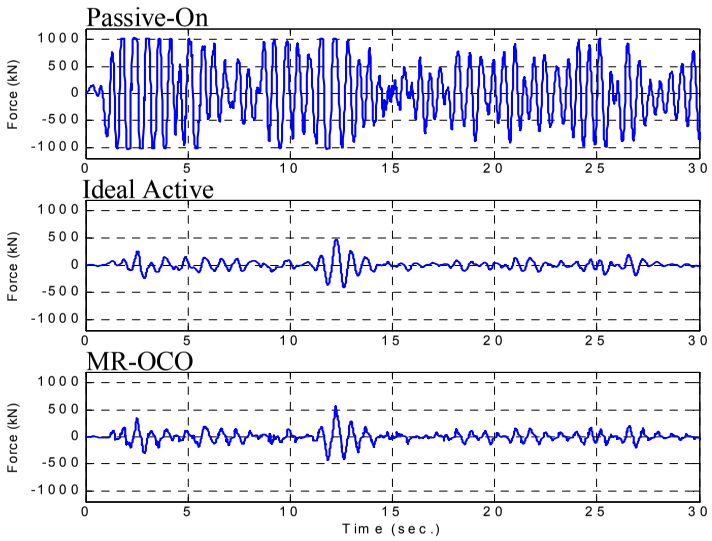

b) Control Forces in y-direction at X116 on 1FL

FIGURE 6-39. Representative Control Forces (El Centro 1.5).

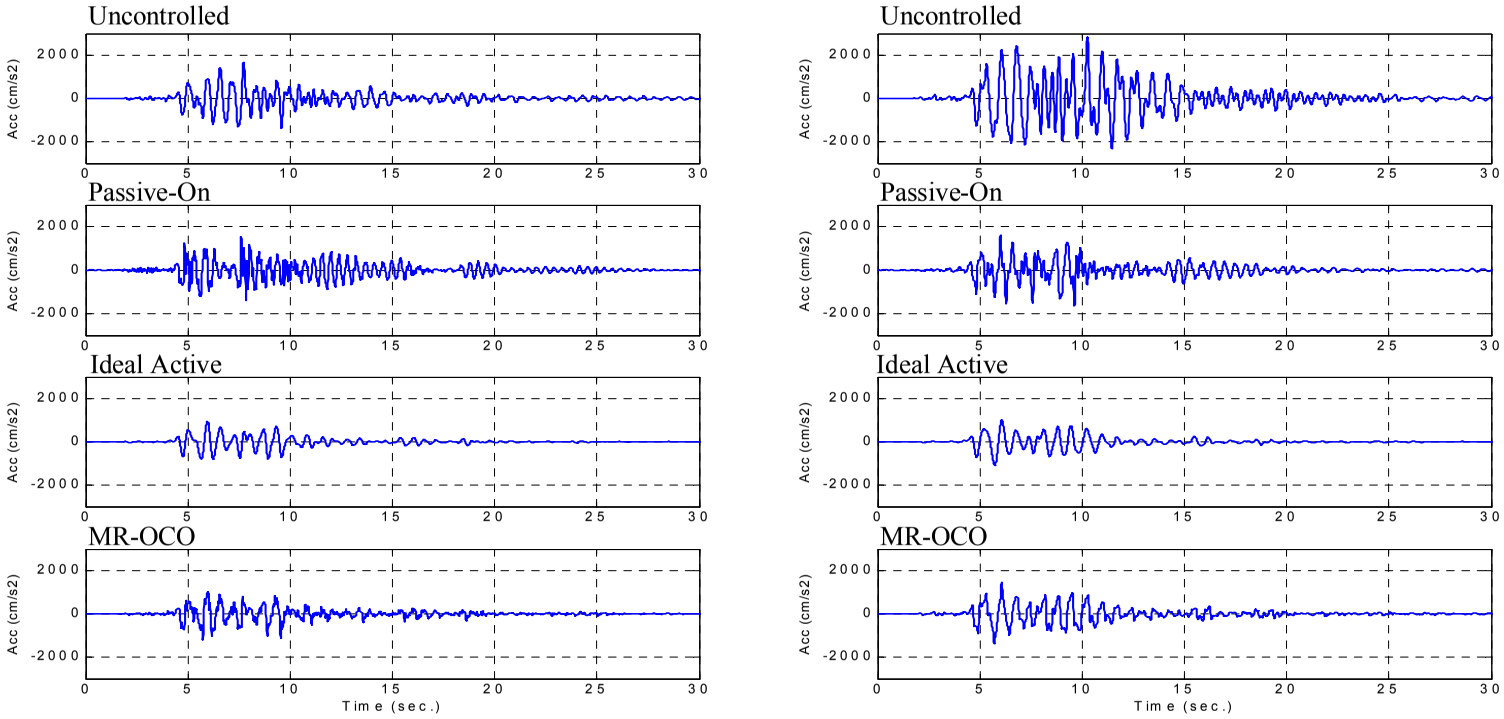

a) Acceleration Responses in x-direction at Y-163.35 on 8FL

b) Acceleration Responses in x-direction at Y107 on 8FL

FIGURE 6-40. Representative Acceleration Responses in x-direction (Kobe 0.5).

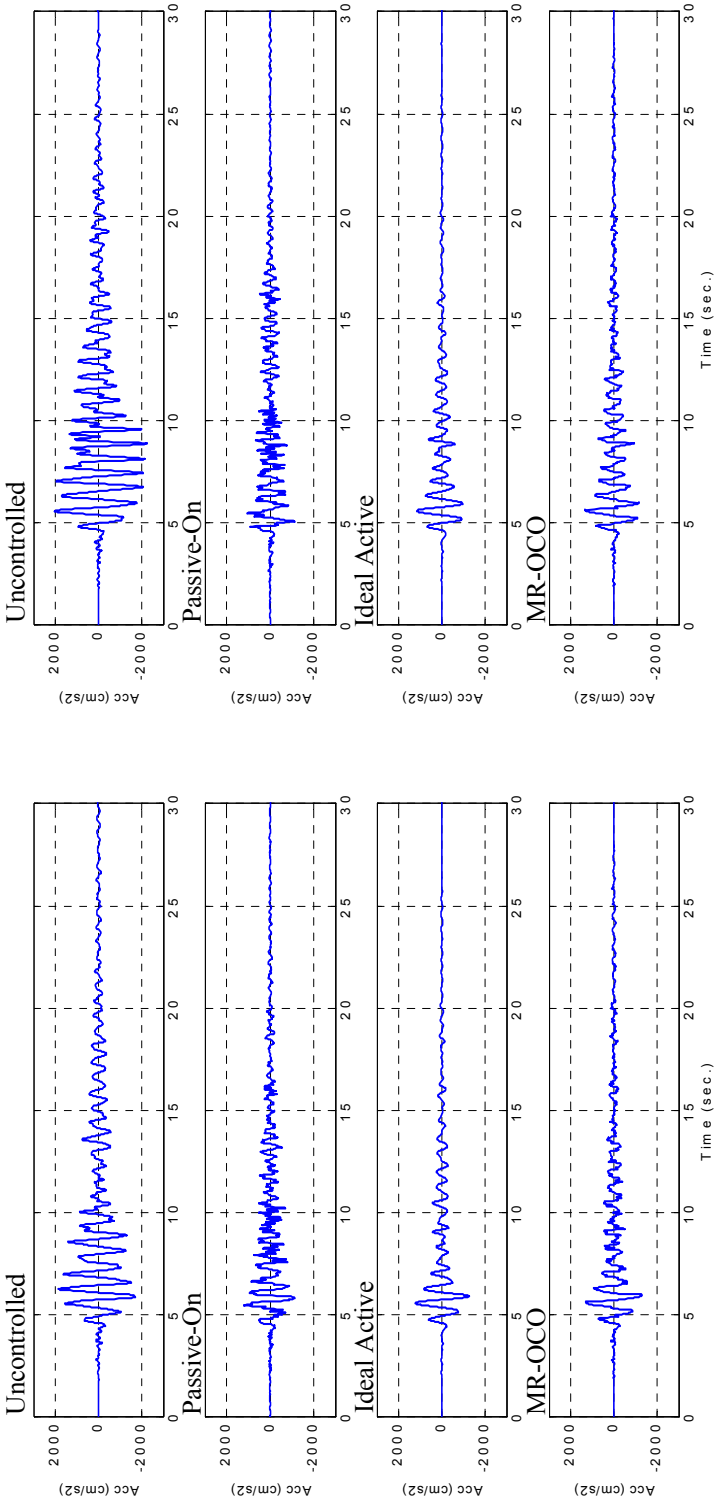

a) Acceleration Responses in y-direction at X-62 on 8FL

b) Acceleration Responses in y-direction at X52.05 on 8FL

FIGURE 6-41. Representative Acceleration Responses in y-direction (Kobe 0.5).

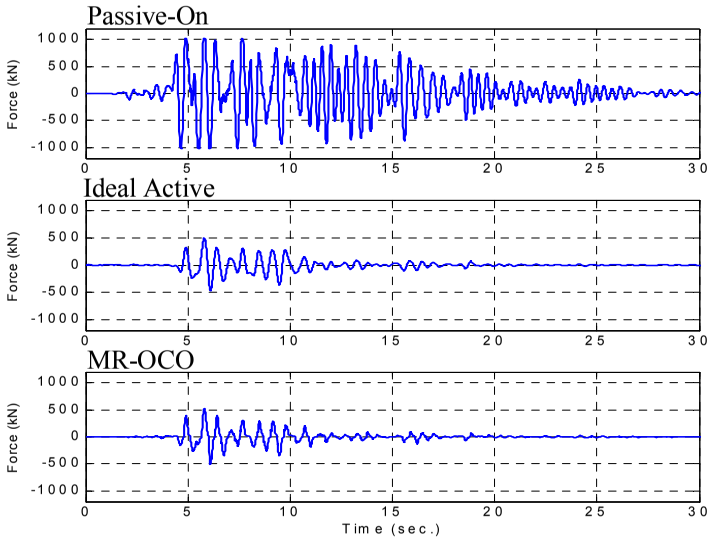

a) Control Forces in x-direction at Y-163.35 n 1FL

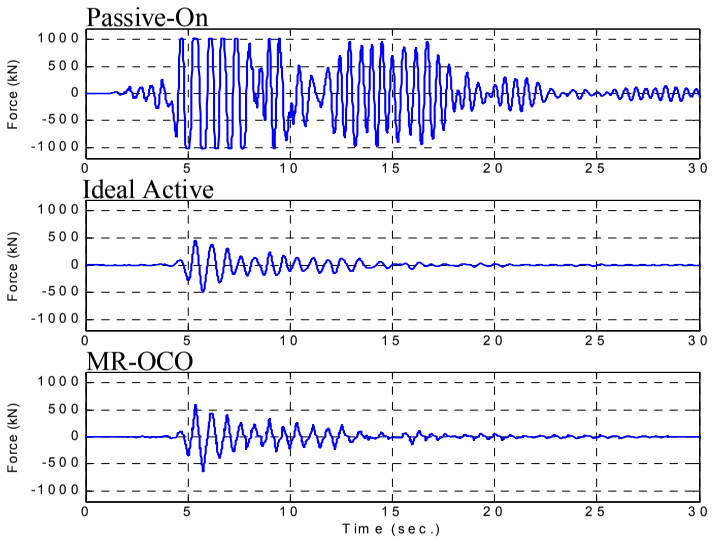

b) Control Forces in y-direction at X116 on 1FL

FIGURE 6-42. Representative Control Forces (Kobe 0.5).

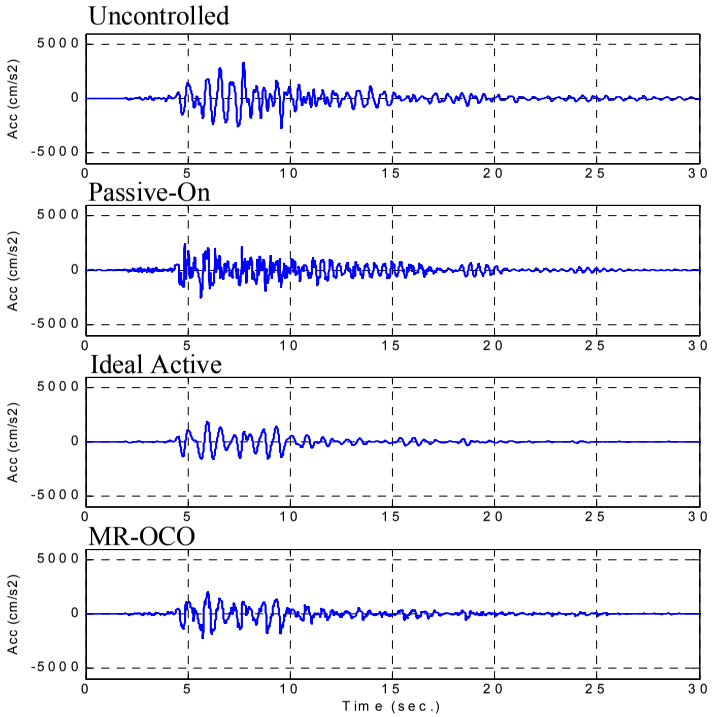

a) Acceleration Responses in x-direction at Y-163.35 on 8FL

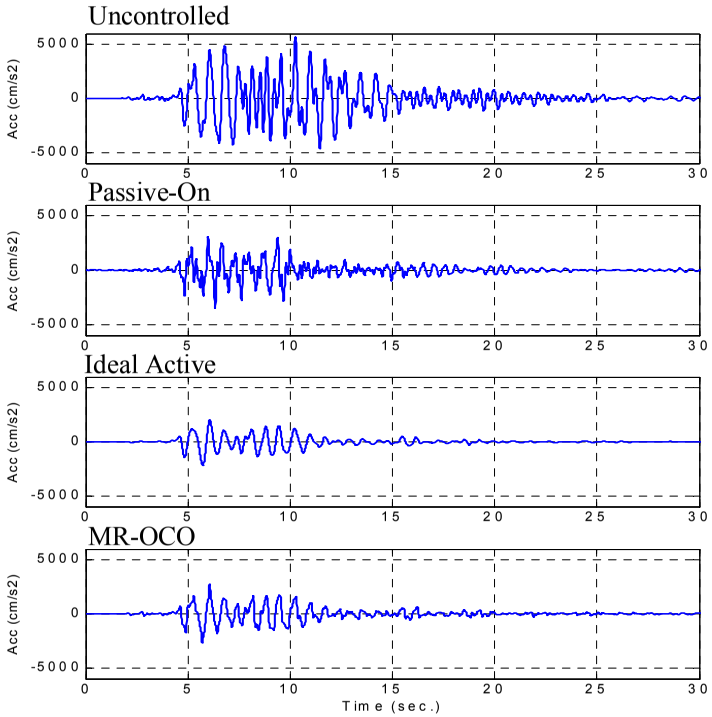

b) Acceleration Responses in x-direction at Y107 on 8FL

FIGURE 6-43. Representative Acceleration Responses in x-direction (Kobe 1.0).

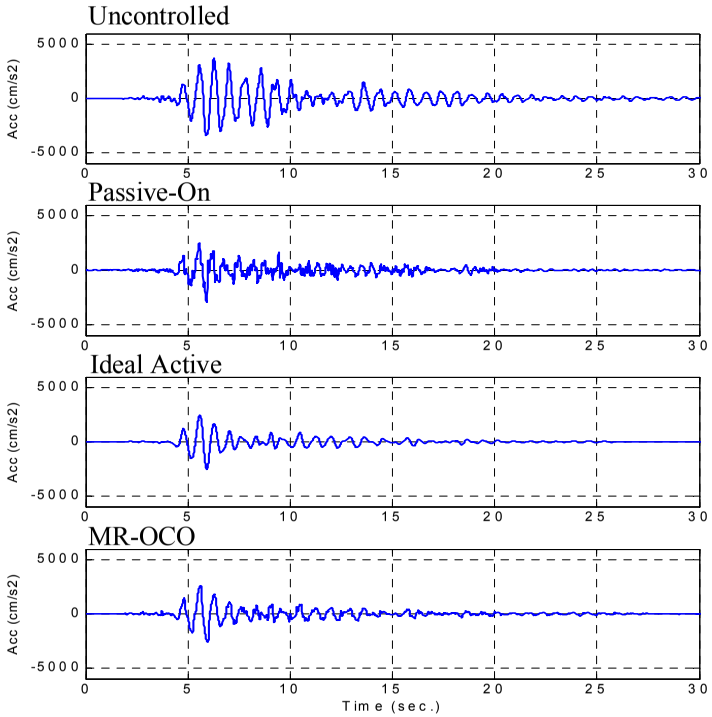

a) Acceleration Responses in y-direction at X-62 on 8FL

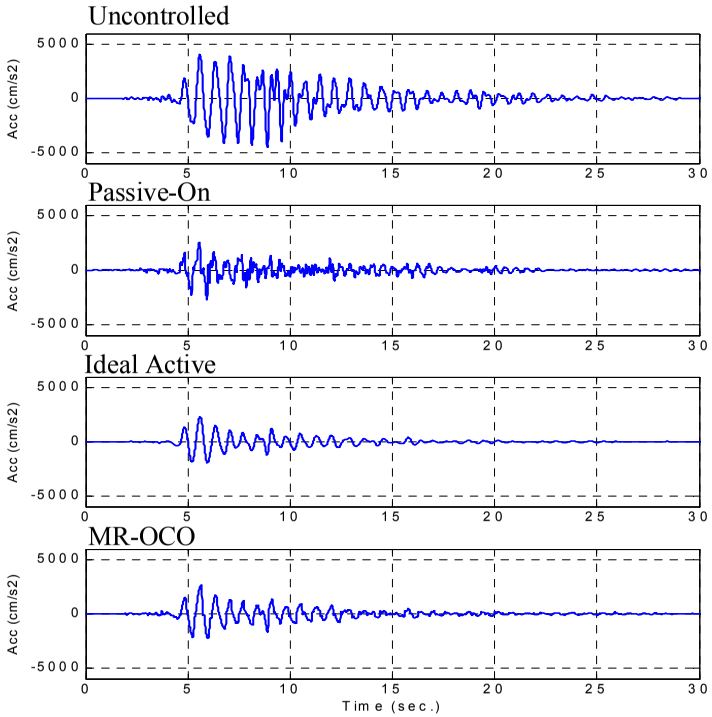

b) Acceleration Responses in y-direction at X52.05 on 8FL

FIGURE 6-44. Representative Acceleration Responses in y-direction (Kobe 1.0).

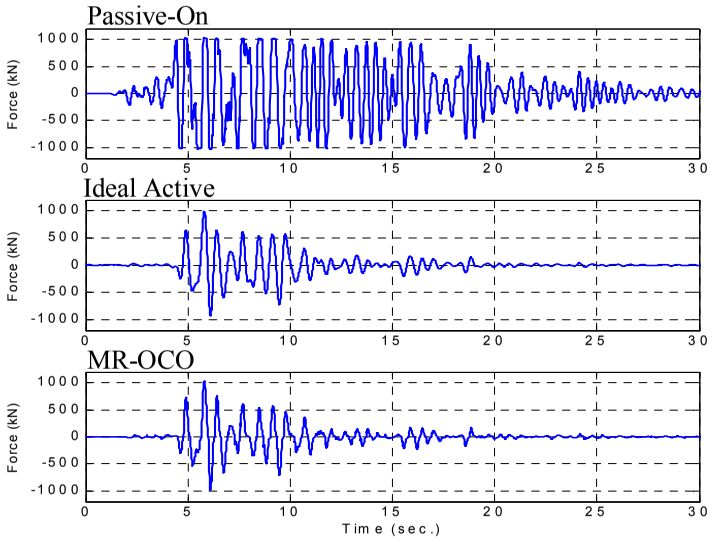

a) Control Forces in x-direction at Y-163.35 n 1FL

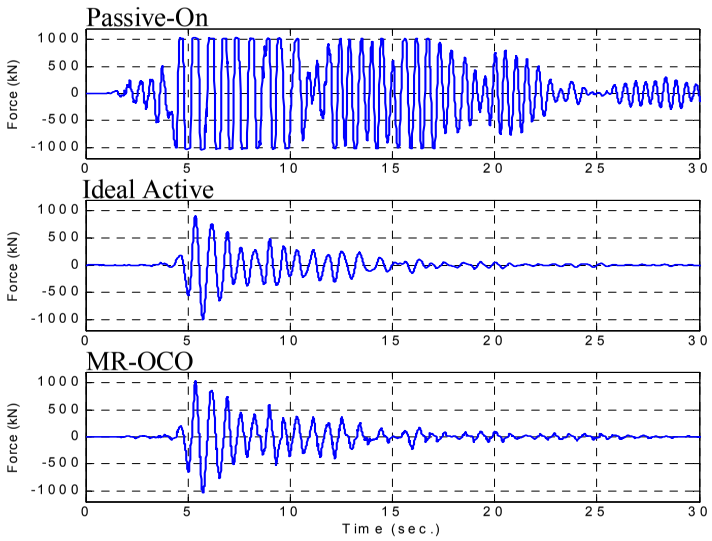

b) Control Forces in y-direction at X116 on 1FL

FIGURE 6-45. Representative Control Forces (Kobe 1.0).

representation of the evaluated responses is shown in Figure 6-46. The results obtained in this case study basically agree with the one in the previous case, but are discussed here again.

In comparing the clipped-optimal controller and the ideal active controller, similar performance is achieved by both control systems in general. The clipped-optimal controller reduces the maximum acceleration responses by 40–52% for the El Centro 1940 earthquake and by 49–51% for the Kobe 1995 earthquakes, and the maximum interstory drift is reduced by 45–48% for the El Centro 1940 earthquakes and by 46–47% for the Kobe 1995 earthquakes. In reducing acceleration responses the ideal active controller achieves a modest improvement over the clipped-optimal controller, while in reducing interstory drift due to the Kobe earthquakes, the clipped-optimal performs better than the ideal active controller.

When comparing the clipped-optimal controller and the passive-on controller, the clipped-optimal controller has significant advantages in reducing the acceleration responses, both in terms of maximum and normed values. This observation is more pronounced for the acceleration responses due to smaller earthquakes. Note that the normed acceleration response of the passive-on controller for El Centro 0.5 is increased compared to the uncontrolled building, while the clipped-optimal controller can reduce this response effectively. As for reducing the interstory drift, both the clipped-optimal controller and the passive-on controller have similar performance. In some cases, such as El Centro 0.5 and all levels of Kobe earthquakes, the passive-on control performs slightly better in reducing the maximum interstory drift responses. In the other cases, such as El Centro 1.0 and El Centro 1.5, the clipped-optimal controller is slightly better. It is also noted that the passive-on controller applies larger forces than the clipped-optimal controller, while achieving much lower performance level.

TABLE 6-12. Results for Evaluation Criteria.

	J_1	J_2	J_3	J_4	J_5
El Centro 0.5					
Passive-Off	0.9110	1.0318	0.7066	0.8063	0.000149
Passive-On	0.5202	0.7694	0.5191	1.7947	0.006931
Ideal Active	0.5161	0.4052	0.4491	0.3265	0.001871
Original Clipped-Optimal	0.5514	0.6009	0.4065	0.5103	0.002335
Modified Clipped-Optimal	0.5650	0.5627	0.4666	0.5889	0.001688
El Centro 1.0					
Passive-Off	0.9360	0.9983	0.8026	0.8367	0.000150
Passive-On	0.5414	0.7177	0.4170	0.8982	0.007002
Ideal Active	0.5161	0.4052	0.4491	0.3265	0.003742
Original Clipped-Optimal	0.5263	0.4944	0.4079	0.4412	0.004197
Modified Clipped-Optimal	0.5406	0.5240	0.4373	0.5021	0.003511
El Centro 1.5					
Passive-Off	0.9511	0.9864	0.8499	0.8623	0.000151
Passive-On	0.5633	0.7457	0.4106	0.6316	0.007033
Ideal Active	0.5161	0.4052	0.4491	0.3265	0.005614
Original Clipped-Optimal	0.5150	0.4755	0.4121	0.4129	0.005874
Modified Clipped-Optimal	0.5325	0.5050	0.4331	0.4652	0.005026
Kobe 0.5					
Passive-Off	0.8635	0.8646	0.8557	0.8558	0.000150
Passive-On	0.4374	0.5762	0.3679	0.7085	0.006992
Ideal Active	0.5858	0.4420	0.4361	0.3251	0.003425
Original Clipped-Optimal	0.5373	0.5123	0.4123	0.4117	0.004753
Modified Clipped-Optimal	0.5555	0.4990	0.4455	0.4511	0.004393
Kobe 1.0					
Passive-Off	0.9154	0.9148	0.9130	0.9069	0.000152
Passive-On	0.4448	0.6091	0.3847	0.4511	0.007103
Ideal Active	0.5858	0.4420	0.4361	0.3251	0.006850
Original Clipped-Optimal	0.5311	0.4839	0.4143	0.3868	0.007078
Modified Clipped-Optimal	0.5446	0.4844	0.4269	0.4149	0.007073

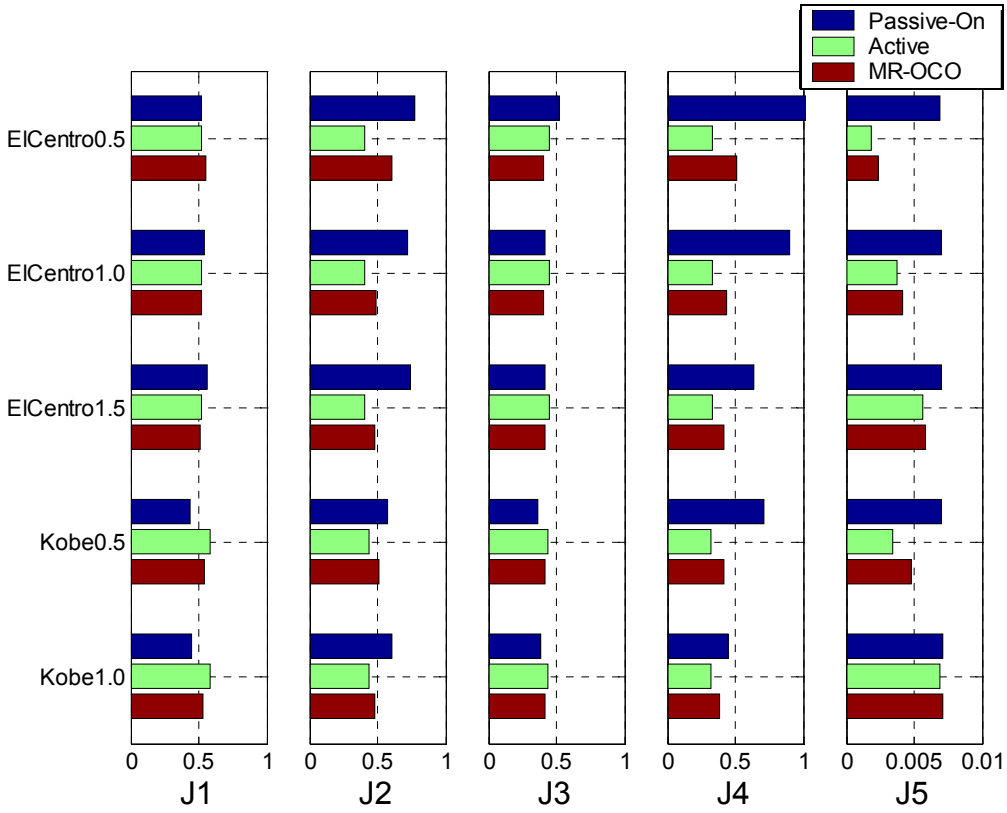

FIGURE 6-46. Evaluation Criteria for Case II.

6.7 Summary

In this chapter, the semiactive control systems proposed for torsional response control were applied to numerical models of two full scale buildings, and the performance when subjected to earthquake excitations was evaluated. One building studied here was a 9-story building with an irregular plan. The second was an L-shaped, 8-story building with vertical irregularities (setbacks). GAs were used to determine the optimal layout of the control devices for each structure. A bi-directional earthquake input was considered in the second case. Several evaluation criteria were selected to assess the performance of the proposed passive, active and semiactive designs.

The results of these studies indicated that, in general, the semiactive clipped-optimal controller using MR damper achieves similar performance to an ideal active control system in reducing the evaluated responses due to earthquakes. With a few exceptions, the ideal active controller performed slightly better than the clipped-optimal controller, although the clipped-optimal controller achieved higher reductions in interstory drift responses in some cases.

When comparing the semiactive clipped-optimal controller using MR dampers and the passive-on controllers, the clipped-optimal controller offered significant performance gains in reducing acceleration responses. In reducing interstory drift responses, in some cases, the clipped-optimal performed slightly better, and the other cases, the passive-on control performed slightly better. In comparing two semiactive control algorithms used with MR dampers, almost same performance were shown, but the original clipped-optimal control algorithm was found to be moderately better than the modified version of this algorithm.

Chapter 7

Conclusions and Future Work

This dissertation has focused on the development and validation of control systems that can effectively reduce the seismic responses due to torsional coupling in asymmetric building structures. Due to their attractive characteristics for seismic response control, semiactive control systems using MR dampers were specifically examined in the numerical and experimental studies. Two candidate control algorithms were presented for the semiactive control system, the clipped-optimal control algorithm as well as the modified version of this algorithm.

Initially, to verify the performance of the proposed semiactive control systems, the approach developed herein was applied to a simple numerical model of a full scale symmetric building. The building selected for this study was the 20-story building used for the 3rd Generation Benchmark Problem on Structural Control [36,37], developed as part of the activities of the IASC-ASCE Task Group on Structural Control Benchmarks. To investigate the requirements and achievable capabilities of the control system, the performance of the semiactive control systems were compared to those of an active control system and an ideal semiactive control system. In comparing the active, ideal semi-active and MR control systems, it was observed that similar performance could typically be achieved by all of these systems, reinforcing the result obtained by previous studies that semiactive systems can achieve similar performance levels to that of active systems. In comparing the two control algorithms used with the MR damper, the modified clipped-optimal control algorithm was found to be significantly more effective

at reducing the accelerations of this structure while achieving nearly the same reduction in interstory drifts. Of particular interest was the result that the permanent offset in the interstory drifts was generally reduced by a significant margin in the controlled results. The number of plastic connections formed was also reduced significantly by the controllers.

Next, the basic behavior of torsional responses of asymmetric building was examined. Additionally, as a preliminary numerical control study, a passive control system and active control systems were implemented on several asymmetric building models. Parametric studies were conducted using a model of a single story building with an asymmetric stiffness distribution along one axis. The results demonstrated that increasing asymmetry results in an increase in torsional response and a decrease in translational response, which concentrates the deformation at some columns and amplifies the maximum acceleration of the floors. In controlling the responses of asymmetric buildings, active control systems were found to reduce the responses more than passive control systems. This effect was more pronounced as the number of stories in the building increased and as the eccentricity increased. The application of active control clearly has advantages over passive here.

To experimentally verify the applicability of the proposed semiactive control system to torsional coupling responses of an asymmetric building, laboratory studies were conducted using a 2-story, asymmetric test structure with four degrees of freedom. To obtain a control-oriented model of this experimental structure, an automated procedure was developed to identify a control-oriented model of the system to be controlled. The analytical model of the system was developed based on the structural parameters, and this model was modified to have the frequencies observed in the experimental system. The ERA technique was used to experimentally identify frequencies and mode shapes of the test structure. The parameters for the MR damper model were identified for the integrated system model, which considers the test structure combined with the MR dampers.

The integrated system model obtained was found to adequately represent the experimental system. The optimal nominal controller was designed through a series of parametric studies. High performance controllers were designed by placing a higher weighting on the acceleration responses of the weak side on the 2nd floor. The experimental results demonstrate that the performance of a semiactive controller using MR dampers was significantly better than passive control system where constant voltages are applied to the MR dampers. When a large constant voltage was applied to the MR damper, the first floor became rigid and the second floor was able to move freely with its own natural frequency, resulting in an increase in the maximum response, especially for small ground excitations. However, when the proposed semiactive controller was applied, all responses of the structure were effectively reduced at all input amplitudes.

Furthermore, the proposed semiactive control systems was numerically applied to two simple numerical models of full scale buildings, and their performance due to earthquake excitations was evaluated. Case I considered a 9-story building with an irregular plan, and Case II considered an L-shaped 8-story building with additional vertical irregularity. GAs were used to find the optimal location of the control devices. A bi-directional earthquake input was employed in Case II. In general, the semiactive clipped-optimal controller using MR dampers achieved similar performance to that of the ideal active control system in reducing the responses due to earthquakes. When comparing the semiactive clipped-optimal controller using MR dampers and the passive-on controller, the clipped-optimal controller was significantly better at reducing acceleration responses. In comparing the two semiactive control algorithms, clipped-optimal and modified clipped-optimal, almost the same performance as observed for both. The original clipped-optimal controller was found to be slightly better than the modified version.

Through the series of studies conducted within this dissertation, semiactive control systems using MR dampers were found to be effective for the reduction of responses in torsionally coupled symmetric building structures.

Some potential topics for future work related to this dissertation are discussed herein.

Two semiactive control algorithms were proposed and applied in this dissertation, clipped-optimal control algorithm and the modified version. The modified version was found to be more effective than the original clipped-optimal control algorithm in reducing the acceleration responses for the 20-story symmetric building, while their performances were similar and the original clipped-optimal controller is slightly better than the modified version for the 9-story and L-shaped 8-story asymmetric buildings. The most likely reason for this result is the difference in the values of the natural frequencies of the structures. The fundamental natural frequency of the 20-story building is 0.26Hz, which is much smaller than those of the 9-story (0.83Hz) and the L-shaped 8-story building (1.26Hz). A systematic parametric study is needed develop an approach to select the most appropriate algorithm for each application.

GAs are used to identify the optimal control device placement for the 9-story and the L-shaped 8-story buildings. In many cases, the control device locations found to be optimal by the GA look reasonable, while in other cases the results are suspicious. Further investigation is needed on the use of GAs for control device placement.

In general, semiactive control systems using MR dampers are attractive because their control performance is significantly better than those of passive control systems, and is as good as active control systems (in some cases better) with significantly less power requirements. According to the studies conducted in this dissertation, to reduce the maximum responses by 2/3 to 1/2, the required total force capacities are nearly the weight of the building. It is true that the number of MR dampers needed to achieve these performance is not small, but this is within reasonable parameters. In fact, several buildings currently exist which are equipped with a number of passive dampers inside the building frames on every floors. The semiactive control systems requires several elements above and beyond the needs of such a passive system. For instance, sensors, CPUs, and cables

are required, possibly on every floor throughout the structure. This task seems quite complex and expensive, not only for installation but also for maintenance of the system. One approach to solve this problem is the development of wireless technologies. If the sensors and control devices are able to communicate with CPUs wirelessly, there are no need for cables to be installed, reducing the overall cost of such a system considerably. So, the development of wireless technologies could be a key to encouraging the application of semiactive control systems to full scale buildings.

Furthermore, it would be ideal for a semiactive control system at least function as a passive control system mechanically if the power to the system were to fail. For example, if the semiactive system were designed with a permanent magnet such that the maximum damping forces are generated when zero voltage is applied, simulating a system failure, the behavior of a given device if a failure were to occur would correspond to that of a passive-on device. The first priority during severe earthquakes is to protect the structures from being significantly damaged and collapsed. This outcome can be achieved in many cases even with passive control systems. Considering the design of a system for fail-safe behavior is another key issue for the widespread application of semiactive control systems to full scale structures.

References

[1] Abdullah, M., Richardson, A., and Hanif, J. (2001). "Placement of Sensors/ Actuators on Civil Structures Using Genetic Algorithms." *Earthquake Engineering and Structural Dynamics*, Vol. 30, pp. 1167–1184.

[2] Akbay, Z., and Aktan, H. M. (1991). "Actively Regulated Friction Slip Devices." *Proc. of the 6th Canadian Conference on Earthquake Engineering*, pp. 367–374.

[3] Antoniou, A. (1993). *Digital Filters: Analysis, Design, and Applications*. McGraw-Hill, Inc., New York, pp. 444–446.

[4] Burton, S. A., Makris, N., Konstantopoulos, I. and Antsaklis, P. J. (1996). "Modeling the Response of ER Damper: Phenomenology and Emulation," *Journal of Engineering Mechanics*, ASCE, Vol. 122, No. 9, pp. 897–906.

[5] Carlson, J. D. (1994). "The Promise of Controllable Fluids." *Proc. of Actuator 94* (H. Borgmann and K. Lenz, Eds.), AXON Technologie Consult GmbH, pp. 266–270.

[6] Carlson, J. D., and Spencer Jr., B. F. (1996). "Magneto-Rheological Fluid Dampers: Scalability and Design Issues for Application to Dynamic Hazard Mitigation." *Proc. 2nd Int. Wkshp. on Struc. Control*, Hong Kong, pp. 99–109, Dec.

[7] Carlson, J. D., and Weiss, K. D. (1994). "A Growing Attraction to Magnetic Fluids," *Machine Design*, August, pp. 61–64.

[8] Chi, Y., Sain, M. K., Pham, K. D., Spencer Jr., B. F. (2000) "Structural Control Paradigms for an Asymmetric Buildings." *Proc. of 8th ASCE Special Conference on Probabilistic Mechanics and Structural Reliability*, PMC2000-152.

[9] Constantinou, M. C., and Symans, M. D. (1994). "Semi-Active Fluid Viscous Dampers for Seismic Response Control." *Proc. of the First World Conf. on Structural Control,* Pasadena, CA.

[10] Dyke, S. J., and Spencer Jr., B. F., (1996). "Seismic Response Control Using Multiple MR Dampers." *Proc. of the 2nd Intl. Workshop on Structural Control*, Hong Kong, pp. 163–173.

[11] Dyke, S. J., and Spencer Jr., B. F. (1997). "A Comparison of Semi-Active Control Strategies for the MR Damper." *Proc. of the International Conference on Intelligent Information Systems*, Bahamas, December 8–10.

[12] Dyke, S. J., Spencer Jr., B. F., Sain, M. K., and Carlson, J. D. (1996). "Modeling and Control of Magnetorheological Dampers for Seismic Response Reduction." *Smart Materials and Structures*, Vol. 5, pp. 565–575.

[13] Dyke, S. J., Spencer Jr., B. F., Sain, M. K. and Carlson, J. D. (1996). "Seismic Response Reduction Using Magnetorheological Dampers." *Proc. of the IFAC World Congress*, San Francisco, CA, June 30–July 5.

[14] Dyke, S. J., Spencer Jr., B. F., Sain, M. K., and Carlson, J. D. (1998). "An Experimental Study of MR Dampers for Seismic Protection." *Smart Materials and Structures: Special Issue on Large Civil Structures*, Vol. 7, pp. 693–703.

[15] Dyke, S. J., Yi, F., and Carlson, J.D. (1999). "Application of Magnetorheological Dampers to Seismically Excited Structures." *Proc. of the Intl. Modal Anal. Conf.*, Kissimmee, Florida, February 8–11.

[16] Ehrgott, R. C., and Masri, S. F. (1994). "Structural Control Applications of an Electrorheological Device." *Proc. of the International Workshop on Structural Control*, USC Publication Number CE-9311, pp. 115–129.

[17] FEMA (1991). *1991 Edition NEHRP Recommended Provisions for the Development of Seismic Regulations for New Buildings - Part2 Commentary*, FEMA223.

[18] Feng, Q., and Shinozuka, M. (1990). "Use of a variable Damper for Hybrid Control of Bridge Response Under Earthquake." *Proc., U.S. Nat. Workshop on Struct. Control Res.*, USC Publ. No. CE-9013.

[19] Ferhi, A., and Truman, K. Z. (1996). "Behaviour of asymmetric building systems under a monotonic load - I." *Engineering Structures*, Vol. 18, No. 2, pp. 133–141.

[20] Ferhi, A., and Truman, K. Z. (1996). "Behaviour of asymmetric building systems under a monotonic load - II." *Engineering Structures*, Vol. 18, No. 2, pp. 142–153.

[21] Fujino, Y., Soong, T. T., and Spencer Jr., B. F. (1996). "Structural Control: Basic Concepts and Applications." *Proc. of the ASCE Struct. Cong.*, Chicago, Illinois, pp. 361–370.

[22] Fujitani, H., Soda, S., Iwata, N., Sodeyama, H., Hata, K., Sunakoda, K., and Komatsu, Y. (2001). "Dynamic Performance Evaluation of Magneto-rheological Damper by Experimental and Analytical Methods." *Proceedings of the US-Japan Workshop on Smart Structures for Improved Seismic Performance in Urban Regions*, Seattle, Washington, August 14, pp. 237–248.

[23] Gavin, H., and Alhan, C. (2002) "Control of Torsionally Asymmetric Structures." *Proc. of the American Control Conference,* Anchorage, AK, May 8–10.

[24] Gavin, H. P., Hose, Y. D., and Hanson, R. D. (1994). "Design and Control of Electrorheological Dampers." *Proc. of the First World Conference on Structural Control*, Pasadena, CA, August 3-5, Vol. 1, pp. WP3-83 through WP3-92.

[25] Giacosa, L. M., Yoshida, O., and Dyke, S. J. (2002). "Control-oriented System Identification Using ERA," *Proc. of the Third World Conf. on Structural Control*, Como, Italy.

[26] Jansen, L. M., and Dyke, S. J., (2000). "Semiactive Control Strategies for MR Dampers: Comparison Study." *Journal of Engineering Mechanics*, ASCE, Vol. 126, No. 8, pp 795–803.

[27] Juang, J.N. and Pappa, R.S. (1985). "An Eigensystem Realization Algorithm for Modal Parameter Identification and Model Reduction," *J. of Guidance Control and Dynamics*, 8, pp. 620–627.

[28] Kan, C. L., and Chopra, A. K. (1977). "Effect of Torsional Coupling on Earthquake Force in Buildings," *Journal of the Structural Division*, ASCE, 103, pp. 805–820.

[29] Kawashima, K., Unjoh, S., and Shimizu, K. (1992). "Experiments on Dynamics Characteristics of Variable Damper," *Proc. of the Japan National Symposium on Structural Response Control*, Tokyo, Japan, pp. 121.

[30] Klass, D. L., and Martinek, T. W. (1967). "Electroviscous Fluids I: Rheological Properties," *Journal of Applied Physics*, Vol. 38(1), pp. 67–74.

[31] Klass, D. L., and Martinek, T. W. (1967). "Electroviscous Fluids II: Electrical Properties," *Journal of Applied Physics*, Vol. 38(1), pp. 75–80.

[32] Li, Q. S., Liu, D. K., Zhang. N. Tam, C. M., and Yang L. F. (2001). "Multi-level design model and genetic algorithm for structural control system optimization," *Earthquake Engineering and Structural Dynamics*, Vol. 30, pp. 927–42.

[33] Makris, N., Burton, S. A., Hill, D. and Jordan, M. (1996). "Analysis and Design of ER Damper for Seismic Protection of Structures," *Journal of Engineering Mechanics*, ASCE, Vol. 122, No. 10, pp. 1003–11.

[34] Narasimhan, S., Nagarajaiah, S., Gavin, H., and Johnson, E. A. (2002). "Benchmark Problem for Control of Base Isolated Buildings," *Proc. of 15th ASCE Engineering Mechanics Conference*, New York, NY, June 2-5.

[35] Obayashi Corporation Technical Research Institute, Internal Report No. 63024-6 (2002). (in Japanese, not open to public)

[36] Ohtori, Y., Christenson, R.E., Spencer, Jr. B.F., and Dyke, S.J. (2000). "Summary of Benchmark Control Problems for Seismically Excited Nonlinear Buildings," *Proc. of the 2000 Engineering Mechanics Conf.,* ASCE, Austin, Texas, May 21–24.

[37] Ohtori, Y., Christenson, R.E., Spencer, Jr. B.F., and Dyke, S.J. (2002). "Benchmark Control Problems for Seismically Excited Nonlinear Buildings," *Journal of Engineering Mechanics: Special Issue on Structural Control Benchmark Problems*, ASCE (in press).

[38] Pohlheim, H., (1999). "Evolutionary Algorithms: Overview, Methods and Operators." Documentation for: Genetic Evolutionary Algorithm Toolbox for Use with Matlab version: toolbox 1.92 documentation 1.92 (*http:// www.geatbx.com/*).

[39] Sack, R. L., and Patten, W., (1994). "Semi-active Hydraulic Structural Control." *Proc. of the International Workshop on Structural Control*, USC Publication No. CE-9311, pp. 417-431.

[40] Sadek, F., and Mohraz, B. (1998). "Semi-active Control Algorithm For Structures With Variable Dampers." *Journal of Engineering Mechanics*, ASCE, Vol. 124, No. 9, pp. 981–999.

[41] Sakamoto, M., Kobori, T., Yamada, T., and Takahashi, M. (1994). "Practical Application of Active and Hybrid Response Control Systems and Their Verification by Earthquake and Strong Wind Observations." *Proc. of First World Conference on Structural Control*, Los Angels, CA, August 3–5, pp.WP2:90–99.

[42] Singh, M. P., Singh, S., and Moreschi, L. M. (2002). "Tuned Mass Dampers for Response Control of Torsional Buildings." *Earthquake Engineering and Structural Dynamics*, Vol. 31, pp. 749–769.

[43] Singh, M. P., and Moreschi, L. M. (2002). "Optimal placement of dampers for passive response control." *Earthquake Engineering and Structural Dynamics*, Vol. 31, pp. 955–976.

[44] Sodeyama, H., Sunakoda, K., Suzuki, K., Carlson, J. D., and Spencer Jr., B. F. (2001a). "Development of Large Capacity Semi-active Vibration Control Device using Magnetorheological Fluid." *Seismic Engineering*, ASME, PVP Vol. 428-2, pp. 109–114.

[45] Sodeyama, H., Sunakoda, K., Suzuki, K., Carlson, J. D., and Spencer Jr., B. F. (2001b). "A Basic Study on Dynamic Characteristics of MR Dampers." *Seismic Engineering,* ASME, PVP Vol. 428-2, pp. 115–120.

[46] Soong, T.T. and Grigoriu, M., (1992). *Random Vibration of Mechanical and Structural Systems*, Prentice Hall, Englewood Cliffs, New Jersey.

[47] Spencer Jr., B. F. (1996). "Recent Trends in Vibration Control in the U.S." *Proc. of the 3rd Int. Conf. on Motion and Vibration Control*, Chiba, Japan, Vol. 2, pp. K1–K6.

[48] Spencer Jr., B. F. and Sain, M. K. (1997). "Controlling Buildings: A New Frontier in Feedback," *IEEE Control Systems Magazine: Special Issue on Emerging Technologies* (Tariq Samad Guest Ed.), Vol. 17, No. 6, pp. 19–35.

[49] Spencer Jr., B. F., Dyke, S. J., Sain, M. K., and Carlson, J. D., (1997a). "Phenomenological Model for Magnetorheological Dampers." *Journal of Engineering Mechanics*, ASCE, Vol. 123, No. 3, pp 230–238.

[50] Spencer Jr. B. F., Carlson, J. D., Sain, M. K., and Yang, G. (1997b). "On the Current Status of Magnetorheological Dampers: Seismic Protection of Full-Scale Structures." *Proc. of the Amer. Control Conf*., pp. 458–62.

[51] Spencer Jr., B. F., Dyke, S. J., and Deoskar, H. S. (1998a). "Benchmark Problems in Structural Control - Part I: Active Mass Driver System, and Part II: Active Tendon System." *Earthquake Engineering and Structural Dynamics,* Vol. 27, No. 11, pp.1127–1139 & pp. 1140–1147.

[52] Spencer Jr., B. F., Christenson, R. E., and Dyke, S. J. (1998b). "Next Generation Benchmark Control Problem for Seismically Excited Buildings." *Proceedings of the Second World Conference on Structural Control*, Wiley, Kyoto, JAPAN, June 29–July 2.

[53] Suzuki, T., Kageyama, M., Nobata, A., Inaba, S., and Yoshida, O. (1994). "Active Vibration Control System Installed in a High-rise Building." *Proc. of First World Conference on Structural Control*, Los Angels, CA, August 3–5, pp. FP3:3–11.

[54] Tezcan, S. S. and Alhan, C. (2001). "Parametric Analysis of Irregular Structures under Seismic Loading According to the New Turkish Earthquake Code." *Engineering Structures*, Vol. 23, No.6, pp. 600–609.

[55] Wen, Y. K. (1976). "Method of Random Vibration of Hysteretic Systems." *Journal of Engineering Mechanics Division*, ASCE, Vol. 102, No. EM2, pp. 249–263.

[56] Yang, G., Spencer Jr., B. F., Carlson, J. D., and Sain, M. K. (2001a). "Large-scale MR fluid dampers: modeling and dynamic performance considerations." *Engineering Structures* (submitted).

[57] Yang, G., Jung, H. J., and Spencer Jr., B. F. (2001b). "Dynamic Model of Full-Scale MR Dampers for Civil Engineering Applications." *Proceedings of the US-Japan Workshop on Smart Structures for Improved Seismic Performance in Urban Regions*, Seattle, Washington, August 14, pp. 213–224.

[58] Yang, J. N., Wu, J. C., Samali, B., and Agrawal, A. K. (1998). "A Benchmark Problem for Response Control of Wind-excited Tall Buildings." *Proceedings of the Second World Conference on Structural Control*, Wiley, Kyoto, JAPAN, June 29-July 2.

[59] Yang, J. N., Agrawal, A. K., Samali, B., and Wu, J. C. (2002). "A Benchmark Problem For Response Control of Wind-Excited Tall Buildings." *Journal of Engineering Mechanics: Special Issue on Structural Control Benchmark Problems*, ASCE (in press).

[60] Yi, F., Dyke, S. J., Caicedo, J. M., and Carlson, J. D. (1999). "Seismic Response Control Using Smart Dampers." *Proceedings of the 1999 American Control Conference*, San Diego, California, June 23–25, pp. 1022–26.

[61] Yi, F., Dyke, S. J., Caicedo, J. M., and Carlson, J. D. (2001). "Experimental Verification of Multi-Input Seismic Control Strategies for Smart Dampers." *Journal of Engineering Mechanics*, ASCE, Vol. 127, No. 11, Nov., pp. 1152–1164.

[62] Yoshida, O., and Dyke, S. J. (2002). "Seismic Control of a Nonlinear Benchmark Building Using Smart Dampers," *Journal of Engineering*

Mechanics: Special Issue on Structural Control Benchmark Problems, ASCE (in press).

[63] Yoshida, O., Dyke, S. J., Giacosa, L. M., and Truman, K. Z. (2002). "Torsional Response Control of Asymmetric Buildings Using Smart Dampers," *Proc. of 15th ASCE Engineering Mechanics Conference*, New York, NY, June 2–5.

[64] Yoshida, O., Dyke, S. J., Giacosa, L. M., and Truman, K. Z. (2002). "An Experimental Study on Seismic Response Control of Asymmetric Buildings Using MR Dampers," *Proc. of The 11th Japan Earthquake Engineering Symposium*, Tokyo, Japan, November 20–22.

[65] Yoshida, O., Dyke, S. J., Giacosa, L. M., and Truman, K. Z. (2002). "Experimental Verification on Torsional Response Control of Asymmetric Buildings Using MR Dampers," *Earthquake Engineering and Structural Dynamics* (submitted).

Vita

Osamu Yoshida

EDUCATION

- Washington University, St. Louis, MO, D. Sc.: Civil Engineering, 2003
- The University of Tokyo, Tokyo, Japan, M.S.: Mechanical Engineering, 1993
- The University of Tokyo, Tokyo, Japan, B.S.: Mechanical Engineering, 1991

PROFESSIONAL HISTORY

- Research Engineer - Obayashi Corporation, Technical Research Institute, Tokyo, Japan (April 1993 - to date)

May 2003

Short Title: Torsional Response Control, Yoshida, D.Sc., 2003